行政院國家科學委員會專題研究計畫 成果報告

阻斷克雷伯氏菌複製叉重啟之研究(2/2)
研究成果報告(完整版)

計 畫 類 別 ：個別型
計 畫 編 號 ：NSC 99-3112-B-040-001-
執 行 期 間 ：99 年 05 月 01 日至 100 年 04 月 30 日
執 行 單 位 ：中山醫學大學生物醫學科學學系（所）

計 畫 主 持 人 ：黃晟洋

計畫參與人員：碩士級-專任助理人員：李彥陵
碩士級-專任助理人員：謝惠娟
碩士班研究生-兼任助理人員：陳政傑
碩士班研究生-兼任助理人員：林柏宏
碩士班研究生-兼任助理人員：黃彥華
碩士班研究生-兼任助理人員：莊立勤
大專生-兼任助理人員：謝玉亭
大專生-兼任助理人員：洪丹青
大專生-兼任助理人員：楊姿筠
大專生-兼任助理人員：鄭雅尹
大專生-兼任助理人員：黃喬霞
大專生-兼任助理人員：林宜加
大專生-兼任助理人員：郭易緯
大專生-兼任助理人員：楊凱植
大專生-兼任助理人員：楊舜銓
大專生-兼任助理人員：侯宗緯
大專生-兼任助理人員：曹懷文
大專生-兼任助理人員：林欣賢
大專生-兼任助理人員：何雅燁

報 告 附 件 ：出席國際會議研究心得報告及發表論文

處 理 方 式 ： 本計畫涉及專利或其他智慧財產權，2 年後可公開查詢

中 華 民 國 100 年 07 月 05 日

目　　錄

一、 計畫摘要

1a. 中文摘要 (一頁為限) ---------- page 2

1b. 英文摘要 (一頁為限) ---------- page 3

二、 背景介紹

2a. 研究目的 ---------- page 4

2b. 文獻探討 ---------- page 4

2c. 研究方法 ---------- page 7

三、 研究內容

3a. 研究成果 ---------- page 8

3b. 分析與討論 ---------- page 28

3c. 所遭遇之困難與因應對策 ---------- page 28

四、 成果自評 (整合型計畫之總計畫主持人需另針對整體計畫評估)

4a. 研究成果與原設定目標之相符程度 ---------- page 29

4b. 達成預期目標情形 ---------- page 29

4c. 研究成果之學術或應用價值 ---------- page 29

4d. 學術期刊發表情形 ---------- page 29

五、 參考文獻 ---------- page 30

六、 附件

學術論文 ---------- page 32

一、計畫摘要

1a. 中文摘要

關鍵詞：克雷伯氏肺炎桿菌，PriA，PriB，PriC，SSB，DnaB，DnaC，DnaG，DnaT，引子合成體，DNA 複製重啟體，複製重啟，複製叉，類黃酮，以結構為依據的藥物設計，單股 DNA 結合模式，蛋白質-蛋白質交互作用，蛋白質-DNA 交互作用，巨分子組裝，蛋白質結晶結構。

細菌利用 DNA 複製重啟之引子合成體 (DNA replication restart primosome) 來重新啟動 DNA 複製對其存活而言已被確認為必需，此蛋白質-核酸複合體包含八個蛋白質有次序的互相結合於停滯的複製叉上，分別為 PriA、PriB、PriC、SSB、DnaB、DnaC、DnaG 與 DnaT。克雷伯氏肺炎桿菌是台灣最常被分離出的病原菌之一，為了對抗被克雷伯氏肺炎桿菌感染的威脅，阻斷其 DNA 複製叉重啟的能力也許可行。這個計畫在兩年的時間已完成的工作如下：(1) 此八個蛋白質的基因選殖、大量表達、純化與蛋白質晶體之高速篩選。(2) PriB 與 SSB 的單股 DNA 結合模式之分析。(3) PriB 與 DnaT 蛋白質晶體之獲得。(4) PriB 結晶結構解出至 2.07Å。(5) 類黃酮物質能抑制 DnaB 活性。(6) PriB 與引子合成體蛋白質-蛋白質間結合作用分析。(7) DnaB 與其抑制劑 galangin 蛋白質複合晶體之獲得。希望這些結果能逐步引導以結構為依據的標靶藥物設計來針對克雷伯氏肺炎桿菌的 DNA 複製重啟體組裝，尤其是 PriB、SSB 與 DnaB。

一、計畫摘要

1b. 英文摘要

Keywords: *Klebsiella pneumoniae*, PriA, PriB, PriC, SSB, DnaB, DnaC, DnaG, DnaT, primosome, DNA replication restart primosome, DNA replication restart, replication forks, flavonols, structure-based drug design, single-strand DNA binding mode, protein-protein interactions, protein-DNA interactions, macromolecular assembly, protein crystal structure.

It has been recognized that the ability of DNA replication restart primosome is essential for bacterial survival. These primosomal proteins, PriA, PriB, PriC, SSB, DnaB, DnaC, DnaG and DnaT, sequentially associated together and then restart arrested DNA replication forks. *Klebsiella pneumoniae* (KP) is one of the most commonly isolated bacterial pathogens in Taiwan. To combat the threat of KP infections, blocking the restart of replication fork of KP may be useful. The accomplished experiments of this project are: (1) Gene cloning, expression, and purification of these primosomal proteins. (2) The analyses of ssDNA binding modes of PriB and SSB. (3) PriB and DnaT protein crystals are obtained. (4) Crystal structure of PriB has been solved to 2.07 Å by synchrotron radiation X-ray source at Beamline 13C1 of NSRRC. (5) The flavonols are found to inhibit the activity of DnaB. (6) Analyses of interactions of PriB with the primosomal proteins. (7) Crystal of DnaB in complex with the inhibitor galangin. We hope these results will lead the structure-based drug design to target KP replication restart primosome, especially PriB, SSB and DnaB.

二、背景介紹

2a. 研究目的

2b. 文獻探討

Initiation of chromosomal DNA replication in bacteria for genome duplication is a complex process that relies on divergent multi-protein assembly for entry of the replicative DNA helicase at the replication origin (1-4). In *Escherichia coli*, replication starts by loading the DnaB helicase at the unique site *oriC* (origin of chromosomal replication), accomplished by an *oriC*-specific recognition protein DnaA and a molecular escort protein DnaC, and continues bidirectionally around the chromosome until the two replication forks meet in the terminus region opposite to the *oriC* (5-8). During DNA replication, the DnaG primase interacts with the DnaB helicase to synthesize short RNA primers, which are used to generate the Okazaki fragments that are essential for the progression of replication fork extended by the DNA polymerase (9). However, replication forks initiated at *oriC* often collapse or disintegrate spontaneously, leading to fail to completion around the chromosome (4,10). It has become apparent that some exogenous and endogenous sources of DNA damage can inactivate a large proportion of replication forks (4,11). The replication forks could accidentally be arrested anywhere along the DNA, so reloading DnaB helicase for o*riC*-independent re-initiation of DNA replication is required (10,11).

In the past few years, it has been recognized that the ability to restart replication at sites of DNA damage on the template is essential for bacterial survival (11). The replication restart primosome, is a protein-DNA complex that re-activates stalled DNA replication at forks (4). Eight crucial proteins (PriA, PriB, PriC, DnaB, DnaC, DnaT, DnaG, and SSB) are involved in the restart of DNA replication (10). During replication restart, *in vitro* evidences indicate that PriA-directed replication restart primosome is located at the D-loop, a three-way-junction DNA structure that is an intermediate in recombination repair (12-14). The PriA-directed replication restart primosome assembly on the D-loop DNA is an ordered process: (i) PriA recognizes and binds to SSB-coated D-loop DNA. (ii) PriB joins PriA to form a PriA-PriB-DNA complex. (iii) DnaT participates in this complex to form a tri-protein complex on the D-loop DNA. (iv) DnaB is then transferred from a DnaB-DnaC complex to the PriA-PriB-DnaT-DNA complex to form a pre-primosome assembly that consists of PriA, PriB, DnaT and DnaB on the DNA. Finally, DnaG adds to this complex by interacting with DnaB, and completes assembly of the PriA-directed replication restart primosome (4,15).

The *PriA* mutant of *E. coli* exhibit complex phenotypes that include reduced viability, chronic induction of SOS response, rich media sensitivity, decreased homologous recombination, sensitivity to UV irradiation, defective double-stranded break repair, and both induced and

constitutive stable DNA replication (10,15-17). The *priBC* double mutant displays phenotypes that are identical to those of the *priA* mutant, in addition to a very poor viability and a growth rate that is even much slower than that of the *priA* mutant (15). These results suggest that preventing re-initiation of DNA replication or blocking the activities of the replication restart primosome will decrease the bacterial growth significantly. Fortunately, due to their distinct mechanisms in DNA replication re-initiation, we found that bacterial PriA, PriB, PriC, and DnaT proteins have no homologs in eukaryotic cells. Thus these prokaryotic primosomal proteins may be novel targets for antibiotics development.

Klebsiella are ubiquitous opportunistic pathogens which colonize at the mucosal surfaces of humans, and can give rise to severe diseases such as septicemia, pneumonia, urinary tract infections, and soft tissue infection (18). These nosocomial infections are mainly caused by *Klebsiella pneumoniae* (KP), the medically most important species of the genus. KP primarily attacks immunocompromised patients who are hospitalized or suffering from severe underlying diseases, such as diabetes mellitus, chronic alcoholism, or pulmonary obstruction, and commonly results in a high fatality rate if untreated (18). In spite of advances in treatment and prevention, KP still poses a major threat on public health worldwide. In Taiwan, KP is one of the most commonly isolated bacterial pathogens and is reported to be more prevalent and virulent than other regions of the world (19). Although KP strains are generally susceptible to some antibiotics such as cephalosporins, to which many clinical strains of KP are highly resistant (19-21). These extended-spectrum beta-lactamase (ESBL)-producing KP strains have restricted effective treatments in current therapy (22). Several critical pathogenicity factors of *Klebsiella* infections have been identified, including capsular antigens, pili (fimbriae), lipopolysaccharide, serum resistance, and siderophores (18,23-26). These gene clusters of pathogenicity factors have been sequenced, classified and studied by both *in vitro* and *in vivo* models to investigate the interaction of bacterial cells with the host. Nevertheless, the ability of pathogenic bacteria to cause disease in a susceptible host is determined by multiple virulence factors acting individually or together at different stages of infection, thereby complicating the analyses of these dynamic infection mechanisms and virulence factors-based drug design.

To combat the threat of invading KP infections, discovering virulence factors and identifying novel targets for drug developments and/or new cures would be highly needed for public health. Since inhibition of either activity of the replication restart primosomal proteins will be detrimental to bacterial survival, targeting to these proteins should be a legitimate way to reduce viability of KP. Some crystal structures of primosomal proteins such as PriA (27), PriB (28,29), DnaB (5-7), and DnaG (30) have been determined, and these results have significantly advanced the knowledge of the molecular mechanisms of replication restart primosome assembly. It seems likely that antibiotics' development by rational design for these target proteins of KP may

be achieved as soon. However, we found that several primosomal proteins identified previously are not conserved among Gram-negative bacteria including KP, for example as PriB protein (28,29,31). It is therefore difficult and inappropriate to apply the primosome information studied from other system directly to that of KP. In addition, little is reported on replication restart primosome of KP (31-33). In this project, we propose to study the 3-D structure and function of these KP primosomal proteins. We believe the resultant information can provide the deeper knowledge of the KP replication restart primosome, whereby to advance our understanding as to how DNA replication restart of KP can be blocked.

2c. 研究方法

New and emerging pathogenic bacteria and the rise in multi-drug-resistant bacterial strains are driving the need to discover novel antibiotics. *Klebsiella pneumoniae* (KP) is one of the most commonly isolated bacterial pathogens in Taiwan. It has been recognized that the ability to restart arrested DNA replication forks is essential for bacterial survival. Thus, in order to combat the threat of KP infections, blocking the restart of replication fork of KP may be useful. Eight crucial proteins (PriA, PriB, PriC, DnaB, DnaC, DnaT, DnaG, and SSB) are involved in assembly of replication restart primosome. To obtain better knowledge as to how the activities of these primosomal proteins can be blocked, our objective is to provide structural and functional information to assist in drug development targeting KP.

(1) Crystallization, and structural determination of KP primosomal proteins. To provide the molecular information of these KP primosomal proteins, we aim to obtain the crystals of PriA, PriB, PriC, DnaT, DnaC, DnaB, DnaG, and SSB or their complexes with DNA or RNA.

(2) Characterization of DNA binding properties of KP primosomal proteins. PriA, PriB, DnaC, DnaB, DnaG, SSB are known to have ssDNA binding ability. Biochemical analyses of these Protein-DNA complexes are vital to understand the assembly mechanisms of KP PriA-directed primosome. We study the stoichiometry, the structure-function relationship, base specificity, and binding affinity of the protein by use of electrophoretic mobility shift assay (EMSA), mutational analysis, and filter binding assay. The cooperativity of the binding process and the binding modes of the protein are also analyzed quantitatively.

(3) Knowledge-based selection of inhibitors. Some small compounds possessing anti-DNA binding or anti-ATPase activities have been reported. We use these nucleic acid analogues as inhibitors to characterize the DNA binding affinity of the protein, and the ability of the replication restart primosome assembly of KP. To find more and more inhibitors, program-based docking with the protein's structure is also used. There may be some inhibitors as potential drug candidates that can block the restart of replication fork of KP.

(4) Determination of crystal structure of the protein in complex with the drug candidate. An inhibitor is selected to co-crystallize with the protein, and solve the complexed structure. This information may provide a molecular insight into how modify the inhibitor can make a better drug.

三、研究內容

3a. 研究成果

(1) Gene cloning, expression, and purification of PriA, PriB, PriC, DnaT, DnaC, DnaB, DnaG, and SSB from KP. The genes encoding KP replication restart primosomal proteins were amplified by polymerase-chain reaction (PCR). The expression pET-21b vector containing a six-histidine affinity tag at the C-terminus of the cloning site was used to overexpress these proteins.

(2) Crystallization of PriB, DnaT, and DnaB from KP.

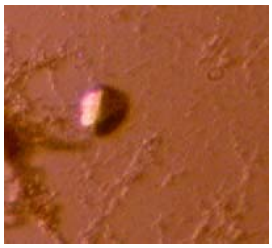

PriB

DnaT

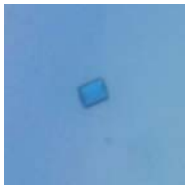

DnaB

(3) Crystal structure of *Klebsiella pneumoniae* PriB. The structure of PriB from KP has been solved at 2.07Å resolution and submitted to the Protein Data Bank (PDB) with **accession no. 2xrr**.

Table Data collection and refinement statistics for *Kp*PriB

Data collection	
Crystal	*Kp*PriB
Wavelength (Å)	0.97622
Resolution (Å)	2.1
Space group	C2
Cell dimension (Å)	a = 64.7
	b = 36.9 β = 113.7
	c = 39.4
Completeness (%)	96.7(99.8)
<*I*/σ*I*>	40.7 (6.4)
*R*symb (%)	6.4 (25.9)
Redundancy	3.4 (3.6)
Refinement	
Resolution (Å)	30-2.1
No. reflections	5096
*R*work / *R*free	23.4/23.8
No. atoms	
Portein	784
Water	12
R.m.s deviation	
Bond lengths (Å)	0.007
Bond angles (°)	1.5
Ramachandran Plot	
In preferred regions	80 (90.9%)
In allowed regions	7 (7.9%)
outliers	1 (1.1%)

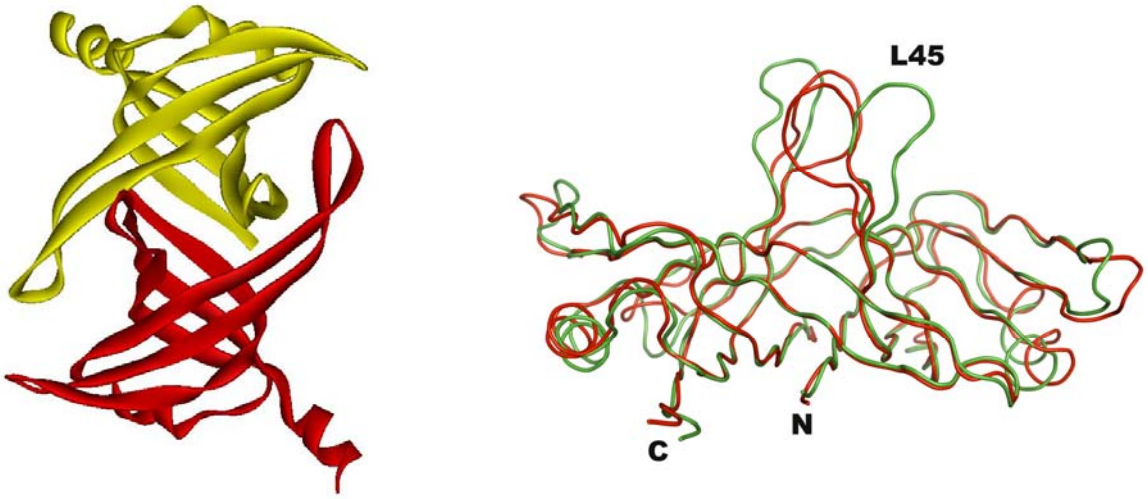

Crystal structure of the full length version of PriB from KP; accession no. 2xrr. The structure of KP PriB (2.1Å) compared with that of *E coli* PriB. Their ssDNA binding sites (Loop 45; L45) are very different.

(4) A novel PriB protein from KP.

4.1. Sequence analysis

The gene *KPN_04595* encoding the putative *Kp*PriB is described in the NCBI database. Based on the known nucleotide sequence, the predicted *Kp*PriB monomer protein has a length of 55 aa and a molecular mass of 7 kDa. This differs from the well-studied 104-aa *Ec*PriB protein. Analysis of the primary structure of *Kp*PriB by RPS-BLAST revealed the presence of an RPA OB fold-like domain. The figure shows alignment of the amino acid sequences of *K. pneumoniae*, *P. carotovorum* (*Pc*), *Y. ruckeri* (*Yr*), *S. enterica* (*Se*), *E. coli*, and *Neisseria gonorrhoeae* (*Ng*) PriB. The primary structures of these PriBs are similar; however, *Kp*PriB, *Pc*PriB, *Yr*PriB, and *Se*PriB are shorter in length than *Ec*PriB and *Ng*PriB. Specifically, the N-terminal 1－49 aa region of *Ec*PriB is absent in *Kp*PriB. This region in *Ec*PriB contains several important residues crucial for ssDNA binding, such as K18, R34, and W47. In addition, the W47 residue of *Ec*PriB has been proven to stimulate PriA helicase. These residues, conserved in most PriB families, are not found in *Kp*PriB, *Pc*PriB, and *Yr*PriB, due to their truncated gene products. The evolutionary tree for these PriBs is shown: they could be classified into at least 3 groups.

```
KpPriB  ------------------------------------------------------MPVII  5
PcPriB  ------------------------------------------------------MPVIV  5
YrPriB  ------------------------------------------------------MPVIV  5
SePriB  ---------------------------------MLEHRSVQEEAGFHRQAWCQMPVIV  25
EcPriB  --MTNRLVLSGTVCRAPLRKVSPSGIPHCQFVLEHRSVQEEAGFHRQAWCQMPVIV  54
NgPriB  MGFTNLVSLAALIEKAFPIRYTPAGIPVLDIILKHESWQEENGQQCLVQLEIPARI  56

KpPriB  SGHENQAITHSITVGSAVTVRGFISCHKAKNGLSKMVLHAEQIELIDSGD  55
PcPriB  SGLSSQAVTHSITVGTQLTVHGFISCHQGRNGLSKIVLHAEQIELIDSGD  55
YrPriB  SGHQSQALTHSITVGSQLTVEGFISCHQGRNGLNKLVLHAEQIELIDSGD  55
SePriB  SGHENQAITHSITVGSRITVQGFISCHKAKNGLSKMVLHAEQIELIDSGD  75
EcPriB  SGHENQAITHSITVGSRITVQGFISCHKAKNGLSKMVLHAEQIELIDSGD  104
NgPriB  LGRQAEEWQYRQ--GDCATVEGFL-AQKSRRSLMP-MLRIQNIKEYK-G-  100
```

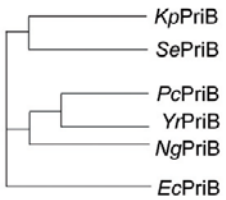

4.2. Oligomerization of KpPriB in solution

To determine whether the length of the gene product affects its oligomerization state, we analyzed *Kp*PriB and *Ec*PriB by gel filtration chromatography. *Ec*PriB exists as a dimer and a tetramer (solid line). However, analysis of purified *Kp*PriB by gel filtration chromatography revealed a single peak (dotted line). Assuming that *Kp*PriB has a structure and partial specific volume similar to the standard proteins, the native molecular mass of *Kp*PriB was estimated to be ~7 kDa. Thus, the single peak suggests that *Kp*PriB, unlike *Ec*PriB, is a stable monomer.

To assess whether *Kp*PriB forms dimer or oligomer in the presence of ssDNA, we incubated the protein with glutaraldehyde in order to cross-link lysine residues in the presence and absence of dT30. Addition of dT30 resulted in a significant increase in the amount of cross-linked species, which may correspond to the presence of dimers (~15 kDa) and tetramers (~30 kDa) of *Kp*PriB. Taken together with the gel filtration data, these studies suggest that *Kp*PriB is a monomer in solution, and that oligomers (mainly dimers) are formed, only in the presence of ssDNA.

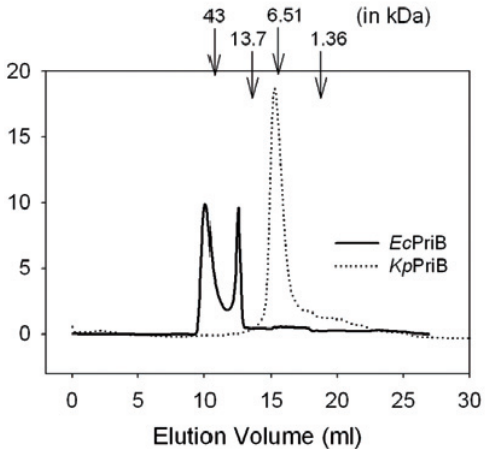

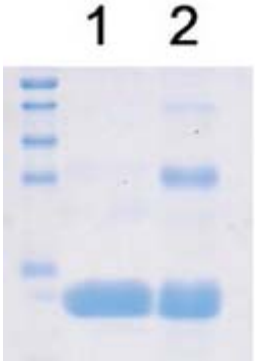

4.3. KpPriB binds ssDNA

To assess whether *Kp*PriB binds ssDNA, we assessed binding of *Kp*PriB to dT20, dT25, dT30, dT35, dT40, dT45, dT50, dT55, and dT60 with different protein concentrations using EMSA. No significant band shift was observed when *Kp*PriB was incubated with dT20, indicating that *Kp*PriB could not form a stable complex with dT20 during electrophoresis. In contrast to dT20, the longer dT homopolymers bind to *Kp*PriB, forming a single complex. These interactions appear to be highly cooperative since only 1 complex of *Kp*PriB molecules bound per ssDNA is visible when the length of the dT homopolymers is further increased to 60 nt; there is no other distinctive complex or intermediate form. Thus, the shorter *Kp*PriB can bind ssDNA, and the length of ssDNA required for forming a stable complex with *Kp*PriB molecule(s) is approximately 25 nt, as determined using EMSA.

4.4. Base preference for ssDNA binding of KpPriB

To test the base preference for *Kp*PriB binding to purine and pyrimidine, we used dT30, dC30, and dA30 to bind to *Kp*PriB. Like *Ec*PriB, *Kp*PriB shows a higher preference for dT30

than for dA30. In addition, this study revealed that the binding preference of *Kp*PriB follows the given order: dT > dC > dA, i.e., *Kp*PriB preferentially binds to pyrimidine than to purine. However, the *in vitro* base preference of PriB, as well as other SSBs, is still unknown.

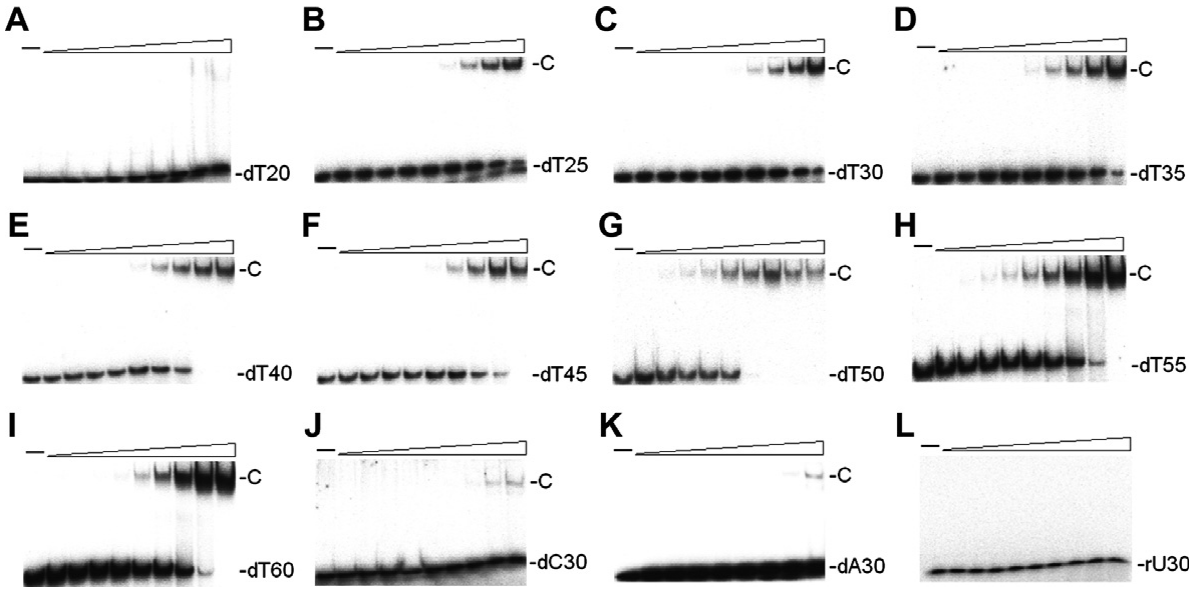

4.5. RNA binding activity of KpPriB

It has been previously reported that *Ec*PriB binds ssRNA (U35) with an affinity that is comparable to its affinity for ssDNA dT35. In order to assess whether the ability of PriB to bind to RNA is conserved, we assessed the binding of rU30 and dT30 to *Kp*PriB. Unexpectedly, *Kp*PriB did not bind to rU30 with the same affinity as it did for dT30. Thus, the RNA-binding activity of PriB among different species is not conserved and therefore is likely to be unnecessary in the *K. pneumoniae* primosome assembly.

4.6. Cooperative binding of KpPriB to ssDNA

The ssDNA binding ability of *Kp*PriB was studied via a filter-binding assay using dT15. Since dT20 or longer homopolymers give high background noise on binding to nitrocellulose filters, they were excluded from the assays. The titration curves for *Kp*PriB are shown in the figure, and the estimated apparent K_d values are summarized in the Table. The binding affinity of *Kp*PriB for dT15 (filled circle) increased significantly within a narrow range of protein concentrations, indicating that the formation of the *Kp*PriB-dT15 complex is a positive cooperative process. The Hill coefficient (*h*) for *Kp*PriB-dT15 binding was determined to be 3.41 ± 0.56, which is significantly higher than that for *Ec*PriB-dT15 (1.5 ± 0.1). The strong cooperative binding of *Kp*PriB to ssDNA has important implications for the nature of the protein-protein interactions within the complex and the position of the ssDNA-binding sites on *Kp*PriB. This is especially important considering that *Kp*PriB lacks several important residues for ssDNA binding, as compared with *Ec*PriB.

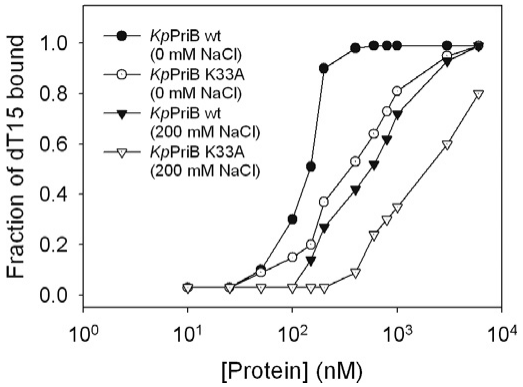

ssDNA-binding parameters of *Kp*PriB.

	[NaCl] (mM)	Apparent K_d (nM)	*h*
*Kp*PriB wt	0	140 ± 20	3.41 ± 0.56
*Kp*PriB K33A	0	380 ± 20	1.26 ± 0.08
*Kp*PriB wt	200	580 ± 50	1.33 ± 0.12
*Kp*PriB K33A	200	2600 ± 400	1.28 ± 0.19

The errors are standard deviations determined using 2–4 independent titration experiments.

4.7. Salt effect on ssDNA binding of KpPriB

The ssDNA-binding surface of *Ec*PriB is highly electropositive and interacts directly with both the bases and the phosphate backbone of ssDNA. Although *Kp*PriB lacks the N-terminal 1 – 49 aa region seen in *Ec*PriB, the most important residues for ssDNA binding, K33, K35, and K40, corresponding to positions K82, K84, and K89, respectively, in *Ec*PriB, are conserved. To investigate whether the electrostatic interactions play a role in ssDNA binding, we examined the binding of *Kp*PriB to dT15 at high salt concentrations (200 mM NaCl). As expected, the binding affinity of *Kp*PriB for dT15 is salt dependent, and is approximately 4-fold lower than that measured in the absence of salt. Furthermore, the Hill coefficient (*h*) is reduced to 1.26 ± 0.08, indicating lower cooperativity in these conditions.

4.8. Role of K33 in KpPriB-ssDNA binding

To investigate the contribution of K33 in *Kp*PriB-ssDNA binding, a mutant was created with an alanine substitution at the position corresponding to K82 in loop L_{45} of *Ec*PriB. Binding was assessed in the absence and presence of 200 mM NaCl. The K33A mutant has a K_d value (380 ± 20 nM) that is 2.7-fold higher than that of the wild-type *Kp*PriB (140 ± 20 nM) in the absence of additional NaCl. In the presence of 200 mM NaCl, the K33A mutant has a K_d value (2600 ± 400 nM) that is ~19-fold higher than that of the wild-type *Kp*PriB assayed without additional salt. The Hill coefficient of the K33A mutant is 1.26 ± 0.08 and 1.28 ± 0.19, when in the absence and presence of 200 mM NaCl, respectively. These data indicate that *Kp*PriB binds to ssDNA mainly through electrostatic interactions, especially within the positive charge region. Hence, the K33 position in *Kp*PriB appears to be involved not only in ssDNA binding, but also in the intra- or/and inter-molecular cooperative binding to other residue(s) of *Kp*PriB.

4.9. Comparison with EcPriB

The homodimeric arrangement of OB folds in *Ec*PriB is roughly conserved among known PriB homologs. In this study, we reported a novel PriB from *K. pneumoniae* that is shorter and monomeric compared with the known PriBs, which are polymeric. It has been previously reported that the monomeric interactions found in the *Ec*PriB dimer are tightly packed by hydrophobic interactions involving the residues Leu5, Leu7, Met50, and Ile78. Two of these residues, Met1 and Ile29, exist in the shorter *Kp*PriB homolog. The lack of the 2 Leu residues results in the failure to homodimerize, but the remaining residues are sufficient for mediating

ssDNA binding.

Previous investigations of *Ec*PriB demonstrated that aromatic stacking, mediated by residues Phe42 and Trp47, plays an important role in ssDNA binding and in stimulating PriA helicase. These residues, however, do not exist in *Kp*PriB. Therefore, the mechanisms and the binding modes of *Kp*PriB, as well as other *K. pneumoniae* primosomal proteins, to ssDNA remain to be explored.

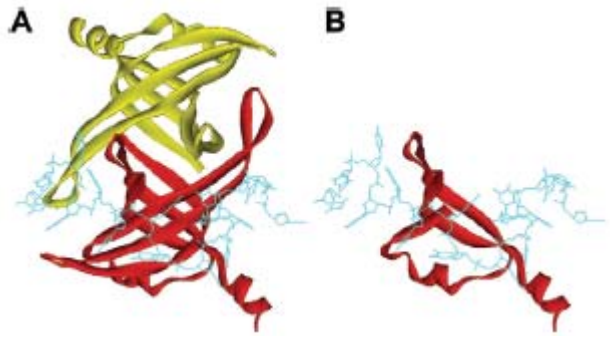

(5) The putative *Kp*PriB gene (*Kp*PriBc), *KPN_04595*, described in the NCBI database, is incorrect.

5.1. Identification of KpPriB gene in K. pneumoniae

Because the yeast 2-hybrid analysis of *Kp*PriBc revealed that PriB from *K. pneumoniae* did not interact with any primosomal proteins used, we aimed to discover other forms of PriB. We found a DNA fragment of *K. pneumoniae* chromosome that could be specifically amplified by using primers for cloning the *Ec*PriB gene, suggesting that there was a region in *K. pneumoniae* chromosome highly similar to that of the *Ec*PriB gene. As expected, on searching the NCBI database, we found a positive hit at 5023576－5023890 nt in the *Kp* chromosome. To test whether this region, designated as *KpPriB*, could be expressed, the total RNA of *K. pneumoniae* was extracted and reverse transcribed, and then analyzed by Q-PCR using specific primers for *KpPriBc* and *KpPriB*. The expression plasmid pET21b-*Kp*PriB served as a quantitative standard. We found that this region of *KpPriB*, as well as of *KpPriBc*, was expressed; the C_T values were 22.59 and 22.40 for *KpPriBc* and *KpPriB*, respectively. Because the region of *KpPriBc* completely overlapped the C-terminal region of *KpPriB*, comparison of C_T values from Q-PCR experiments revealed that mRNA levels of *KpPriBc* and *KpPriB* were nearly equal. This suggests that only 1 *PriB* gene was expressed in *K. pneumoniae*, most likely *KpPriB*.

5.2. Sequence analysis

The putative *KpPriB* is not described in the NCBI database, but we have identified its expression here. Based on the known nucleotide sequence, the predicted *Kp*PriB monomer protein has a length of 104 aa and a molecular mass of 12 kDa. This is highly similar to the well-studied 104-aa *Ec*PriB protein. The figure shows the alignment of the amino acid sequences of the PriB in *K. pneumoniae*, *P. carotovorum* (*Pc*), *Y. ruckeri* (*Yr*), *S. enterica* (*Se*), *E. coli*, and *Neisseria gonorrhoeae* (*Ng*). The primary structures of these PriBs are similar; however, *Kp*PriBc, *Pc*PriB, *Yr*PriB, and *Se*PriB are shorter in length than *Ec*PriB and *Ng*PriB. Since we identified that *Kp*PriB, another form of PriB, exists, these shorter PriBs, namely *Kp*PriBc, *Pc*PriB, *Yr*PriB,

and *Se*PriB, as well as other unidentified PriBs among different bacterial species, may need to be reassessed in terms of gene length.

In addition to identifying the expression of *KpPriB*, we also tried to locate its promoter as predicted by several programs. By using online promoter analysis tools (http://molbiol-tools.ca/Promoters.htm), we found no significant promoter for *KpPriB* expression. Thus, it seems difficult and inappropriate to apply the gene expression information from *E. coli* or other systems directly to that of *K. pneumoniae*. Therefore, the regulation and expression of the primosomal proteins such as *KpPriB* should be further investigated in *K. pneumoniae*.

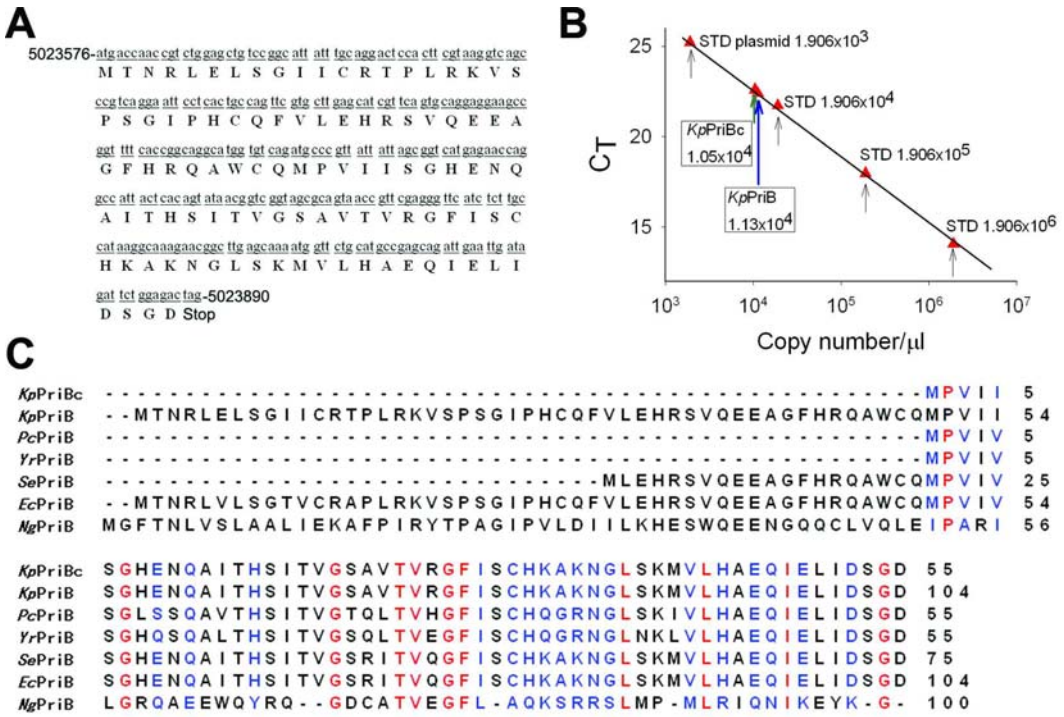

5.3. Yeast 2-hybrid analyses

PriB is known to interact with the primosomal protein PriA and DnaT *in vitro*. To address whether PriB binds to other primosomal proteins and to map the interacting region of PriB, 2 yeast 2-hybrid systems, strains Y187 and AH109, were used to identify proteins interacting with *Kp*PriB (right lanes) or *Kp*PriBc (middle lands). cDNA corresponding to *Kp*PriBc or *Kp*PriB was fused to the GAL4-binding domain used as the bait to bind a possible 2-hybrid. *Kp*PriA, *Kp*PriB, *Kp*DnaA, *Kp*DnaB, *Kp*DnaC, *Kp*DnaG, and *Kp*DnaT fused to the activation domain were used as the prey, and the empty pACT2 vector was used as a control. An interaction between PriB (*Kp*PriBc or *Kp*PriB) and the protein will result in strong β-galactosidase activity of the Y187 strain, shown in blue after cell lysis. In addition, to ascertain this interaction, the AH109 strain was tested for its ability to grow on histidine and urea-free plates. The filter papers show blue smears, identifying the interactions of *Kp*PriB-*Kp*PriA, *Kp*PriB-*Kp*PriB, and *Kp*PriB-DnaT pairs. These interactions were also verified in the AH109 strain; the yeast grew well on histidine and urea-free plates. Thus, *Kp*PriB clearly showed strong interactions with *Kp*PriA, *Kp*DnaT, and *Kp*PriB itself as examined by these yeast 2-hybrid analyses.

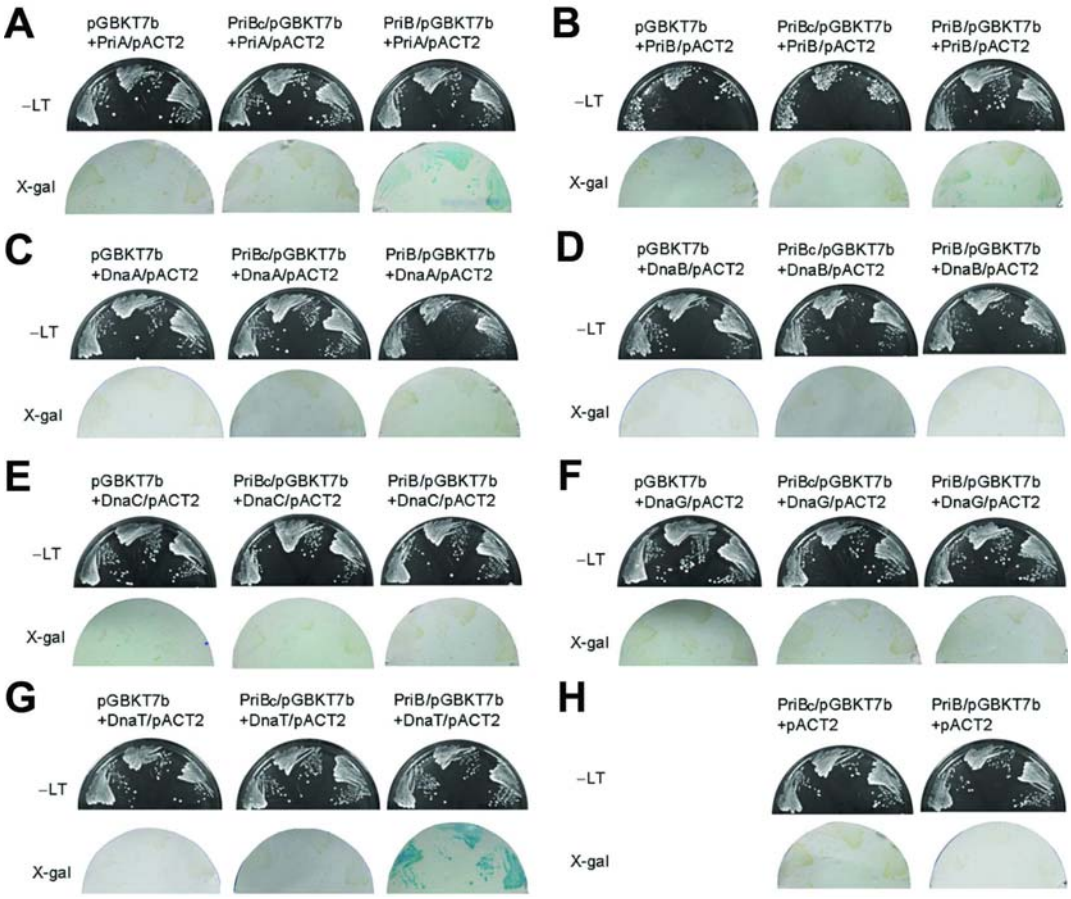

Y187 strain

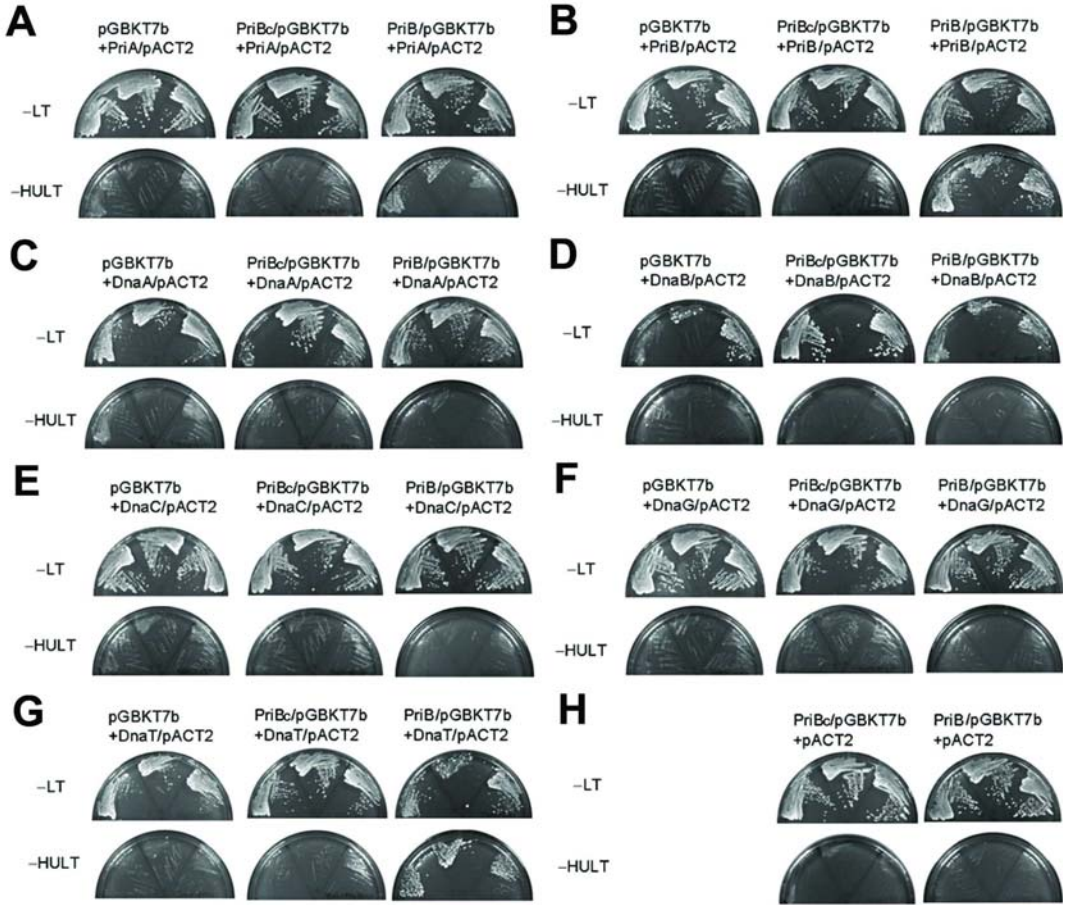

AH109 strain

Table 1. The yeast 2-hybrid analyses of *Kp*PriBc and *Kp*PriB

Strain	Y187		AH109	
	PriBc	PriB	PriBc	PriB
PriA	—	++	—	++
PriB	—	+	—	+++
DnaA	—	—	—	—
DnaB	—	—	—	—
DnaC	—	—	—	—
DnaG	—	—	—	—
DnaT	—	+++	—	++
Ctrl	—	—	—	—

For

5.4. KpPriB binds ssDNA

To assess whether *Kp*PriB binds ssDNA, we assessed binding of *Kp*PriB to dT20, dT25, dT30, dT35, dT40, dT45, dT50, dT55, and dT60 with different protein concentrations using EMSA. No significant band shift was observed when *Kp*PriB was incubated with dT20, indicating that *Kp*PriB could not form a stable complex with dT20 during electrophoresis. In contrast to dT20, the longer dT homopolymers bind to *Kp*PriB, forming a single complex. These interactions appear to be highly cooperative since only 1 complex of *Kp*PriB molecules bound per ssDNA is visible when the length of the dT homopolymers is further increased to 60 nt; there is no other distinctive complex or intermediate form. Thus, *Kp*PriB can bind ssDNA, and the length of ssDNA required for forming a stable complex with *Kp*PriB molecule(s) is approximately 25 nt, like *Kp*PriBc, as determined using EMSA.

5.5. Base preference for ssDNA binding of KpPriB

To test the base preference for *Kp*PriB binding to purine and pyrimidine, we used dT30 and dA30 to bind to *Kp*PriB. Like *Ec*PriB and *Kp*PriBc, *Kp*PriB shows a higher preference for dT30 than for dA30, i.e., *Kp*PriB preferentially binds to pyrimidine than to purine. However, the *in vitro* base preference of PriB, as well as other SSBs, is still unknown.

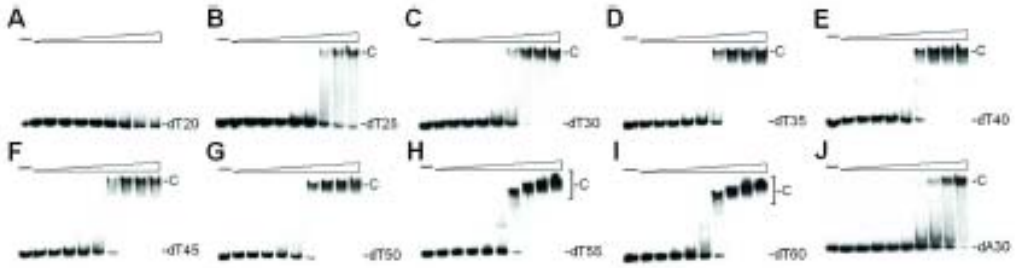

5.6. An annotation of K. pneumoniae PriB in NCBI is incorrect

In this study, we have shown a new or second PriB gene (5023576－5023890 nt) in *K. pneumoniae* by using Q-PCR and bioinformatic approaches. This one seems to have a longer, N-terminal extension, relative to the previous documented PriB gene (*KPN_04595*, designated as *KpPriBc* in this study), and is ~98% identical to the *E. coli* gene. It is also exactly the same length as the *E. coli* gene. Because the region of *KpPriBc* completely overlaps the C-terminal

region of *KpPriB*, comparison of C_T values from Q-PCR experiments reveals that mRNA levels of *KpPriBc* and *KpPriB* are nearly equal. Since there is no evidence that there are two biologically meaningful forms of PriB, these results suggest that only 1 *PriB* gene is expressed in *K. pneumoniae*, most likely *KpPriB*.

5.7. KpPriBc does not interact with KpPriA, KpPriB, KpDnaA, KpDnaB, KpDnaC, KpDnaG, and KpDnaT proteins

The *PriB* gene in *K. pneumoniae*, originally described as *KPN_04595* in the NCBI database, has been identified recently and designated as *KpPriBc* here. Contrary to our initial expectation, *Kp*PriBc does not show interacting activity with the primosomal *Kp*PriA, *Kp*PriB, *Kp*DnaA, *Kp*DnaB, *Kp*DnaC, *Kp*DnaG, and *Kp*DnaT proteins in our yeast 2-hybrid analyses in the both strains Y187 and AH109. We, therefore, reinvestigate the presence of other forms of PriB. The only difference between *Kp*PriBc and *Kp*PriB is the length, in which the N-terminal 1－49 aa region of *Kp*PriB is absent in *Kp*PriBc, indicating that this N-terminal domain contains several residues crucial for both *Kp*PriA and *Kp*DnaT binding, as well as *Kp*PriB self-association.

5.8. KpPriB does not interact with KpDnaA

It is well established that the components of primosome assembly are different in gram-positive and gram-negative bacteria. Furthermore, it has been proposed that gram-positive bacterial primosome assembly should be similar to that of the gram-negative bacteria, in which DnaD and PriB assemble to their respective PriA proteins. In addition to binding to PriA, DnaD also interacts with another initiator protein, DnaA, to initiate the DnaA-directed DNA replication pathway. To test whether *Kp*PriB interacts with *Kp*DnaA, we performed yeast 2-hybrid analyses, and the results revealed that *Kp*PriB does not interact with *Kp*DnaA. Thus, *Kp*PriB, unlike DnaD, may not initiate DnaA-directed pathway for DNA replication in gram-negative bacteria.

5.9. KpPriB does not interact with KpDnaC, KpDnaB, and KpDnaG

It has been proposed that DnaT binding to PriB, causing the release of ssDNA by PriB, is a driving force in the recruitment of the DnaB/C complex to the primosome, perhaps through direct contact with DnaT. To test whether PriB interacts with the DnaB/C complex, we performed yeast 2-hybrid analyses. The results revealed no interaction between *Kp*DnaC, *Kp*DnaB, and *Kp*DnaG. If PriA does not interact with the DnaB/C complex, we can speculate that DnaT may interact with the DnaB/C complex alone and cause further loading onto the forked DNA. However, this speculation needs to be confirmed by further biochemical experiments.

5.10. KpPriBc maintains interaction with ssDNA but loses interactions with KpPriA and KpDnaT

It has been shown that the residues E39 and R44 in *Ec*PriB are crucial for *Ec*PriA binding, and these residues along with W47 are involved in *Ec*DnaT binding, in which some binding residues partially overlap to bind to *Ec*PriA. Taken together with our yeast 2-hybrid identifications of PriB domains important for protein binding, and the data that *Kp*PriBc can bind ssDNA well, the conserved N- and C-terminal regions in the PriB family could be clearly defined

in terms of function. The N-terminal 1 – 49 aa region of PriB is the protein-protein interaction domain for PriA and DnaT binding, and for self-dimerization, while the C-terminal 50 – 104 aa region of PriB is the ssDNA-binding domain.

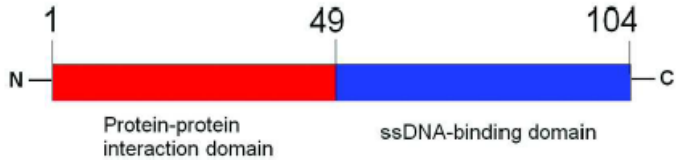

(6) ssDNA binding modes of SSB.

6.1. Sequence analysis

The gene *KPN04446*, encoding *K. pneumoniae* SSB, was initially found using a database search through the National Center for Biotechnology Information (NCBI). Based on the known nucleotide sequence, the predicted *Kp*SSB monomer protein has a length of 174 amino acid residues and a molecular mass of 19 kDa. Analysis of the primary structure of *Kp*SSB by RPS-BLAST revealed the presence of a putative OB-fold domain that is common in all known SSBs. The figure shows an alignment of the amino acid sequences of *K. pneumoniae*, *Salmonella enterica* Serovar Typhimurium LT2, *Pseudomonas aeruginosa*, *Helicobacter pylori*, *E. coli*, *Mycobacterium tuberculosis*, and *Mycobacterium smegmatis* SSBs. In the *Ec*SSB–ssDNA complex, 4 essential aromatic residues, Trp40, Trp54, Phe60, and Trp88, participate in ssDNA binding via stacking interactions. These residues are conserved in most SSB families as Phe/Tyr/Trp, and the corresponding residues in *Kp*SSB are Trp41, Trp55, Phe61, and Trp89. The C-terminal tail of SSBs containing several acidic residues, such as "DDDIPF" in *Ec*SSB, is also conserved in *Kp*SSB. In contrast to those motifs, 2 glycine residues in the glycine-rich hinge of *Ec*SSB (Gly125 and Gly128) are not found in *Kp*SSB.

```
KpSSB  MASRGVNKVILVGNLGQDPEVRYMPSGGAVANFTLATSESWRDKQTGEMKE-QTEWHRVVLFG   62
StSSB  MASRGVNKVILVGNLGQDPEVRYMPSGGAVANLTLATSESWRDKQTGEMKE-QTEWHRVVMFG   62
PaSSB  -MARGVNKVILVGNVGGDPETRYMPNGNAVTNITLATSESWKDKQTGQQQE-RTEWHRVVFFG   61
HpSSB  ----MPNKVIMVGRLTRNVELKYLPSGSAAATIGLATSRRFK-KQDGTLGE-EVCFIDARLFG   57
EcSSB  MASRGVNKVILVGNLGQDPEVRYMPNGGAVANITLATSESWRDKATGEMKE-QTEWHRVVLFG   62
MtSSB  --MAGDTTITIVGNLTADPELRFTPSGAAVANFTVASTPRIYDRQTGEWKDGEALFLRCNIWR   61
MsSSB  --MAGDTTITVVGNLTADPELRFTPSGAAVANFTVASTPRMFDRQSGEWKDGEALFLRCNIWR   61

KpSSB  KLAEVAGEYLRKGSQVYIEGQLRTRKWTDQSGQDKYTTEV-VVNVGGTMQMLGGRQGGGAPAG  124
StSSB  KLAEVAGEYLRKGSQVYIEGQLRTRKWTDQSGQERYTTEINVPQIGGVMQMLGGRQGGGAPAG  125
PaSSB  RLAEIAGEYLRKGSQVYVEGSLRTRKWQGQDGQDRYTTEI-VVDINGNMQLLGGR-----PSG  121
HpSSB  RTAEIANQYLSKGSSVLIEGRLTYESWKDQTGKKNSRHTITADSLQFMDKKSDNPQANAMQDS  120
EcSSB  KLAEVASEYLRKGSQVYIEGQLRTRKWTDQSGQDRYTTEV-VVNVGGTMQMLGGRQGGGAPAG  124
MtSSB  EAAENVAESLTRGARVIVSGRLKQRSFETRSGEKRTVIEVEVDEIGPSLRYATAKVNKASRSG  124
MsSSB  EAAENVAESLTRGSRVIVTGRLKQRSFETRSGEKRTVVEVEVDEIGPSLRYATAKVNKASRSG  124

KpSSB  ------GGQQQQGGWGQPQQPQ---GGNQFSGGAQSRPQQQAPAAPSNEPPMD-FDDDIPF   174
StSSB  -------GQQQQGGWGQPQQPQQPQGGNQFSGGAQSRPQQSAP-APSNEPPMD-FDDDIPF   176
PaSSB  -------DDSQRAPREPMQRP------QQAPQQQSRPAPQQQPAPQPAQDYDSFDDDIPF   165
HpSSB  IMHENSNNAYPANHNAPSQDPFN-QAYAQMAYAKENLQAQPSKYQMSVPEINIDEEEIPF   179
EcSSB  GNI--GGGQPQGGWGQPQQPQ---GGNQFSGGAQSRPQQSAPAAPSNEPPMD-FDDDIPF   178
MtSSB  ------------GFGSGSRPA-------PAQTS-SASGDDPWGSAPASGSFGGGDDEPPF   164
MsSSB  ------------GGGGGFGSG-------GGSRQSEPKDDPWGSAPASGSFSGADDEPPF   165
```

6.2. Oligomerization of KpSSB in solution

Analysis of purified protein by gel filtration chromatography revealed a single peak. Assuming that *Kp*SSB has a shape and partial specific volume similar to the standard proteins, the native molecular mass of *Kp*SSB was estimated to be ~80 kDa. The native molecular mass for *Kp*SSB is approximately 4.1 times the molecular mass of a *Kp*SSB monomer (19 kDa). Thus, we concluded that *Kp*SSB in solution is a stable tetramer, similar to *Ec*SSB.

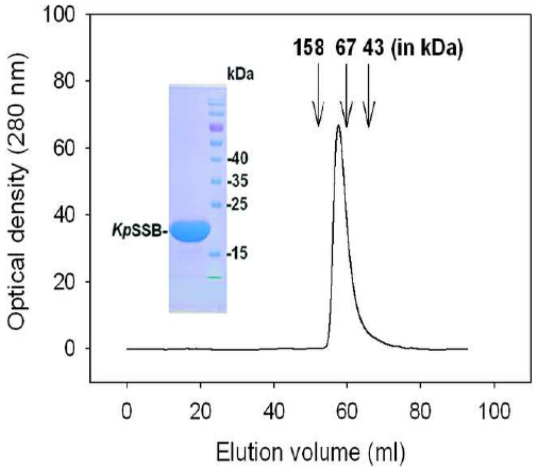

6.3. DNA binding monitored by quenching of intrinsic tryptophan fluorescence

It is well established that the fluorescence quench and the estimated size of the binding sites of SSBs depend on the salt concentration of the SSB solution. *Kp*SSB has 3 tryptophan residues (Trp41, Trp55, and Trp89) in the OB-fold domain, allowing an analysis of ssDNA binding by tryptophan fluorescence quenching. The protein displayed strong intrinsic fluorescence with a peak wavelength of 348 nm when excited at 295 nm, consistent with tryptophan fluorescence. As dT50 was titrated into the *Kp*SSB solution, the intrinsic fluorescence of the protein was progressively quenched. On addition of a saturating quantity of ssDNA in the presence of 20 and 300 mM NaCl, the intrinsic fluorescence at 348 nm was quenched by 65% and 89%, respectively. The estimated binding-site sizes of *Kp*SSB in 20 and 300 mM NaCl were about of 27 ± 2 nt and 38 ± 2 nt, respectively.

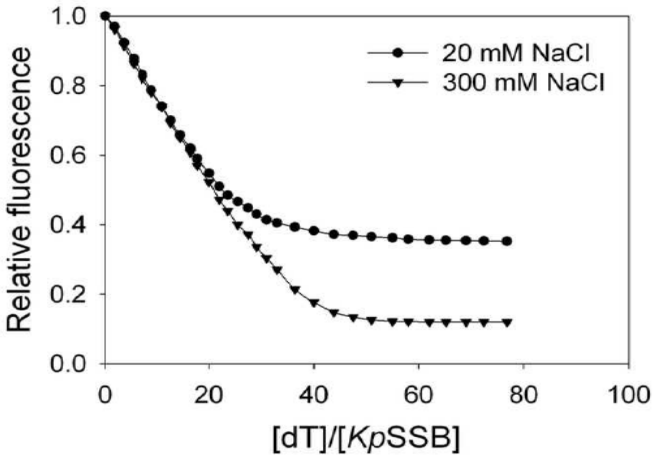

6.4. KpSSB binding to dT25–50 forms a single complex

To investigate the length of nucleotides sufficient for the formation of the *Kp*SSB-ssDNA complex and the ssDNA-binding ability of *Kp*SSB, we studied the binding of *Kp*SSB to dT20, dT25, dT30, dT35, dT40, dT45 and dT50 with different protein concentrations using EMSA. As shown in the figure, no significant band shift was observed when *Kp*SSB was incubated with dT20, indicating that *Kp*SSB could not form a stable complex with this homopolymer. Because some smears were observed, it appears that *Kp*SSB interacts with dT20, but it could not form a stable complex with dT20 during electrophoresis. It is considered that dT20 is too short to form a stable complex with *Kp*SSB. In contrast to dT20, longer dT homopolymers, dT25–50, bind to *Kp*SSB and form a single complex. Thus, the EMSA results suggest that the length of ssDNA required for *Kp*SSB binding ranges between 20–25 nt.

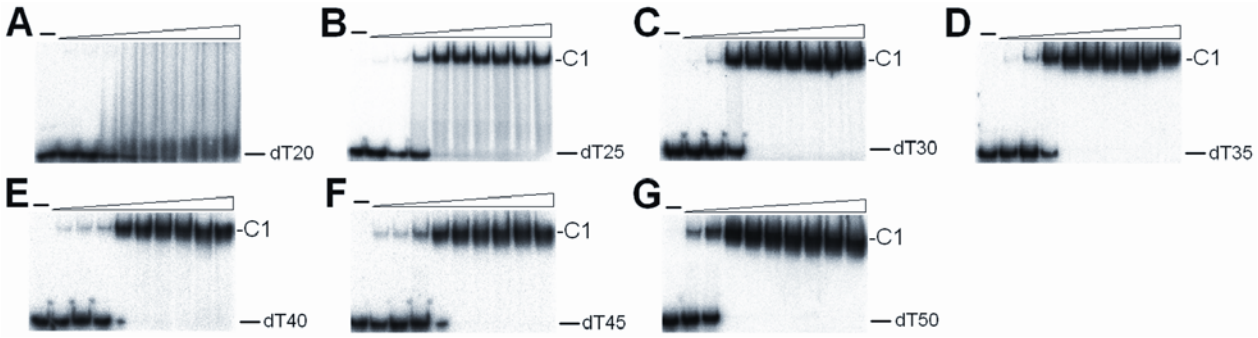

6.5. Two different complexes are formed when KpSSB binds to dT55–75

To examine the minimal nucleotide length necessary for the binding of a second *Kp*SSB tetramer to ssDNA pre-bound to *Kp*SSB, we studied the binding of *Kp*SSB to longer dT homopolymers of 55–75 nt. Although dT55 is only 5 nt longer than dT50, the pattern of the *Kp*SSB-ssDNA complexes observed using EMSA is very different. At lower protein concentrations, *Kp*SSB forms a single complex with dT55, similar to that observed with dT50; however, when the *Kp*SSB concentration is increased, another slower-migrating complex appears. The appearance of the second complex results from the increasing *Kp*SSB concentration, which suggests that it may contain at least 2 *Kp*SSB tetramers per oligonucleotide. As the minimal length of ssDNA required for *Kp*SSB binding ranges between 20–25 nt, the presence of an extra 5 nt in dT55, as compared with dT50, provides enough interaction space for the binding of a second *Kp*SSB tetramer, which occupies around 27 nt ssDNA. Furthermore, the stoichiometry of the 2 *Kp*SSB tetramers bound per ssDNA did not change when the length of the dT homopolymers was further increased to 75 nt. These results from EMSA suggest that the length of ssDNA required for efficient binding of *Kp*SSB is 26 ± 1 nt.

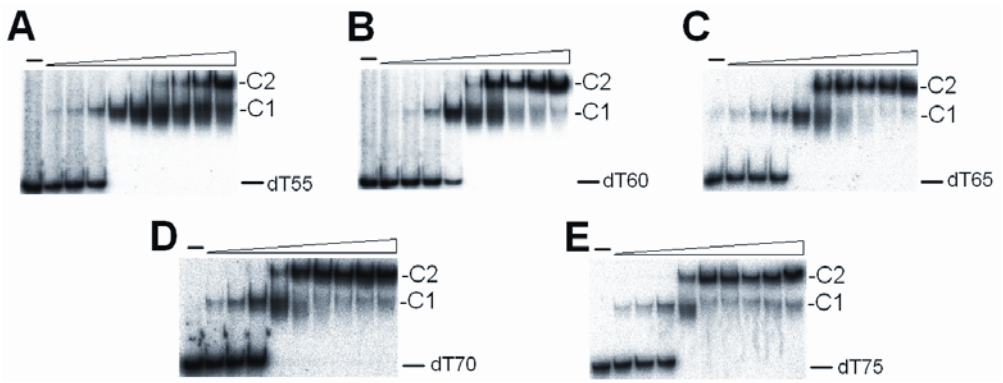

6.6. The binding constants of the KpSSB-ssDNA complexes

The binding constants of the *Kp*SSB-ssDNA complexes (K_d values) are summarized in the table. The formation of the *Kp*SSB-ssDNA complex 1 (C1) is nearly ssDNA-length independent, suggesting that the protein-DNA contact for each C1 is similar. In contrast, the ability of a second *Kp*SSB tetramer (the K_{d2} value) to bind to ssDNA already bound by *Kp*SSB tetramer was length-dependent. In fact, increases in ssDNA length were associated with higher binding ability (lower K_{d2} value), indicating that the second *Kp*SSB prefers to bind to long ssDNA segments to which *Kp*SSB tetramer(s) is already bound.

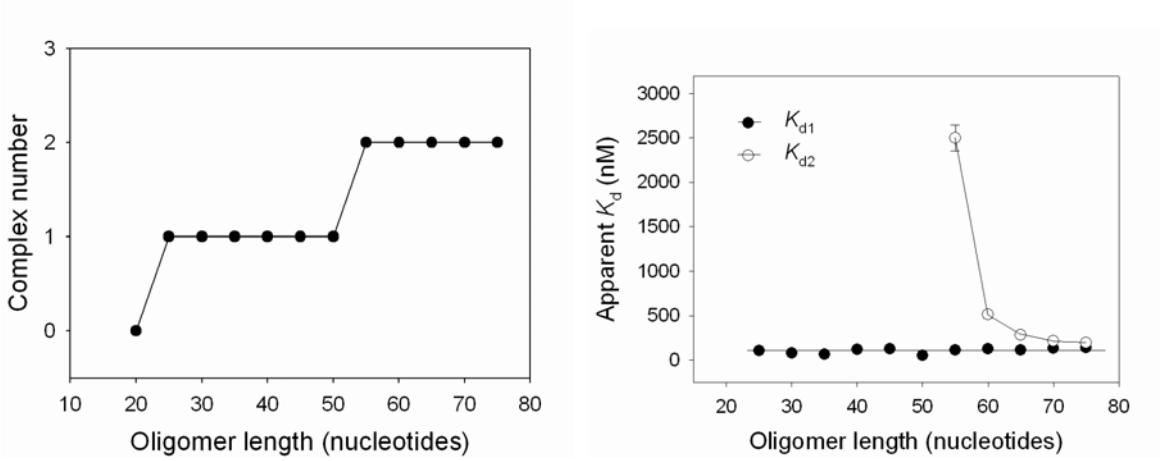

Table 1. ssDNA-binding parameters of *Kp*SSB

	*Kp*SSB	
	K_{d1} (nM)	K_{d2} (nM)
dT20		
dT25	108 ± 8	
dT30	78 ± 10	
dT35	67 ± 6	
dT40	118 ± 15	
dT45	123 ± 10	
dT50	51 ± 7	
dT55	112 ± 12	2500 ± 150
dT60	123 ± 10	513 ± 46
dT65	109 ± 14	282 ± 22
dT70	134 ± 15	214 ± 24
dT75	140 ± 18	196 ± 15

Each K_d is calculated as the average of at least three measurements ± S.D.

6.7. Comparison with other SSBs

In this study, we described the cloning, expression, purification, and characterization of SSB from *K. pneumoniae*, which is a ubiquitous opportunistic pathogen that colonizes at the mucosal surfaces in humans and causes severe diseases. In addition, many clinical strains of *K. pneumoniae* are highly resistant to antibiotics. Sequence analysis indicates that the *Kp*SSB monomer possesses an OB-fold domain at its N-terminus and a flexible tail at its C-terminus, as in *Ec*SSB. Analysis of *Kp*SSB by using gel filtration chromatography showed that the protein forms a tetramer in solution.

We showed that the binding of *Kp*SSB to dT50 results in tryptophan fluorescence quenching. In the presence of 20 and 300 mM NaCl, the binding site sizes of *Kp*SSB were 27 ± 2 nt and 38 ± 2 nt per tetramer, respectively; 2 distinct binding modes could be observed between low- and high-salt conditions, as observed in *Ec*SSB. In the case of *Ec*SSB, under high-salt conditions, a 65-nt ssDNA binds to each *Ec*SSB tetramer with almost 90% fluorescence quench; under low-salt conditions, a 35-nt ssDNA exhibits 53% fluorescence quench. In the case of *Hp*SSB, the stoichiometry was 25 ± 2 nt per homotetramer, but the salt effect on its ssDNA-binding mode(s) remains unclear. Human replication protein A, a eukaryotic SSB, binds to DNA noncooperatively and has a binding site of 20–30 nt per heterotrimer under most conditions. The constant binding mode (or "salt-independent" binding mode) of SSBs determined using fluorescence quench at high- and low-salt concentrations has also been reported in SSBs from the *Thermus/Deinococcus* group, *Thermotoga maritima*, *Thermotoga neapolitana*, *Thermoanaerobacter tengcongensis*, and *Pseudomonas aeruginosa* PAO1, possibly because of its low flexibility and/or low number of glycine residues. In fact, 8 glycine residues in the glycine-rich hinge that are found in *Ec*SSB are not found in *Pa*SSB. The amino acid sequences of *Kp*SSB and *Ec*SSB share >80% identity, suggesting the presence of multiple binding modes, even though 2 glycine residues in the glycine-rich hinge of *Ec*SSB (Gly125 and Gly128) are not found in *Kp*SSB. However, this speculation must be confirmed by further biochemical experiments.

Many SSBs bind to ssDNA with some degree of positive cooperativity. Cooperativity can result from direct protein–protein interactions between the nearest neighbors, such as the LAST motif in the T4 gene-32 protein, and the arginine-mediated interaction motif in *Thermus* SSB. Cooperativity can also result from the protein-induced distortion of adjacent DNA as demonstrated by *Sulfolobus* SSB, PriB, and FOXK1a proteins. In the case of *Kp*SSB, binding appears to be noncooperative, for several DNAs, because essentially all the DNA shifts into the fist complex before the appearance of the second complex. In addition, the apparent K_d values are of the first and second complex, as expected for noncooperative binding; for positive cooperative binding, K_{d2} should be less than K_{d1}. Increasing the length of C2 causes its K_d value to match that of C1, suggesting that length dependence reflects the minimal amount of spacing that is optimal for steric considerations.

The EMSA approach used here allowed us to observe the formation of distinct complexes and to determine the ssDNA binding mode of *Kp*SSB. The EMSA results indicate that *Kp*SSB binds to short ssDNAs (dT25–50) to form a complex in which a single tetramer is bound to the ssDNA, and 2 tetramers are bound to dT55–75. Thus, the apparent binding-site size of *Kp*SSB is

26 ± 1 nt. Recently, we have determined that the binding-site sizes of *Pa*SSB and *St*SSB are 29 ± 1 and 22 ± 1 nt using EMSA, respectively. The amino acid sequence of the N-terminal ssDNA-binding/oligomerization domain in these pathogenic SSBs is highly conserved to each other (>90% identity) suggesting that the C-terminal protein-protein interaction domain may also contribute to ssDNA binding, because of their differences in the binding-site size. We have prepared chimeric proteins for these SSBs in which their C-terminal domains were exchanged to further investigate this hypothesis, and the resulting information may be useful in identifying the DNA binding mode(s) of SSB.

Table 2. Summary of the complex formation of some pathogenic SSBs

		ssDNA length for the complex formation		
Source	The binding site size	Unstable complex	Forming a first complex	Forming a second complex
K. pneumoniae	26 ± 1	dT20	dT25–50	dT55–75
S. typhimurium	22 ± 1	dT15	dT20–40	dT45–60
P. aeruginosa	29 ± 1	dT15–20	dT25–55	dT60–80

(7) Inhibition of DnaB helicase by the flavonols

The purpose of this study was to identify some naturally occurring compounds that can inhibit the activity of bacterial replicative helicase(s). The results presented here show that 4 flavonol compounds may be useful in developing anti-*K. pneumoniae* antibiotics.

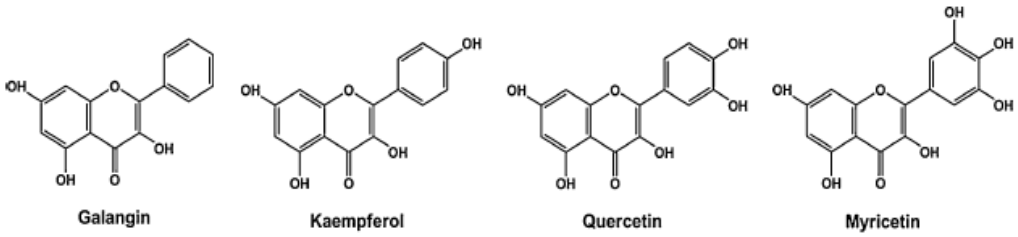

7.1. Fluorescence quenching of KpDnaB by dATP, dTTP, dCTP, or dGTP

The fluorescence emission spectra of *Kp*DnaB quenched with dATP, dTTP, dCTP, and dGTP are shown in the figure. Fluorescence intensity of *Kp*DnaB decreased remarkably with increasing concentrations of dNTP (0–10^{-3} M). At 10^{-3} M, dCTP and dGTP quenched the fluorescence intensity of *Kp*DnaB almost completely, whereas dATP only quenches approximately 80% of the *Kp*DnaB fluorescence intensity. Adding dNTPs resulted in a significant blue shift (~10 nm) of the emission wavelength (λ_{em}) of *Kp*DnaB, indicating an interaction between dNTP and *Kp*DnaB and suggesting formation of a dNTP-*Kp*DnaB complex. The dissociation constant (K_d) values of *Kp*DnaB bound to dATP, dTTP, dCTP, and dGTP determined from the titration curves were 159.8 ± 60, 106.0 ± 30, 60.3 ± 13, and 63.2 ± 16 μM, respectively, meaning that *Kp*DnaB exhibited the strongest binding activity towards dCTP.

7.2. Fluorescence quenching of KpDnaB by flavonols

The fluorescence emission spectra of *Kp*DnaB quenched by Gal, Kae, Que, and Myr are

shown in the figure. Due to the compounds' solubility, 10 μM of each flavonol was used. *Kp*DnaB fluorescence intensity decreased significantly with increasing concentrations of flavonols (0–10 μM). The maximum λ_{em} of these flavonols alone in response to excitation at 280 nm was approximately 520 nm. In addition, these 4 flavonols resulted in a slight blue shift (~1 nm) of the maximum λ_{em} of *Kp*DnaB. Thus, the quenching of *Kp*DnaB fluorescence mainly depended on the formation of a complex between the flavonol and *Kp*DnaB. The titration curves suggest that *Kp*DnaB binds most strongly to Myr, and, in the order of decreasing affinity, to the other flavonols as follows: Myr > Kae > Gal > Que.

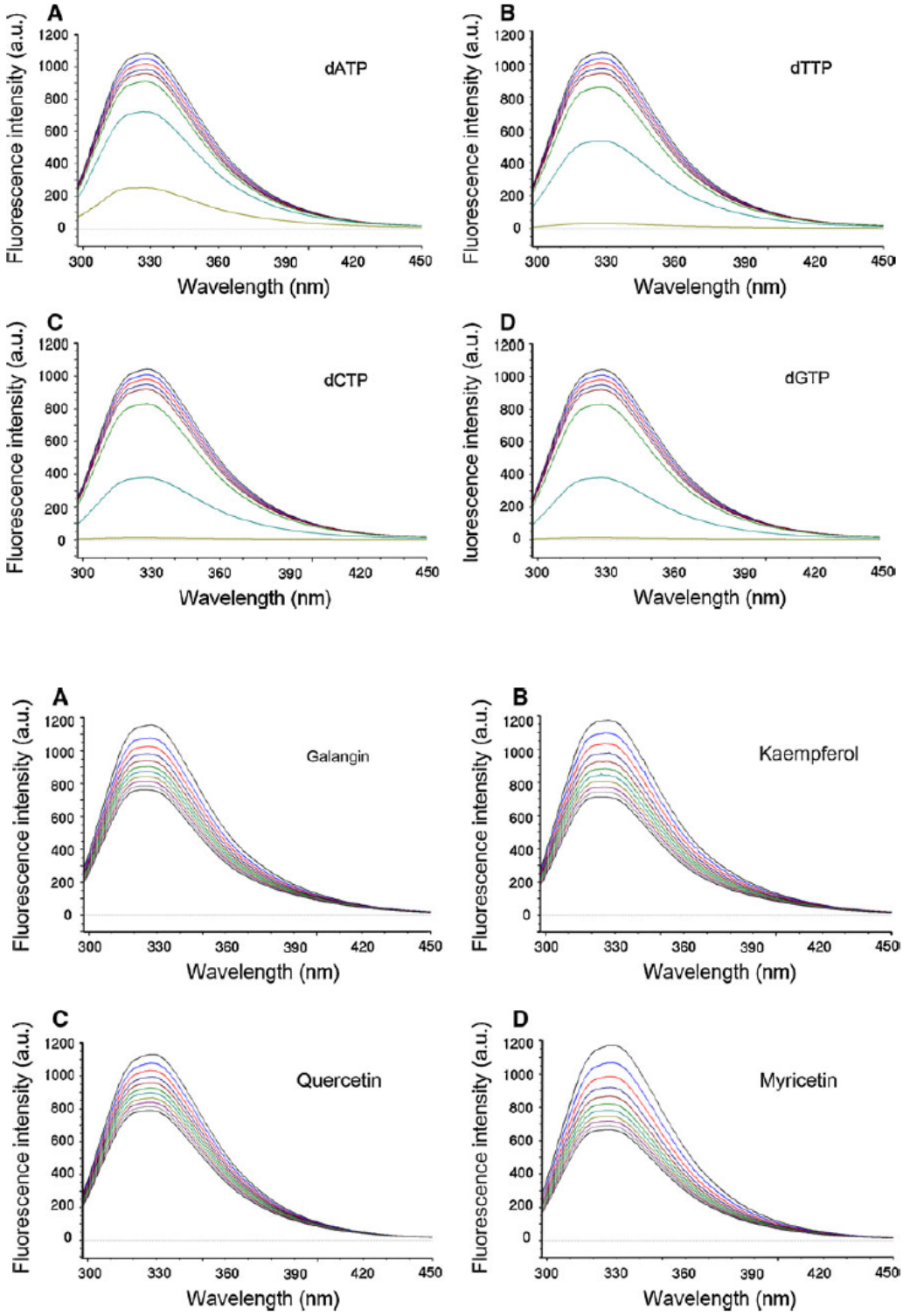

7.3. Fluorescence quenching of KpDnaB by dATP, dTTP, dCTP and dGTP in the presence of Myr, Kae, Gal, or Que

To investigate whether the flavonols can inhibit the binding of *Kp*DnaB to dNTP, we analyzed *Kp*DnaB fluorescence quenching by dATP in the presence of Myr, Kae, Gal, or Que. The interaction of *Kp*DnaB with dATP was much more sensitive to Gal than to Que. Fluorescence quenching of *Kp*DnaB was not obvious until the concentration of dATP increased to 10^{-4} M, indicating that the binding affinity between *Kp*DnaB and dATP was decreased by the presence of Gal, Kae, Que, or Myr in the reaction solution.

To test whether the flavonols inhibit the binding of *Kp*DnaB to other dNTPs, we also analyzed *Kp*DnaB fluorescence quenching by dTTP, dCTP, and dGTP in the presence of Myr, Kae, Gal, or Que. However, the results of these experiments were quite different from those of the experiment with dATP. dTTP, dCTP, and dGTP quenched *Kp*DnaB fluorescence by almost 50% even at 10^{-4} M of the flavonols, suggesting that Myr, Kae, Gal, and Que specifically disrupt the *Kp*DnaB-dATP interaction.

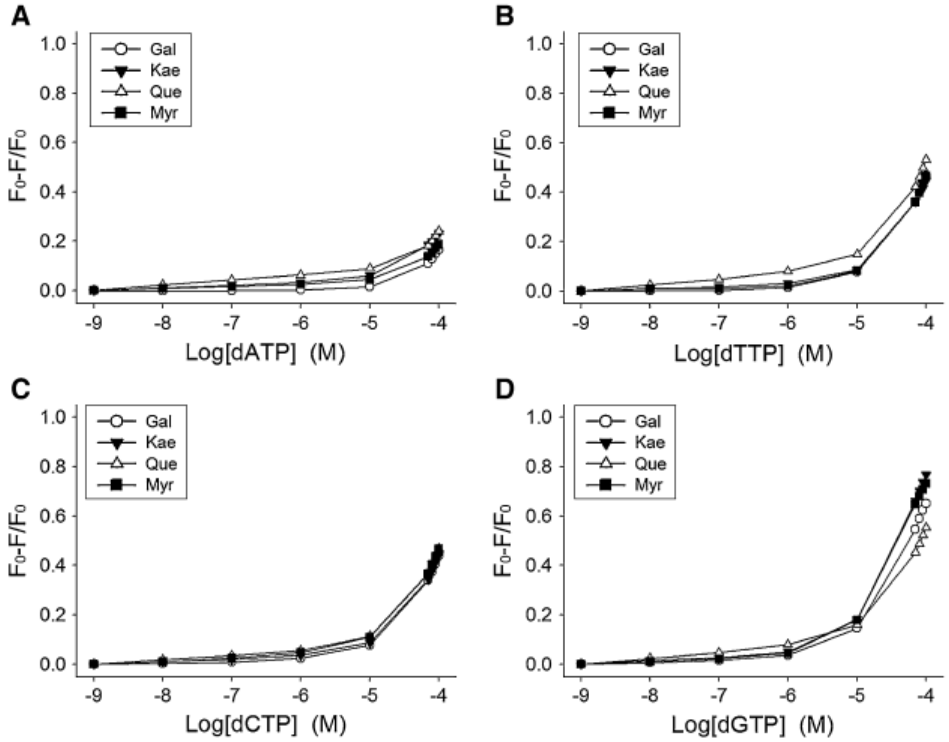

7.4. Inhibition of KpDnaB-dNTP interaction by Gal was the strongest

The figure shows the effects of flavonol on the interaction between *Kp*DnaB and dATP, dTTP, dCTP, or dGTP. *Kp*DnaB-dATP binding was inhibited by flavonoids as follows, in the order of decreasing efficiency: Gal > Myr > Kae > Que. None of the 4 flavonols disrupted dGTP binding to *Kp*DnaB. Among the flavonols, Gal inhibited *Kp*DnaB-dNTP interaction most strongly, although Myr showed the strongest binding to *Kp*DnaB. Thus, the ability of flavonols to inhibit *Kp*DnaB action in general may be dNTP-dependent.

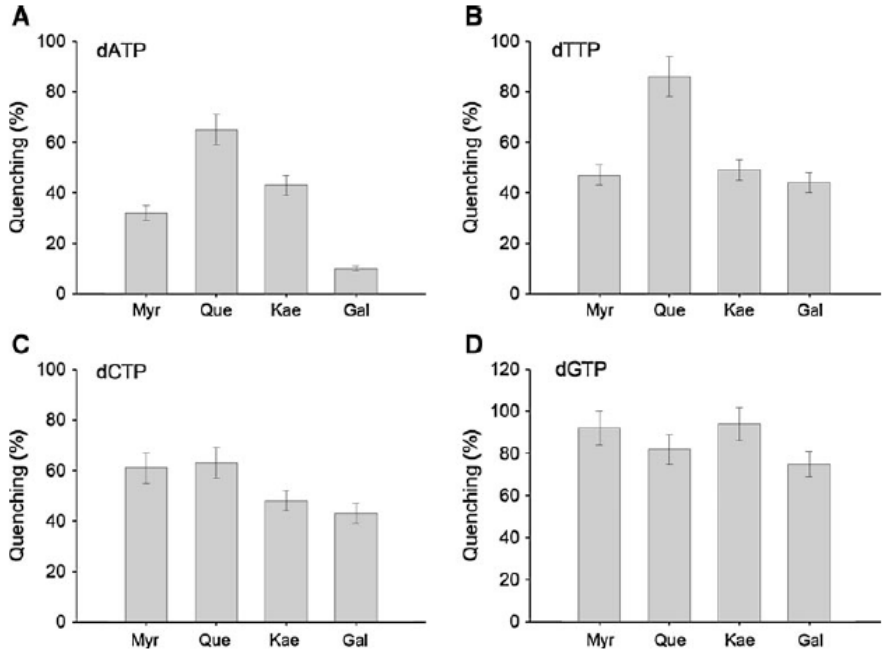

7.5. The flavonoids inhibited growth of K. pneumoniae

To test whether these flavonoids can inhibit growth of *K. pneumoniae*, *K. pneumoniae* cells were grown to 0.5 OD_{600} at 37 °C, and then added 10 μM of Gal, Kae, Que, or Myr into the medium. The figure shows that these 4 flavonoids inhibited growth of *K. pneumoniae*; Gal had a greater inhibitory effect than the others.

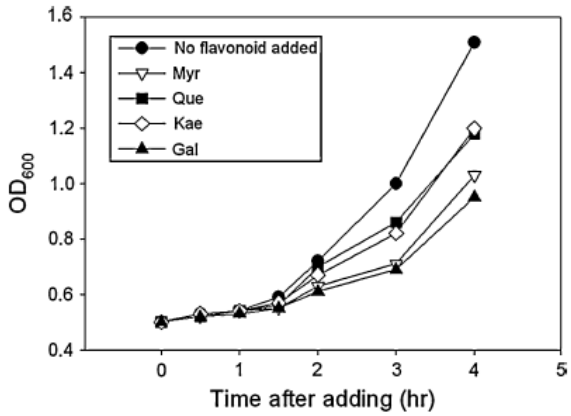

7.6. Inhibitory mechanism of DnaB helicase by the flavonols

DNA replication is one of the most basic biological functions and should be a prime target in antibiotic development. In fact, it is the target of the bactericidal fluoroquinolone class of antibiotics that interferes with DNA gyrase and topoisomerase. Since DNA helicases are important components of the cellular replication machinery in all organisms, inhibition of helicase activity would be detrimental to bacterial survival as well. In this study, we used fluorescence quenching to analyze the interaction of *Kp*DnaB with 4 flavonols, Gal, Kae, Que, and Myr, which contain different numbers of hydroxyl substituent on the aromatic rings. Our results demonstrated that these flavonols were capable of inhibiting the interaction of *Kp*DnaB with dNTPs. The extent of *Kp*DnaB fluorescence quenching induced by dATP in the presence of

a flavonol was much smaller than that of dATP alone, indicating inhibition of *Kp*DnaB-dATP binding by the flavonol. In addition, the inhibition depended not only on the flavonol (with Gal displaying the strongest inhibition), but also on the dNTP used (the inhibition was most specific to dATP binding).

Binding and hydrolysis of NTP cofactors by the DnaB helicase before association with ssDNA are essential processes that induce and modulate a high affinity conformation of the enzyme that can bind to ssDNA. Although the primary replicative helicase can hydrolyze all NTPs, our studies indicate that *Kp*DnaB has a preference for dCTP over other nucleotides. Thus, other compounds similar to dCTP may be useful in inhibiting *Kp*DnaB.

Other studies have shown that Myr non-competitively inhibits *E. coli* DnaB helicase and RSF1010 RepA helicase, with IC_{50} of approximately 10 and 50 μM, respectively. In this study, we found that 10 μM of Gal, Kae, Que, or Myr can inhibit dNTP binding to *Kp*DnaB. Although it is well established that flavonoids have several hydroxyl groups and thus have marked potentials to bind (any) proteins, the strength of the inhibition in dNTP binding of *Kp*DnaB was not correlated with the number of hydroxyl substituent on the aromatic rings of the flavonols.

Although Myr binds to *Kp*DnaB with the highest affinity among the flavonols, it did not display the highest inhibition of dNTP-*Kp*DnaB binding. Based on these results, we propose that these flavonols may inhibit dNTP binding to *Kp*DnaB in 2 possible ways. First, these 4 flavonols may not bind to the active site of *Kp*DnaB, or only partially occupy the active site. Second, since DnaB helicase binding to dNTP causes a large conformational change, these flavonols may inhibit the conformational change itself, thereby causing varying degree of inhibition. The inhibition of *Kp*DnaB by these flavonols appeared to be dNTP-dependent, and, thus, neither of these possibilities can be dismissed.

Our crystal structure of *Geobacillus kaustophilus* helicase in complex with ssDNA and the non-hydrolysable NTP analogue ATPγs revealed that ATP hydrolysis may drive the movement of the helicase toward the 3′ end of the lagging strand. In addition, the dNTP-binding site of the helicase at loop I, part of the Walker B motif, is adjacent to the DNA interaction site. From these results, we speculate here that 1 flavonol molecule is enough to bind to the empty active sites of 6 *Kp*DnaB subunits to shut down and lock the enzyme in the dNTP-unbound state. We have prepared a crystal of *Kp*DnaB in complex with Gal to further investigate this hypothesis, and the resulting information may be useful in designing compounds that fit more precisely into helicase active sites.

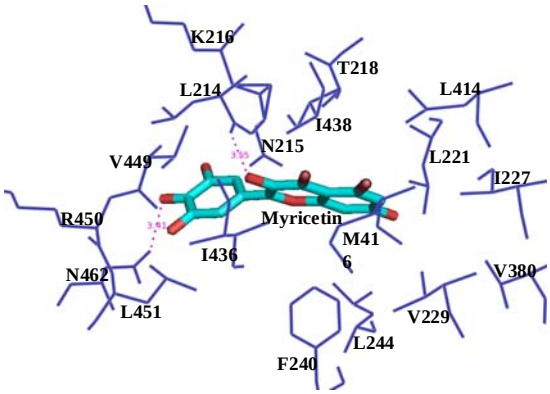

3b. 分析與討論

We have expressed and purified these eight recombinant primosomal proteins with high yield, and carried out the experiments as planned, describing into seven parts as following: (1) Gene cloning, expression, and purification of these primosomal proteins. (2) The analyses of ssDNA binding modes of PriB and SSB. (3) PriB and DnaT protein crystals are obtained. (4) Crystal structure of PriB has been solved to 2.07 Å by synchrotron radiation X-ray source at Beamline 13C1 of NSRRC. (5) The flavonols are found to inhibit the activity of DnaB. (6) Analyses of interactions of PriB with the primosomal proteins. (7) Crystal of DnaB in complex with the inhibitor galangin.

Since the flavonol compounds were found to inhibit the binding activity of DnaB to dNTP, we will combine this knowledge with DnaB structure to do molecular docking. In addition, we also found that these small compounds possessing anti-DNA binding and anti-ATPase activities on the DnaB's action. This information may provide a molecular insight into how the inhibitor can be modified as a "better" drug.

3c. 所遭遇之困難與因應對策

The most commonly difficult experiment for this project is to get "good" protein crystals for X-ray diffraction. We have obtained several crystals such as PriB and DnaT crystals for their structure determinations, but other primosomal proteins' crystals are still needed to be produced. We will conduct mutated version of these proteins with lower flexibility (e.g. loop(s)-deletion forms) or co-crystallize these proteins with some additives. More and more proteins will be produced for high-throughput screening of crystallization trials.

四、成果自評

4a. 研究成果與原設定目標之相符程度
4b. 達成預期目標情形

We have expressed and purified these recombinant primosomal proteins with high yield, solved some structures, and discovered some inhibitors for the DnaB action. These results are highly correlated with the original goals of the project. Some results of the current project are, however, not significant for the drug development. For example, inhibition of the DnaB helicase by the natural product flavonols is only in μM scale. We will continue the optimization of the inhibitor(s) for these proteins.

4c. 研究成果之學術或應用價值
4d. 學術期刊發表情形

1. Huang, Y.H., Huang, W., Lee, Y.L., **Huang, C.Y.*** (2011) Role of the conserved N- and C-terminal regions of PriB, a primosomal DNA replication protein. ***Genes Cells***, In revision. (SCI)
2. Huang, Y.H., Lee, Y.L., **Huang, C.Y.*** (2011) Characterization of a single-stranded DNA binding protein from *Salmonella enterica* serovar Typhimurium LT2. ***Protein J.***, 30, 102-108. (SCI)
3. Hsieh, H.C., **Huang, C.Y.*** (2011) Identification of a novel protein, PriB, in *Klebsiella pneumoniae*. ***Biochem. Biophys. Res. Commun.***, 404, 546-551. (SCI)
4. Chen, C.C., **Huang, C.Y.*** (2011) Inhibition of *Klebsiella pneumoniae* DnaB helicase by the flavonol galangin. ***Protein J.***, 30, 59-65. (SCI)
5. Jan, H.C., Lee, Y.L., **Huang, C.Y.*** (2011) Characterization of a single-stranded DNA-binding protein from *Pseudomonas aeruginosa* PAO1. ***Protein J.***, 30, 20-26. (SCI)

五、參考文獻

1. Reyes-Lamothe, R., Sherratt, D. J., and Leake, M. C. (2010) *Science* **328**, 498-501
2. Masai, H., Tanaka, T., and Kohda, D. (2010) *Bioessays* **32**, 687-697
3. Gabbai, C. B., and Marians, K. J. (2010) *DNA Repair (Amst)* **9**, 202-209
4. Heller, R. C., and Marians, K. J. (2006) *Nat Rev Mol Cell Biol* **7**, 932-943
5. Lo, Y. H., Tsai, K. L., Sun, Y. J., Chen, W. T., Huang, C. Y., and Hsiao, C. D. (2009) *Nucleic Acids Res* **37**, 804-814
6. Wang, G., Klein, M. G., Tokonzaba, E., Zhang, Y., Holden, L. G., and Chen, X. S. (2008) *Nat Struct Mol Biol* **15**, 94-100
7. Bailey, S., Eliason, W. K., and Steitz, T. A. (2007) *Science* **318**, 459-463
8. Benkovic, S. J., Valentine, A. M., and Salinas, F. (2001) *Annu Rev Biochem* **70**, 181-208
9. Singleton, M. R., Dillingham, M. S., and Wigley, D. B. (2007) *Annu Rev Biochem* **76**, 23-50
10. Cox, M. M., Goodman, M. F., Kreuzer, K. N., Sherratt, D. J., Sandler, S. J., and Marians, K. J. (2000) *Nature* **404**, 37-41
11. McGlynn, P., and Lloyd, R. G. (2002) *Nat Rev Mol Cell Biol* **3**, 859-870
12. Tanaka, T., Mizukoshi, T., Sasaki, K., Kohda, D., and Masai, H. (2007) *J Biol Chem* **282**, 19917-19927
13. Nurse, P., Liu, J., and Marians, K. J. (1999) *J Biol Chem* **274**, 25026-25032
14. Liu, J., and Marians, K. J. (1999) *J Biol Chem* **274**, 25033-25041
15. Sandler, S. J., and Marians, K. J. (2000) *J Bacteriol* **182**, 9-13
16. Lee, E. H., and Kornberg, A. (1991) *Proc Natl Acad Sci U S A* **88**, 3029-3032
17. Masai, H., Asai, T., Kubota, Y., Arai, K., and Kogoma, T. (1994) *EMBO J* **13**, 5338-5345
18. Podschun, R., and Ullmann, U. (1998) *Clin Microbiol Rev* **11**, 589-603
19. Yu, W. L., Chuang, Y. C., and Walther-Rasmussen, J. (2006) *J Microbiol Immunol Infect* **39**, 264-277
20. Bush, K., and Macielag, M. J. (2010) *Expert Opin Ther Pat* **20**, 1277-1293
21. Bush, K. (2010) *Curr Opin Microbiol* **13**, 558-564
22. Kumarasamy, K. K., Toleman, M. A., Walsh, T. R., Bagaria, J., Butt, F., Balakrishnan, R., Chaudhary, U., Doumith, M., Giske, C. G., Irfan, S., Krishnan, P., Kumar, A. V., Maharjan, S., Mushtaq, S., Noorie, T., Paterson, D. L., Pearson, A., Perry, C., Pike, R., Rao, B., Ray, U., Sarma, J. B., Sharma, M., Sheridan, E., Thirunarayan, M. A., Turton, J., Upadhyay, S., Warner, M., Welfare, W., Livermore, D. M., and Woodford, N. (2010) *Lancet Infect Dis* **10**, 597-602
23. Chen, L., Yang, J., Yu, J., Yao, Z., Sun, L., Shen, Y., and Jin, Q. (2005) *Nucleic Acids Res* **33**, D325-328
24. Zhou, C. E., Smith, J., Lam, M., Zemla, A., Dyer, M. D., and Slezak, T. (2007) *Nucleic Acids Res* **35**, D391-394
25. Wu, H. J., Wang, A. H., and Jennings, M. P. (2008) *Curr Opin Chem Biol* **12**, 93-101
26. Yang, J., Chen, L., Sun, L., Yu, J., and Jin, Q. (2008) *Nucleic Acids Res* **36**, D539-542

27. Sasaki, K., Ose, T., Okamoto, N., Maenaka, K., Tanaka, T., Masai, H., Saito, M., Shirai, T., and Kohda, D. (2007) *EMBO J* **26**, 2584-2593
28. Liu, J. H., Chang, T. W., Huang, C. Y., Chen, S. U., Wu, H. N., Chang, M. C., and Hsiao, C. D. (2004) *J Biol Chem* **279**, 50465-50471
29. Huang, C. Y., Hsu, C. H., Sun, Y. J., Wu, H. N., and Hsiao, C. D. (2006) *Nucleic Acids Res* **34**, 3878-3886
30. Keck, J. L., Roche, D. D., Lynch, A. S., and Berger, J. M. (2000) *Science* **287**, 2482-2486
31. Hsieh, H. C., and Huang, C. Y. (2011) *Biochem Biophys Res Commun* **404**, 546-551
32. Chen, C. C., and Huang, C. Y. (2011) *Protein J*
33. Wang, C. C., Tsau, H. W., Chen, W. T., and Huang, C. Y. (2010) *Protein J* **29**, 445-452
34. Terwilliger, T. C., and Berendzen, J. (1999) *Acta Crystallogr D Biol Crystallogr* **55**, 849-861
35. Clardy, J., Fischbach, M. A., and Walsh, C. T. (2006) *Nat Biotechnol* **24**, 1541-1550
36. Griep, M. A., Blood, S., Larson, M. A., Koepsell, S. A., and Hinrichs, S. H. (2007) *Bioorg Med Chem* **15**, 7203-7208

六、附件

學術論文

Biochemical and Biophysical Research Communications 404 (2011) 546–551

Contents lists available at ScienceDirect

Biochemical and Biophysical Research Communications

journal homepage: www.elsevier.com/locate/ybbrc

Identification of a novel protein, PriB, in *Klebsiella pneumoniae*

Hui-Chuan Hsieh [a], Cheng-Yang Huang [a,b,*]

[a] Department of Biomedical Sciences, Chung Shan Medical University, No. 110, Sec. 1, Chien-Kuo N. Rd., Taichung City, Taiwan
[b] Department of Medical Research, Chung Shan Medical University Hospital, No. 110, Sec. 1, Chien-Kuo N. Rd., Taichung City, Taiwan

ARTICLE INFO

Article history:
Received 2 December 2010
Available online 6 December 2010

Keywords:
PriB
PriA
Primosome
ssDNA binding
SSB

ABSTRACT

PriB is a primosomal protein required for the reinitiation of replication in bacteria. Here, we report the identification and characterization of a novel PriB protein in *Klebsiella pneumoniae* (KPN_04595; *Kp*PriB). Unlike the well-studied *Escherichia coli* PriB protein (*Ec*PriB), which exists as a homodimer comprising 104-aa polypeptides, *Kp*PriB forms a monomer of only 55 aa, due to the absence of the 49 aa N-terminus in *Kp*PriB. Although this N-terminal region (1–49 aa) in *Ec*PriB contains several important residues, such as K18, R34, and W47, which are crucial for ssDNA binding, we found that *Kp*PriB binds ssDNA, but not ssRNA, with comparable affinity as that for *Ec*PriB. Results from filter-binding assays demonstrate that the *Kp*PriB–ssDNA interaction is cooperative and salt-sensitive. Substituting the residue K33 in *Kp*PriB with alanine, the position corresponding to the classic ssDNA-binding residue K82 of *Ec*PriB located in loop L_{45}, significantly reduced ssDNA-binding activity and cooperativity. These results reveal that the 1–49 aa region of the classical PriB protein is unnecessary for ssDNA binding. On the basis of these findings, the structure–function relationships of *Kp*PriB are discussed.

© 2010 Elsevier Inc. All rights reserved.

1. Introduction

The ability to reinitiate replication after DNA damage is essential for bacterial survival [1,2]. The replication restart primosome is a multi-protein complex that reactivates stalled DNA replication at the forks after DNA damage [3–5]. In *Escherichia coli*, the primosome includes 7 essential proteins (PriA, PriB, PriC, DnaB, DnaC, DnaT, and DnaG). There are 2 overlapping mechanisms for reassembly of the replication forks; initiation is induced by either PriA helicase or PriC [6–8]. In the PriA-directed pathway, PriB is the second protein to be assembled in the protein–DNA complex [9], where it then stimulates PriA helicase activity [10]. PriB also stabilizes the binding of PriA to DNA hairpins and therefore facilitates the association of DnaT with the primosome [11]. In an ATP- and DnaC-dependent manner, DnaB helicase is then loaded onto the complex and forms the complete primosome upon binding with DnaG primase [12–14]. Recruitment of DnaB helicase to the DNA results in reactivation of the repaired replication forks, allowing bidirectional DNA synthesis to resume.

PriB exists as a homodimer [15–18] with 104-aa polypeptide chains. The PriB monomer has an oligonucleotide/oligosaccharide binding (OB)-fold structure [19,20], and it can bind both ssDNA and ssRNA [18]. The DNA-binding site of PriB is located in loop L_{45} centrally within the dimer [21], and this site occupies 12 ± 1 nt of the total site-size [22]. Furthermore, PriB shares structural similarity with the DNA-binding domain of *E. coli* ssDNA-binding protein (*Ec*SSB) [16–18,23,24], but they differ in their ssDNA-binding modes [21,22].

While significant progress has been made in understanding the structure and function of *Ec*PriB, study of these proteins in other bacterial species is limited. Many prokaryotic genomes do not contain the full component of the primosome genes [15]. In addition, several PriBs, such as *Kp*PriB, *Pc*PriB, and *Yr*PriB from *Klebsiella pneumoniae*, *Pectobacterium carotovorum* (*Pc*), *Yersinia ruckeri* (*Yr*), and *Salmonella enterica* (*Se*) are shorter in length than *Ec*PriB, specifically lacking the N-terminal 1–49 aa fragment present in *Ec*PriB (Fig. 1A). This N-terminal region in *Ec*PriB contains several important residues for binding to other primosomal proteins and ssDNA, and for dimerization [9,15]. Therefore, the PriBs lacking such a region must have mechanisms for primosome assembly that are distinct from that of *Ec*PriB.

Previously, we described the crystal structures of *Ec*PriB [18] and its complex with ssDNA [21]. Here, we aimed to determine whether the shorter 55-aa PriB polypeptides bind ssDNA and dimerize. In order to do so, *KPN_04595*, the gene encoding a putative PriB from *K. pneumoniae* was cloned and expressed, and its

Abbreviations: ssDNA, single-stranded DNA; SSB, single-stranded DNA-binding protein; EMSA, electrophoretic mobility shift analysis; nt, nucleotides; aa, amino acids; K_d, the apparent dissociation constant; OB, oligonucleotide/oligosaccharide binding; *Ec*SSB, *E. coli* ssDNA-binding protein.

* Corresponding author at: Department of Biomedical Sciences, Chung Shan Medical University, No. 110, Sec. 1, Chien-Kuo N. Rd., Taichung City, Taiwan. Fax: +886 4 23248187.

E-mail address: cyhuang@csmu.edu.tw (C.-Y. Huang).

0006-291X/$ - see front matter © 2010 Elsevier Inc. All rights reserved.
doi:10.1016/j.bbrc.2010.12.023

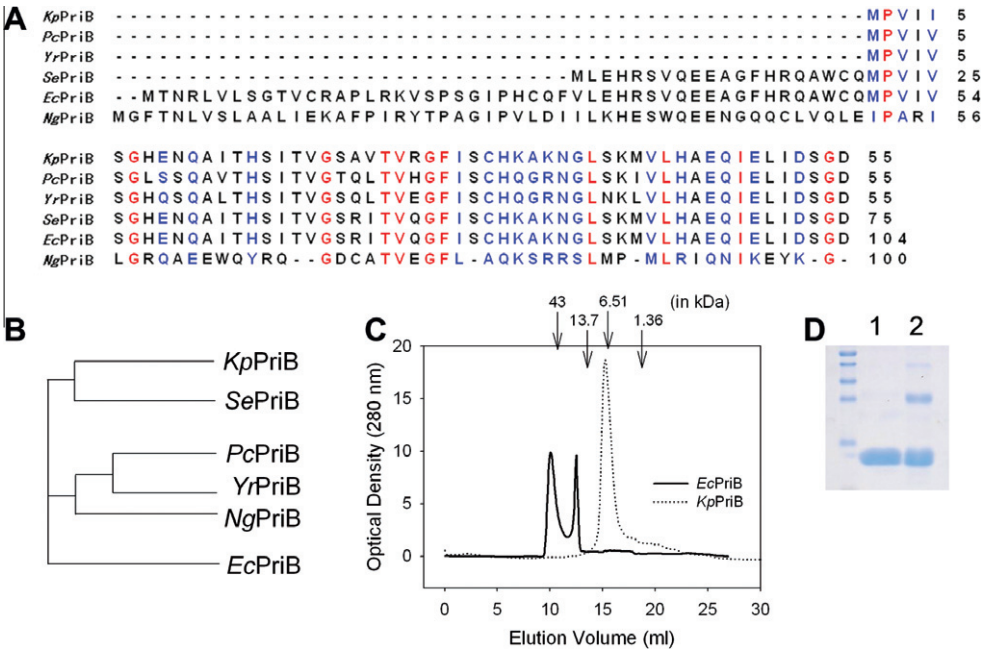

Fig. 1. (A) Multiple amino acid sequence alignment of PriB from *K. pneumoniae* (*Kp*), *P. carotovorum* (*Pc*), *Y. ruckeri* (*Yr*), *S. enterica* (*Se*), *E. coli* (*Ec*), and *Neisseria gonorrhoeae* (*Ng*). Alignment was carried out using CLUSTALW2. Amino acid residues displaying 100% homology are highlighted in red, and those displaying similarity are highlighted in blue. (B) The evolutionary tree of these PriB proteins was generated by CLUSTALW2. (C) Gel-filtration chromatographic analysis of *Kp*PriB and *Ec*PriB is shown. Two peaks are found for *Ec*PriB at 10 mg/ml, whereas only a single peak is found for *Kp*PriB under the same conditions. (D) Analysis of the subunit structure of *Kp*PriB (20 μM) assessed by glutaraldehyde (1%) chemical cross-linking in the absence (lane 1) and presence of 5 μM dT30 (lane 2). Retarded species have mobilities consistent with the formation of cross-linked dimers (~15 kDa) and tetramers of *Kp*PriB (~30 kDa). The sizes of the standard proteins, from the top down, are as follows: 40, 35, 25, 15, and 10 kDa. (For interpretation of the references to colour in this figure legend, the reader is referred to the web version of this article.)

gene product was purified and biophysically characterized. Site-directed mutagenesis of the putative DNA-binding residue of *Kp*PriB was also performed, and the structure–function relationship of this novel PriB was elucidated.

2. Materials and methods

2.1. Materials

All restriction enzymes and DNA-modifying enzymes were purchased from New England Biolabs (Ipswich, MA, USA) unless explicitly stated otherwise. All chemicals were purchased from Sigma–Aldrich (St. Louis, MO, USA) unless explicitly stated otherwise. The *E. coli* strains TOP10F′ (Invitrogen, USA) and BL21(DE3)pLysS (Novagen, UK) were used for genetic construction and protein expression, respectively.

2.2. Construction of the KpPriB expression plasmid

KPN_04595, the gene encoding the putative *Kp*PriB, was PCR-amplified using genomic DNA of *K. pneumoniae* subsp. *pneumoniae* MGH 78578 as the template. The forward (5′-GCCGCGAATTCCC CGTTATTATTAGCG-3′) and reverse (5′-GCGGCAAGCTTGTCTCCAGA ATCTATC-3′) primers were designed to introduce unique *Eco*RI and *Hind*III restriction sites (underlined) into *Kp*PriB, permitting the insertion of the amplified gene into the pET21e vector. The pET21e vector was engineered from the pET21b vector (Novagen Inc., Madison, WI, USA), to avoid having the N-terminal T7 tag fused with the gene product [25]. Therefore, the expected gene product expressed by pET21e–*Kp*PriB will have 2 additional artificial residues, EF, introduced by the *Eco*RI site located at the N-terminus, and a C-terminal His tag (KLAAALEHHHHHH), useful for purifying the recombinant protein.

2.3. Site-directed mutagenesis

The *Kp*PriB K33A mutant was generated according to the QuikChange Site-Directed Mutagenesis kit protocol (Stratagene; LaJolla, CA, USA), by using the forward (5′-GGTTCATCTCTTGCCATGC GGCAAAGAACGGCTTGAGC-3′) and the reverse (5′-TGCTCAAGCCGT TCTTTGCCGCATGGCAAGAGATGAACC-3′) primers, and the wild-type plasmid pET21e–*Kp*PriB as a template. The presence of the mutation was verified by DNA sequencing.

2.4. Protein expression and purification

Recombinant wild-type and mutant *Kp*PriB proteins were expressed and purified using the same protocol as described previously for *Ec*PriB [18]. Briefly, *E. coli* cells were transformed with the wild-type or mutant pET21e–*Kp*PriB plasmids and grown to 0.9 OD_{600} at 37 °C in Luria–Bertani medium containing 250 μg/ml ampicillin with rapid shaking. Overexpression of the *Kp*PriB constructs was induced by incubating with 1 mM isopropyl thiogalactoside (IPTG) for 3 h at 37 °C. The cells overexpressing the protein were chilled on ice, harvested by centrifugation, resuspended in Buffer A (20 mM Tris–HCl, 5 mM imidazole, 0.5 M NaCl; pH 7.9) and disrupted by sonication with ice cooling between pulses. The wild-type and mutant *Kp*PriB proteins were purified from the soluble supernatant by Ni^{2+}-affinity chromatography (HiTrap HP; GE Healthcare Bio-Sciences, Piscataway, NJ, USA).

2.5. Gel filtration

Gel-filtration chromatography was carried out by using an AKTA-FPLC system [26]. Briefly, purified *Kp*PriB (10 mg/ml) and *Ec*PriB (10 mg/ml) in buffer (0.1 M NaCl and 20 mM Tris–HCl at pH 7.9) was applied to a Superdex 75 10/300 GL column (GE

Healthcare Bio-Sciences, Piscataway, NJ, USA) equilibrated with the same buffer. The column was operated at a flow rate of 0.5 mL/min, and 0.5-mL fractions were collected. The protein was detected by measuring absorbance at 280 nm. The column was calibrated with samples of known molecular masses: BSA (67 kDa), ovalbumin (43 kDa), ribonuclease A (13.7 kDa), aprotinin (6.512 kDa), and vitamin B_{12} (1.355 kDa) (GE Healthcare Bio-Sciences, Piscataway, NJ, USA).

2.6. Gel shifts

Various lengths of ssDNA oligonucleotides were custom synthesized by MdBio, Inc., Frederick, MD. RNA oligonucleotides (U30 and A30) were obtained from Dharmacon, Inc., Lafayette, CO (Thermo Fisher Scientific). Radiolabeling was carried out with [γ^{32}P]ATP (6000 Ci/mmol; PerkinElmer Life Sciences) and T4 polynucleotide kinase (Promega, Madison, WI, USA). *Kp*PriB (0, 0.2, 0.4, 0.8, 1.6, 3.2, 6.4, 12.5, 25, and 50 μM) were incubated for 30 min at 25 °C with 1.7 nM DNA or RNA substrates (dT5–60, dA30, dC30, rA30, and rU30) in a total volume of 10 μL in 20 mM Tris–HCl pH 8.0 and 100 mM NaCl. Aliquots (5 μL) were removed from each reaction solution and added to 2 μL of gel-loading solution (0.25% bromophenol blue and 40% sucrose). The resulting samples were resolved on a native 8% polyacrylamide gel at 4 °C in TBE buffer (89 mM Tris borate and 1 mM EDTA) for 1 h at 100 V and visualized by autoradiography. Complexed and free DNA or RNA bands were scanned and quantified.

2.7. Filter binding assay

The affinity of *Kp*PriB for ssDNA was examined by a double-filter binding assay using the same protocol as described previously for *Ec*PriB [21,27]. Briefly, ssDNA–*Kp*PriB complexes were generated by incubating 1 nM of ^{32}P-labeled oligonucleotide with various concentrations of *Kp*PriB (10^{-5}–10^{-9} M) for 30 min at 25 °C in binding buffer containing 50 mM Hepes, pH 7.0, and 40 μg/ml BSA. The reaction mixture, in a total volume of 50 μL, was filtered though a nitrocellulose membrane overlaid on a Hybond N+ nylon membrane (GE Healthcare Bio-Sciences, Piscataway, NJ, USA). The membranes have been pre-soaked for 10 min in a washing buffer containing 50 mM Hepes, pH 7.0, and 10 mM NaCl, before being framed into a dot-blotting apparatus. The slots were washed immediately with 100 μL of washing buffer before and after the sample filtering step. The radioactivity on both filters was quantified with a PhosphorImager (Molecular Dynamics), and the fraction of bound ssDNA was estimated.

2.8. Data analysis

Apparent dissociation constants were determined by plotting the fraction of ssDNA bound at each protein concentration and then fitting the data to the following equation: $\theta = [P]/([P] + K_d)$, in which θ is the fraction of ssDNA bound, [P] is the concentration of total protein, and K_d is the apparent dissociation constant. Cooperative binding to ssDNA sites was assessed by plotting the fraction of ssDNA bound over a range of protein concentrations, and the binding data were analyzed by fitting the data to the following equation: $\log(\theta/(1-\theta)) = h \log[P] - h \log K_d$, where h is the Hill coefficient [21,28].

2.9. Glutaraldehyde cross-linking

*Kp*PriB (20 μM) was incubated in the presence or absence of 5 μM dT30 for 10 min, and then added 1% glutaraldehyde for a further 2 min. The reaction was quenched by the addition of 1 M Tris (pH 8.0), and the cross-linked protein solutions were then analyzed after SDS–PAGE (15%).

3. Results and discussion

3.1. Sequence analysis

The gene *KPN_04595* encoding the putative *Kp*PriB is described in the NCBI database. Based on the known nucleotide sequence, the predicted *Kp*PriB monomer protein has a length of 55 aa and a molecular mass of 7 kDa. This differs from the well-studied 104-aa *Ec*PriB protein. Analysis of the primary structure of *Kp*PriB by RPS-BLAST [29] revealed the presence of an RPA OB fold-like domain. Fig. 1A shows alignment of the amino acid sequences of *K. pneumoniae*, *P. carotovorum* (*Pc*), *Y. ruckeri* (*Yr*), *S. enterica* (*Se*), *E. coli*, and *Neisseria gonorrhoeae* (*Ng*) PriB. The primary structures of these PriBs are similar; however, *Kp*PriB, *Pc*PriB, *Yr*PriB, and *Se*PriB are shorter in length than *Ec*PriB and *Ng*PriB. Specifically, the N-terminal 1–49 aa region of *Ec*PriB is absent in *Kp*PriB. This region in *Ec*PriB contains several important residues crucial for ssDNA binding, such as K18, R34, and W47 [17,21]. In addition, the W47 residue of *Ec*PriB has been proven to stimulate PriA helicase [10]. These residues, conserved in most PriB families [15], are not found in *Kp*PriB, *Pc*PriB, and *Yr*PriB, due to their truncated gene products. The evolutionary tree for these PriBs is shown: they could be classified into at least 3 groups (Fig. 1B).

3.2. Oligomerization of KpPriB in solution

To determine whether the length of the gene product affects its oligomerization state, we analyzed *Kp*PriB and *Ec*PriB by gel filtration chromatography. As shown in Fig. 1C, *Ec*PriB exists as a dimer and a tetramer (solid line) [16]. However, analysis of purified *Kp*PriB by gel filtration chromatography revealed a single peak (dotted line). Assuming that *Kp*PriB has a structure and partial specific volume similar to the standard proteins, the native molecular mass of *Kp*PriB was estimated to be ~7 kDa. Thus, the single peak suggests that *Kp*PriB, unlike *Ec*PriB, is a stable monomer.

To assess whether *Kp*PriB forms dimer or oligomer in the presence of ssDNA, we incubated the protein with glutaraldehyde in order to cross-link lysine residues in the presence and absence of dT30. As shown in Fig. 1D, addition of dT30 resulted in a significant increase in the amount of cross-linked species, which may correspond to the presence of dimers (~15 kDa) and tetramers (~30 kDa) of *Kp*PriB. Taken together with the gel filtration data (Fig. 1C), these studies suggest that *Kp*PriB is a monomer in solution, and that oligomers (mainly dimers) are formed, only in the presence of ssDNA.

3.3. KpPriB binds ssDNA

To assess whether *Kp*PriB binds ssDNA, we assessed binding of *Kp*PriB to dT20 (Fig. 2A), dT25 (Fig. 2B), dT30 (Fig. 2C), dT35 (Fig. 2D), dT40 (Fig. 2E), dT45 (Fig. 2F), dT50 (Fig. 2G), dT55 (Fig. 2H), and dT60 (Fig. 2I) with different protein concentrations using EMSA. As shown in Fig. 2A, no significant band shift was observed when *Kp*PriB was incubated with dT20, indicating that *Kp*PriB could not form a stable complex with dT20 during electrophoresis. In contrast to dT20, the longer dT homopolymers bind to *Kp*PriB, forming a single complex (Fig. 2B–I). These interactions appear to be highly cooperative since only 1 complex of *Kp*PriB molecules bound per ssDNA is visible when the length of the dT homopolymers is further increased to 60 nt; there is no other distinctive complex or intermediate form. Thus, the shorter *Kp*PriB can bind ssDNA, and the length of ssDNA required for forming a

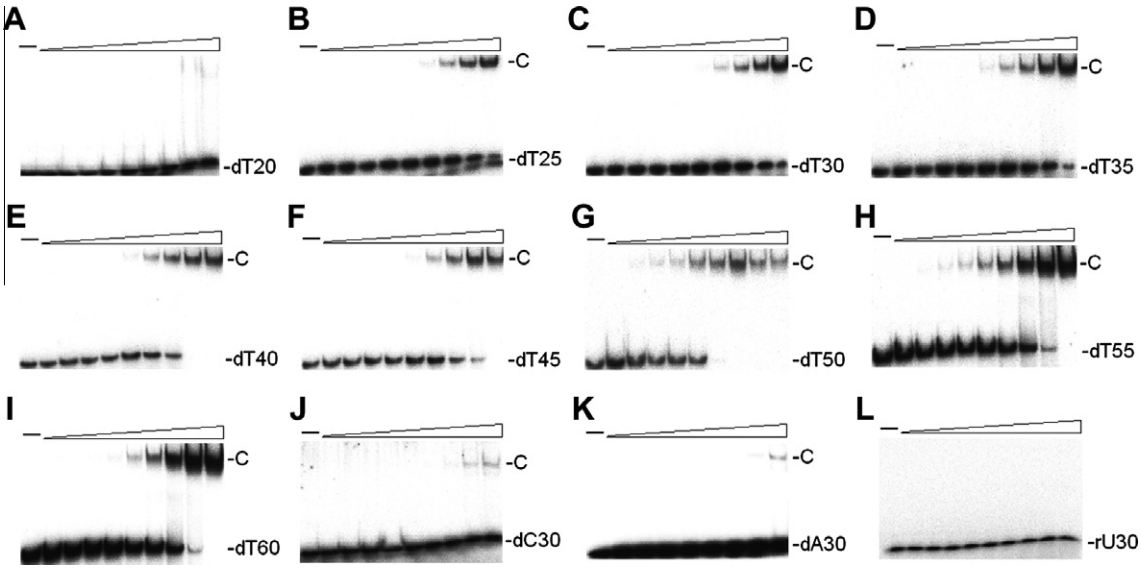

Fig. 2. *Kp*PriB binding affinities to (A–I) dT20–60, (J) dC30, (K) dA30, and (L) U30. The reaction solutions contain 1.7 nM of the oligonucleotide and *Kp*PriB (0–50 μM).

stable complex with *Kp*PriB molecule(s) is approximately 25 nt, as determined using EMSA.

3.4. Base preference for ssDNA binding of KpPriB

To test the base preference for *Kp*PriB binding to purine and pyrimidine, we used dT30 (Fig. 2C), dC30 (Fig. 2J), and dA30 (Fig. 2K) to bind to *Kp*PriB. Like *Ec*PriB [18], *Kp*PriB shows a higher preference for dT30 than for dA30. In addition, this study revealed that the binding preference of *Kp*PriB follows the given order: dT > dC > dA, i.e., *Kp*PriB preferentially binds to pyrimidine than to purine. However, the *in vitro* base preference of PriB, as well as other SSBs [30], is still unknown.

3.5. RNA binding activity of KpPriB

It has been previously reported that *Ec*PriB binds ssRNA (U35) with an affinity that is comparable to its affinity for ssDNA dT35 [18]. In order to assess whether the ability of PriB to bind to RNA is conserved, we assessed the binding of rU30 (Fig. 2L) and dT30 (Fig. 2C) to *Kp*PriB. Unexpectedly, *Kp*PriB did not bind to rU30 with the same affinity as it did for dT30. Thus, the RNA-binding activity of PriB among different species is not conserved and therefore is likely to be unnecessary in the *K. pneumoniae* primosome assembly.

3.6. Cooperative binding of KpPriB to ssDNA

The ssDNA binding ability of *Kp*PriB was studied via a filter-binding assay using dT15. Since dT20 or longer homopolymers give high background noise on binding to nitrocellulose filters, they were excluded from the assays. The titration curves for *Kp*PriB are shown in Fig. 3, and the estimated apparent K_d values are summarized in Table 1. The binding affinity of *Kp*PriB for dT15 (filled circle) increased significantly within a narrow range of protein concentrations, indicating that the formation of the *Kp*PriB–dT15 complex is a positive cooperative process. The Hill coefficient (h) for *Kp*PriB–dT15 binding was determined to be 3.41 ± 0.56, which is significantly higher than that for *Ec*PriB–dT15 (1.5 ± 0.1) [21]. The strong cooperative binding of *Kp*PriB to ssDNA has important implications for the nature of the protein–protein interactions within the complex and the position of the ssDNA-binding sites on *Kp*PriB. This is especially important considering that *Kp*PriB lacks several important residues for ssDNA binding, as compared with *Ec*PriB [9,17,18,21].

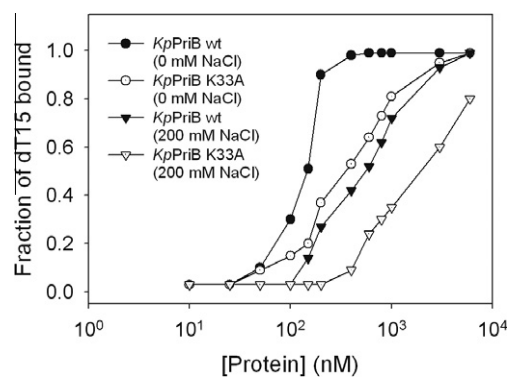

Fig. 3. Filter-binding assay. Titration curves of increasing amounts of *Kp*PriB and the mutant K33A assayed in the absence or presence of 200 mM NaCl, respectively.

Table 1
ssDNA-binding parameters of *Kp*PriB.

	[NaCl] (mM)	Apparent K_d (nM)	h
*Kp*PriB wt	0	140 ± 20	3.41 ± 0.56
*Kp*PriB K33A	0	380 ± 20	1.26 ± 0.08
*Kp*PriB wt	200	580 ± 50	1.33 ± 0.12
*Kp*PriB K33A	200	2600 ± 400	1.28 ± 0.19

The errors are standard deviations determined using 2–4 independent titration experiments.

3.7. Salt effect on ssDNA binding of KpPriB

The ssDNA-binding surface of *Ec*PriB is highly electropositive and interacts directly with both the bases and the phosphate back-

bone of ssDNA [21]. Although *Kp*PriB lacks the N-terminal 1–49 aa region seen in *Ec*PriB, the most important residues for ssDNA binding, K33, K35, and K40, corresponding to positions K82, K84, and K89, respectively, in *Ec*PriB, are conserved [21]. To investigate whether the electrostatic interactions play a role in ssDNA binding, we examined the binding of *Kp*PriB to dT15 at high salt concentrations (200 mM NaCl). As expected, the binding affinity of *Kp*PriB for dT15 is salt dependent, and is approximately 4-fold lower than that measured in the absence of salt (Table 1). Furthermore, the Hill coefficient (h) is reduced to 1.26 ± 0.08, indicating lower cooperativity in these conditions.

3.8. Role of K33 in KpPriB–ssDNA binding

To investigate the contribution of K33 in *Kp*PriB–ssDNA binding, a mutant was created with an alanine substitution at the position corresponding to K82 in loop L_{45} of *Ec*PriB. Binding was assessed in the absence (open circle) and presence of 200 mM NaCl (open triangle) (Fig. 3). As shown in Table 1, the K33A mutant has a K_d value (380 ± 20 nM) that is 2.7-fold higher than that of the wild-type *Kp*PriB (140 ± 20 nM) in the absence of additional NaCl. In the presence of 200 mM NaCl, the K33A mutant has a K_d value (2600 ± 400 nM) that is ~19-fold higher than that of the wild-type *Kp*PriB assayed without additional salt. The Hill coefficient of the K33A mutant is 1.26 ± 0.08 and 1.28 ± 0.19, when in the absence and presence of 200 mM NaCl, respectively. These data indicate that *Kp*PriB binds to ssDNA mainly through electrostatic interactions, especially within the positive charge region. Hence, the K33 position in *Kp*PriB appears to be involved not only in ssDNA binding, but also in the intra- or/and inter-molecular cooperative binding to other residue(s) of *Kp*PriB.

3.9. Comparison with EcPriB

The homodimeric arrangement of OB folds in *Ec*PriB (Fig. 4A) is roughly conserved among known PriB homologs. In this study, we reported a novel PriB from *K. pneumoniae* that is shorter and monomeric compared with the known PriBs, which are polymeric. It has been previously reported that the monomeric interactions found in the *Ec*PriB dimer are tightly packed by hydrophobic interactions [16–18] involving the residues Leu5, Leu7, Met50, and Ile78. Two of these residues, Met1 and Ile29, exist in the shorter *Kp*PriB homolog (Fig. 1A). The lack of the 2 Leu residues results in the failure to homodimerize (Figs. 1C and 4B), but the remaining residues are sufficient for mediating ssDNA binding (Figs. 2–4).

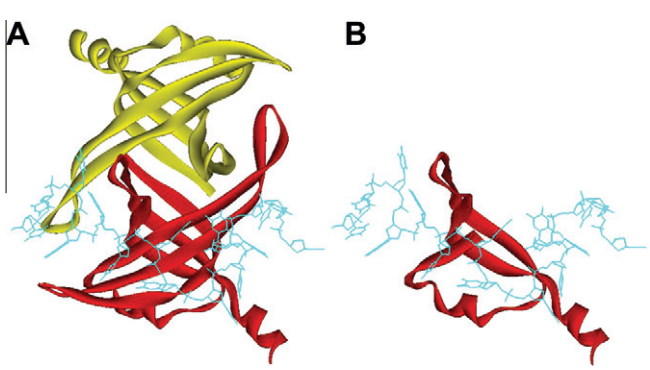

Fig. 4. (A) Crystal structure of *Ec*PriB complexed with ssDNA (derived from PDB code 2CCZ) [21]. A ribbon diagram reveals individual monomers (in gold and red) and ssDNA (cyan). (B) The residues of *Ec*PriB present in *Kp*PriB are shown. (For interpretation of the references to colour in this figure legend, the reader is referred to the web version of this article.)

Previous investigations of *Ec*PriB demonstrated that aromatic stacking, mediated by residues Phe42 and Trp47, plays an important role in ssDNA binding and in stimulating PriA helicase [10]. These residues, however, do not exist in *Kp*PriB. Therefore, the mechanisms and the binding modes of *Kp*PriB, as well as other *K. pneumoniae* primosomal proteins, to ssDNA remain to be explored.

Acknowledgment

This research was supported a grant from the National Research Program for Genome Medicine (NSC 99-3112-B-040-001 to C.Y. Huang).

References

[1] R.C. Heller, K.J. Marians, Replisome assembly and the direct restart of stalled replication forks, Nat. Rev. Mol. Cell Biol. 7 (2006) 932–943.
[2] M.M. Cox, M.F. Goodman, K.N. Kreuzer, D.J. Sherratt, S.J. Sandler, K.J. Marians, The importance of repairing stalled replication forks, Nature 404 (2000) 37–41.
[3] P. McGlynn, R.G. Lloyd, Recombinational repair and restart of damaged replication forks, Nat. Rev. Mol. Cell Biol. 3 (2002) 859–870.
[4] S.J. Sandler, K.J. Marians, Role of PriA in replication fork reactivation in *Escherichia coli*, J. Bacteriol. 182 (2000) 9–13.
[5] K.J. Marians, PriA-directed replication fork restart in *Escherichia coli*, Trends Biochem. Sci. 25 (2000) 185–189.
[6] H. Masai, T. Tanaka, D. Kohda, Stalled replication forks: making ends meet for recognition and stabilization, Bioessays 32 (2010) 687–697.
[7] C.B. Gabbai, K.J. Marians, Recruitment to stalled replication forks of the PriA DNA helicase and replisome-loading activities is essential for survival, DNA Repair (Amst.) 9 (2010) 202–209.
[8] R.C. Heller, K.J. Marians, Replication fork reactivation downstream of a blocked nascent leading strand, Nature 439 (2006) 557–562.
[9] M. Lopper, R. Boonsombat, S.J. Sandler, J.L. Keck, A hand-off mechanism for primosome assembly in replication restart, Mol. Cell 26 (2007) 781–793.
[10] C.J. Cadman, M. Lopper, P.B. Moon, J.L. Keck, P. McGlynn, PriB stimulates PriA helicase via an interaction with single-stranded DNA, J. Biol. Chem. 280 (2005) 39693–39700.
[11] J. Liu, P. Nurse, K.J. Marians, The ordered assembly of the phiX174-type primosome. III. PriB facilitates complex formation between PriA and DnaT, J. Biol. Chem. 271 (1996) 15656–15661.
[12] Y.H. Lo, K.L. Tsai, Y.J. Sun, W.T. Chen, C.Y. Huang, C.D. Hsiao, The crystal structure of a replicative hexameric helicase DnaC and its complex with single-stranded DNA, Nucleic Acids Res. 37 (2009) 804–814.
[13] S. Bailey, W.K. Eliason, T.A. Steitz, Structure of hexameric DnaB helicase and its complex with a domain of DnaG primase, Science 318 (2007) 459–463.
[14] K. Tougu, H. Peng, K.J. Marians, Identification of a domain of *Escherichia coli* primase required for functional interaction with the DnaB helicase at the replication fork, J. Biol. Chem. 269 (1994) 4675–4682.
[15] J. Dong, N.P. George, K.L. Duckett, M.A. DeBeer, M.E. Lopper, The crystal structure of *Neisseria gonorrhoeae* PriB reveals mechanistic differences among bacterial DNA replication restart pathways, Nucleic Acids Res. 38 (2010) 499–509.
[16] S. Shioi, T. Ose, K. Maenaka, M. Shiroishi, Y. Abe, D. Kohda, T. Katayama, T. Ueda, Crystal structure of a biologically functional form of PriB from *Escherichia coli* reveals a potential single-stranded DNA-binding site, Biochem. Biophys. Res. Commun. 326 (2005) 766–776.
[17] M. Lopper, J.M. Holton, J.L. Keck, Crystal structure of PriB, a component of the *Escherichia coli* replication restart primosome, Structure 12 (2004) 1967–1975.
[18] J.H. Liu, T.W. Chang, C.Y. Huang, S.U. Chen, H.N. Wu, M.C. Chang, C.D. Hsiao, Crystal structure of PriB, a primosomal DNA replication protein of *Escherichia coli*, J. Biol. Chem. 279 (2004) 50465–50471.
[19] D.L. Theobald, R.M. Mitton-Fry, D.S. Wuttke, Nucleic acid recognition by OB-fold proteins, Annu. Rev. Biophys. Biomol. Struct. 32 (2003) 115–133.
[20] A.G. Murzin, OB(oligonucleotide/oligosaccharide binding)-fold: common structural and functional solution for non-homologous sequences, EMBO J. 12 (1993) 861–867.
[21] C.Y. Huang, C.H. Hsu, Y.J. Sun, H.N. Wu, C.D. Hsiao, Complexed crystal structure of replication restart primosome protein PriB reveals a novel single-stranded DNA-binding mode, Nucleic Acids Res. 34 (2006) 3878–3886.
[22] M.R. Szymanski, M.J. Jezewska, W. Bujalowski, Interactions of the *Escherichia coli* primosomal PriB protein with the single-stranded DNA. Stoichiometries, intrinsic affinities, cooperativities, and base specificities, J. Mol. Biol. 398 (2010) 8–25.
[23] K.W. Chan, Y.J. Lee, C.H. Wang, H. Huang, Y.J. Sun, Single-stranded DNA-binding protein complex from *Helicobacter pylori* suggests an ssDNA-binding surface, J. Mol. Biol. 388 (2009) 508–519.
[24] S. Raghunathan, A.G. Kozlov, T.M. Lohman, G. Waksman, Structure of the DNA binding domain of *E. coli* SSB bound to ssDNA, Nat. Struct. Biol. 7 (2000) 648–652.

[25] C.C. Wang, H.W. Tsau, W.T. Chen, C.Y. Huang, Identification and characterization of a putative dihydroorotase, KPN01074, from *Klebsiella pneumoniae*, Protein J. 29 (2010) 445–452.
[26] C.Y. Huang, Y.W. Chang, W.T. Chen, Crystal structure of the N-terminal domain of *Geobacillus kaustophilus* HTA426 DnaD protein, Biochem. Biophys. Res. Commun. 375 (2008) 220–224.
[27] I. Wong, T.M. Lohman, A double-filter method for nitrocellulose-filter binding: application to protein–nucleic acid interactions, Proc. Natl. Acad. Sci. USA 90 (1993) 5428–5432.
[28] M. Abbani, M. Iwahara, R.T. Clubb, The structure of the excisionase (Xis) protein from conjugative transposon Tn916 provides insights into the regulation of heterobivalent tyrosine recombinases, J. Mol. Biol. 347 (2005) 11–25.
[29] T.L. Madden, R.L. Tatusov, J. Zhang, Applications of network BLAST server, Methods Enzymol. 266 (1996) 131–141.
[30] T.M. Lohman, M.E. Ferrari, *Escherichia coli* single-stranded DNA-binding protein: multiple DNA-binding modes and cooperativities, Annu. Rev. Biochem. 63 (1994) 527–570.

Protein J (2011) 30:20–26
DOI 10.1007/s10930-010-9297-6

Characterization of a Single-Stranded DNA-Binding Protein from *Pseudomonas aeruginosa* PAO1

Hau-Chern Jan · Yen-Ling Lee · Cheng-Yang Huang

Published online: 4 December 2010
© Springer Science+Business Media, LLC 2010

Abstract Single-stranded DNA-binding protein (SSB) plays an important role in DNA metabolism, such as in DNA replication, repair, and recombination, and is essential for cell survival. We characterized the single-stranded DNA (ssDNA)-binding properties of *Pseudomonas aeruginosa* PAO1 SSB (*Pa*SSB) by using fluorescence quenching measurements and electrophoretic mobility shift analysis (EMSA). Analysis of purified *Pa*SSB by gel filtration chromatography revealed a stable tetramer in solution. In fluorescence titrations, *Pa*SSB bound 22–32 nucleotides (nt) per tetramer depending on salt concentration. Using EMSA, we characterized the stoichiometry of *Pa*SSB complexed with a series of ssDNA homopolymers, and the size of the binding site was determined to be 29 ± 1 nt. Furthermore, EMSA results indicated that the dissociation constants of *Pa*SSB for the first tetramer were less than those for the second tetramer. On the basis of these biophysical analyses, the ssDNA binding mode of *Pa*SSB is expected to be noncooperative.

Keywords SSB · DNA replication · EMSA · ssDNA binding mode

Abbreviations

Ec	*Escherichia coli*
Pa	*Pseudomonas aeruginosa* PAO1
Mt	*Mycobacterium tuberculosis*
Ms	*Mycobacterium smegmatis*
Hp	*Helicobacter pylori*
ssDNA	Single-stranded DNA
SSB	Single-stranded DNA-binding protein
SDS-PAGE	Sodium dodecyl sulphate–polyacrylamide gel electrophoresis
EDTA	Ethylenediamine tetraacetic acid
EMSA	Electrophoretic mobility shift analysis
nt	Nucleotides
K_d	The apparent dissociation constant

H.-C. Jan · Y.-L. Lee · C.-Y. Huang (✉)
Department of Biomedical Sciences, Chung Shan Medical University, No. 110, Sec.1, Chien-Kuo N. Rd., Taichung City, Taiwan
e-mail: cyhuang@csmu.edu.tw

C.-Y. Huang
Department of Medical Research, Chung Shan Medical University Hospital, No. 110, Sec.1, Chien-Kuo N. Rd., Taichung City, Taiwan

1 Introduction

Single-stranded DNA-binding protein (SSB), which is conserved throughout all kingdoms of life, plays an important role in DNA replication, repair, and homologous genetic recombination, and is essential for cell survival [33]. During these reactions, SSB binds to and protects susceptible single-stranded DNA (ssDNA) from nucleolytic digestion and prevents secondary structure formation [22]. The majority of bacterial SSBs and human mitochondrial SSB function as homotetramers [26, 42], in which 4 oligonucleotide/oligosaccharide-binding folds (OB-folds) form a DNA-binding domain [23]. Exceptions to this arrangement exist. For example, SSBs from the bacterial phylum *Deinococcus-Thermus* function as a homodimer in which each monomer contains 2 OB-folds linked by a conserved spacer sequence [6, 8, 13, 40]. SSB from *Sulfolobus solfataricus* is a monomer that includes 1 OB-fold and likely functions as a tetramer when in the presence of DNA [10, 15, 35].

Bacterial SSBs consist of 2 domains, an N-terminal ssDNA-binding/oligomerization domain and a flexible C-terminal protein–protein interaction domain [33]. Generally, the N-terminal domain is separated from the highly conserved and acidic tail of the last 10 C-terminal amino acids of SSB by a long glycine-rich hinge. The C-terminal domain of SSB interacts with other auxiliary proteins that are essential for cell survival [4]. The binding of SSB to ssDNA results in a conformational change in the protein, which makes the glycine-rich region more easily accessible to other proteins such as proteases and DNA polymerase III [3, 39]; however, the C-terminal domain of SSB is disordered, even when bound to DNA [31].

The most thoroughly studied SSB is that of *Escherichia coli* (*Ec*SSB), which binds cooperatively to ssDNA [19]. In fluorescence titrations with poly(dT), the estimated size of the binding sites of SSBs are dependent on salt concentration [19]. *Ec*SSB mainly binds to 35- and 65-nucleotide (nt)-long ssDNA, using the $(SSB)_{35}$- and $(SSB)_{65}$-binding modes, respectively. In the $(SSB)_{35}$-binding mode, 2 subunits of the *Ec*SSB tetramer interact with ssDNA, whereas in the $(SSB)_{65}$-binding mode, all 4 subunits participate in ssDNA binding. These different binding modes of SSB may be required during different stages of DNA metabolism [27, 28].

In the present study, we examined the electrophoretic mobility shift patterns of *Pseudomonas aeruginosa* PAO1 SSB (*Pa*SSB) bound to different length ssDNA. In electrophoretic mobility shift analysis (EMSA), it is expected that, once the nucleotides are of sufficient length to bind to two or more SSB molecules, the electrophoretic mobility of the higher SSB oligomeric tetramers will be lower than that of the smaller SSB oligomeric tetramers. Furthermore, we also studied the binding properties of *Pa*SSB by using fluorescence quenching measurements. The binding-mode transition suggested for *Ec*SSB was not observed for *Pa*SSB when changing the ionic environment from low salt (20 mM NaCl) to high salt (300 mM NaCl).

2 Materials and Methods

2.1 Materials

All restriction enzymes and DNA-modifying enzymes were purchased from New England Biolabs (Ipswich, MA, USA) unless explicitly stated otherwise. All chemicals were purchased from Sigma–Aldrich (St. Louis, MO, USA) unless explicitly stated otherwise. The *E. coli* strains TOP10F' (Invitrogen, USA) and BL21(DE3)pLysS (Novagen, UK) were used for genetic construction and protein expression, respectively.

2.2 Cloning, expression and purification

The gene *PA4232* encoding the *Pa*SSB was PCR-amplified from *P. aeruginosa* genomic DNA [9, 37]. The forward (5′-TTGCTCATATGGCCCGTGGGGTTAACA-3′) and the reverse (5′-TTGCACTCGAGGAACGGAATGTCGTCG-3′) primers were designed to introduce unique NdeI and XhoI restriction sites (underlined) into *Pa*SSB, permitting the insertion of the amplified gene into the pET21b vector (Novagen Inc., Madison, WI, USA) for the protein expression in *E. coli*. *E. coli* cells were transformed with the expression vector and grown to OD_{600} of 0.9 at 37 °C in Lysogeny Broth medium containing 250 µg/mL ampicillin [36]. Overexpression of *Pa*SSB construct was induced with 1 mM isopropyl thiogalactoside (IPTG) for 3 h at 37 °C. The cells overexpressing the protein were chilled on ice, harvested by centrifugation, resuspended in Buffer A (20 mM Tris–HCl, 5 mM imidazole, 0.5 M NaCl; pH 7.9) and disrupted by sonication with ice cooling between pulses. The *Pa*SSB protein was then purified from the soluble supernatant by Ni^{2+}-affinity chromatography (HiTrap HP; GE Healthcare Bio-Sciences, Piscataway, NJ, USA). Protein purity remained greater than 95% as determined by Coomassie-stained SDS–PAGE.

2.3 Gel-Filtration Chromatography

Gel-filtration chromatography was carried out by the same protocol as previously described for DnaD using an AKTA-FPLC system [11]. Briefly, purified *Pa*SSB in buffer (0.1 M NaCl and 20 mM Tris–HCl at pH 8.0) were applied to a Superdex 200 HR 10/30 column (GE Healthcare Bio-Sciences, Piscataway, NJ, USA) equilibrated with the same buffer. The column was operated at a flow rate of 0.5 mL/min, and 0.5-mL fractions were collected. The proteins were detected by measuring absorbance at 280 nm. The column was calibrated with proteins of known molecular masses: γ-globulin (158 kDa), albumin (67 kDa), ovalbumin (43 kDa), chymotrypsinogen A (25 kDa), and ribonuclease A (13.7 kDa).

2.4 Fluorescence Measurement

Fluorescence titrations were carried out in a spectrofluorimeter (Hitachi F-2700; Hitachi High-Technologies, Tokyo, Japan) as described previously [2, 5, 25]. The excitation and emission of tryptophan fluorescence were detected at 295 and 348 nm, respectively. The *Pa*SSB solution (0.4 µM; tetramer) in 2 mL Tris–HCl buffer (20 mM Tris–HCl, and pH 8.0) containing 20 mM or 300 mM NaCl was titrated with rising quantities of dT50 oligonucleotide. After the addition of the ssDNA, the

complex solution was equilibrated for 300 s until no fluorescence change could be observed. The tryptophan fluorescence quenching is used to measure the diminution of fluorescence between the ssDNA-free and the ssDNA-bound proteins. The ssDNA-binding site size (n) was analyzed by the ssDNA-binding curve using the model of Schwarz and Watanabe [32].

2.5 Gel Shifts

Various lengths of ssDNA oligonucleotides were custom synthesized by MdBio, Inc., Frederick, MD. Radiolabeling was carried out with [γ^{32}P]ATP (6000 Ci/mmol; Perkin-Elmer Life Sciences) and T4 polynucleotide kinase (Promega, Madison, WI, USA). *Pa*SSB (0, 19, 37, 77, 155, 310, 630, 1,250, 2,500, and 5,000 nM) was incubated for 30 min at 25 °C with 1.7 nM DNA substrates (dT15–95) in a total volume of 10 μL in 20 mM Tris–HCl pH 8.0 and 100 mM NaCl. Aliquots (5 μL) were removed from each reaction solution and added to 2 μL of gel-loading solution (0.25% bromophenol blue and 40% sucrose). The resulting samples were resolved on a native 8% polyacrylamide gel at 4 °C in TBE buffer (89 mM Tris borate and 1 mM EDTA) for 1 h at 100 V and visualized by autoradiography. Complexed and free DNA bands were scanned and quantified. The binding dissociation constants for the *Pa*SSB-ssDNA tetramer 1 (K_{d1}) were estimated from the protein concentration that binds 50% of the input DNA [7, 12, 18, 21]; the binding dissociation constants for the *Pa*SSB-ssDNA tetramer 2 (K_{d2}) were estimated from the protein concentration that forms 50% of the tetramer 2. In this report, each K_d is calculated as the average of at least three measurements ± S.D.

3 Results

3.1 Sequence Analysis

The gene *PA4232*, encoding *P. aeruginosa* PAO1 SSB, was initially found using a database search through the National Center for Biotechnology Information. Based on the known nucleotide sequence, the predicted *Pa*SSB monomer protein has 165 amino acid residues and a molecular mass of 19 kDa. Analysis of the primary structure of *Pa*SSB by RPS-BLAST [20] revealed the presence of a putative OB-fold domain that is common in all known SSBs. Figure 1 shows an alignment of the amino acid sequences of *P. aeruginosa* PAO1, *E. coli* [26], *Mycobacterium tuberculosis* [29], *Mycobacterium smegmatis* [30], and *Helicobacter pylori* SSBs [2]. In the *Ec*SSB–ssDNA complex [26], 4 essential aromatic residues, Trp40,

```
Pa SSB   -MARGVNKVILVGNVGGDPETRYMPNGNAVTNITLATSESWKDKQTGQQQE-RTEWHRVV 58
Ec SSB   MASRGVNKVILVGNLGQDPEVRYMPNGGAVANITLATSESWRDKATGEMKE-QTEWHRVV 59
Mt SSB   --MAGDTTITIVGNLTADPELRFTPSGAAVANFTVASTPRIYDRQTGEWKDGEALFLRCN 58
Ms SSB   --MAGDTTITVVGNLTADPELRFTPSGAAVANFTVASTPRMFDRQSGEWKDGEALFLRCN 58
Hp SSB   ----MFNKVIMVGRLTRNVELKYLPSGSAAATIGLATSRRFK-KQDGTLGE-EVCFIDAR 54

Pa SSB   FFGRLAEIAGEYLRKGSQVYVEGSLRTRKWQGQDGQDRYTTEIVVDING-NMQLLGGR-- 115
Ec SSB   LFGKLAEVASEYLRKGSQVYIEGQLRTRKWTDQSGQDRYTTEVVVNVGG-TMQMLGGRQG 118
Mt SSB   IWREAAENVAESLTRGARVIVSGRLKQRSFETREGEKRTVIEVEVDEIGPSLRYATAKVN 118
Ms SSB   IWREAAENVAESLTRGSRVIVTGRLKQRSFETREGEKRTVVEVEVDEIGPSLRYATAKVN 118
Hp SSB   LFGRTAEIANQYLSKGSSVLIEGRLTYESWMDQTGKKNSRHTITADSLQFMDKKSDNPQA 114

Pa SSB   ---PSG-----DDSQR-----APREPMQRPQQAPQQQSRPAPQQQPAPQPAQDYDS--FD 160
Ec SSB   GGAPAGGNIGGGQPQGGW--GQPQQPQGGNQFSGGAQSRPQ-QSAPAAPSNEPPMD--FD 173
Mt SSB   KASRSG----------------GFGSGSRPAPAQTS-SASGDDPWGSAPASGSFGG--GD 159
Ms SSB   KASRSG----------------GGGGGFGSGGGGSRQSEPKDDPWGSAPASGSFSG--AD 160
Hp SSB   NAMQDSIMHENSNNAYPANHNAPSQDPFNQAYAQNAYAKENLQAQPSKYQNSVPEINIDE 174

Pa SSB   DDIPF 165
Ec SSB   DDIPF 178
Mt SSB   DEPPF 164
Ms SSB   DEPPF 165
Hp SSB   EEIPF 179
```

Fig. 1 Multiple amino acid sequence alignment of SSB proteins. Sequence alignment of *Pa*SSB, with other SSB proteins from *E. coli* (*Ec*SSB), *Mycobacterium tuberculosis* (*Mt*SSB), *Mycobacterium smegmatis* (*Ms*SSB), and *Helicobacter pylori* (*Hp*SSB), was generated by CLUSTALW2 online [17]. Amino acid residues displaying 100% identity are highlighted in *bold black*, and those displaying similarity are highlighted in *black*

Trp54, Phe60, and Trp88, participate in ssDNA binding via stacking interactions. These residues are conserved in most SSB families as Phe/Tyr/Trp, and the corresponding residues in *Pa*SSB are Trp39, Trp53, Phe59, and Trp87. The C-terminal tail of SSBs containing several acidic residues, such as "DDDIPF" in *Ec*SSB, is also conserved in *Pa*SSB. In contrast to those motifs, the glycine-rich hinge in *Pa*SSB is not as obvious as that of *Ec*SSB. Eight glycine residues in this motif that are found in *Ec*SSB are not found in *Pa*SSB.

3.2 Oligomerization of *Pa*SSB in Solution

Analysis of purified protein by gel filtration chromatography revealed a single peak (Fig. 2). Assuming that *Pa*SSB has a shape and partial specific volume similar to the standard proteins, the native molecular mass of *Pa*SSB was estimated to be ~ 72 kDa. The native molecular mass for *Pa*SSB is approximately 3.8 times the molecular mass of a *Pa*SSB monomer (19 kDa). Thus, we concluded that *Pa*SSB in solution is a stable tetramer, similar to *Ec*SSB.

3.3 DNA Binding Monitored by Quenching of Intrinsic Tryptophan Fluorescence

It is well established that the fluorescence quench and the estimated size of the binding sites of SSBs depend on the salt concentration of the SSB solution [19]. *Pa*SSB has 3

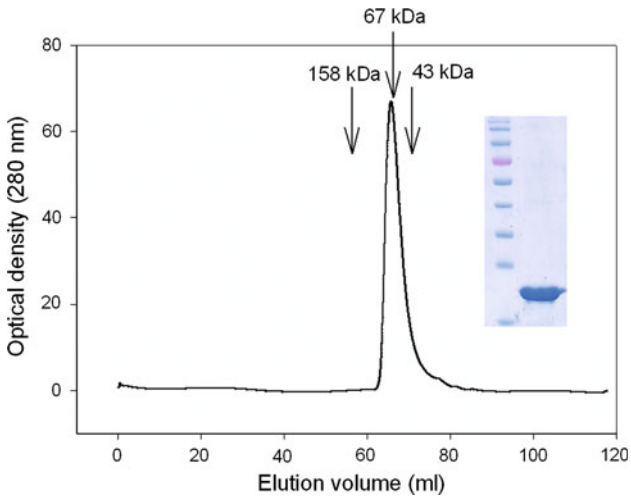

Fig. 2 Gel-filtration chromatographic analysis of *Pa*SSB. The sizes of the molecular mass markers (in kDa) are indicated at the top. The corresponding peak shows the eluted *Pa*SSB. Coomassie Blue-stained SDS–PAGE (12%) of the purified *Pa*SSB and molecular mass standards are also shown. The sizes of the standard proteins, from the *top down*, are as follows: 170, 130, 100, 70, 55, 40, 35, 25, and 15 kDa. The purified *Pa*SSB migrated between the 25 and 15 kDa standards on the SDS–PAGE

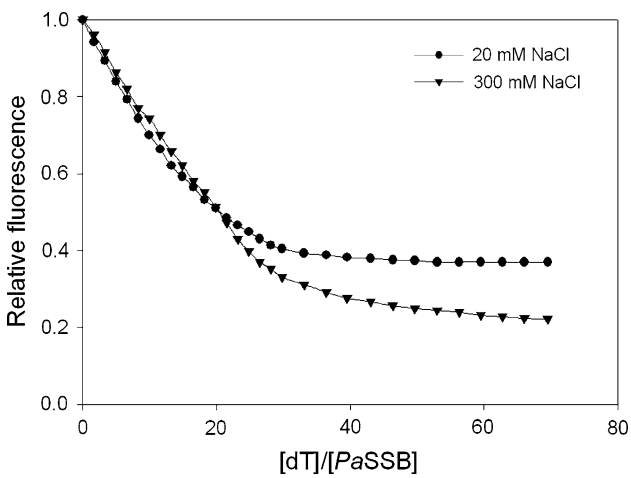

Fig. 3 Fluorescence titration of *Pa*SSB with ssDNA dT50. Tryptophan fluorescence quenching of *Pa*SSB in the presence of 20 mM (*filled circle*) or 300 mM NaCl (*filled triangle*), is shown

tryptophan residues (Trp39, Trp53, and Trp87) in the OB-fold domain, allowing an analysis of ssDNA binding by tryptophan fluorescence quenching (Fig. 3). The protein displayed strong intrinsic fluorescence with a peak wavelength of 348 nm when excited at 295 nm, consistent with tryptophan fluorescence (data not shown). As dT50 was titrated into the *Pa*SSB solution, the intrinsic fluorescence of the protein was progressively quenched. On addition of a saturating quantity of ssDNA in the presence of 20 mM NaCl, the intrinsic fluorescence at 348 nm was quenched by 63%. The estimated binding-site sizes of *Pa*SSB in 20 and 300 mM NaCl were about of 24 ± 2 nt and 30 ± 2 nt, respectively. The ssDNA shows bilinear binding to *Pa*SSB in 20 mM NaCl; ssDNA binding of *Pa*SSB in the presence of 300 mM NaCl, however, follows a hyperbolic curve. This may suggest that ssDNA has higher binding affinity binding for *Pa*SSB under low-salt conditions.

3.4 *Pa*SSB Binding to dT25–55 Forms a Single Complex

To investigate the length of nucleotides sufficient for the formation of the *Pa*SSB–ssDNA complex and the ssDNA-binding ability of *Pa*SSB, we studied the binding of *Pa*SSB to dT15 (Fig. 4a), dT20 (Fig. 4b), dT25 (Fig. 4c), dT30 (Fig. 4d), dT35 (Fig. 4e), dT40 (Fig. 4f), dT45 (Fig. 4g), dT50 (Fig. 4h), and dT55 (Fig. 4i) with different protein concentrations using EMSA. As shown in Fig. 4a, b, no significant band shift was observed when *Pa*SSB was incubated with dT15 or dT20, indicating that *Pa*SSB could not form a stable complex with these homopolymers. Because some smears were observed, it appears that *Pa*SSB interacts with dT15 or dT20, but the ssDNA may be too short to be fully wrapped by *Pa*SSB. In contrast to dT15 or dT20, > 98% of the longer dT homopolymers bind to *Pa*SSB, forming a single complex (Fig. 4c–i). Thus, the EMSA results suggest that the length of ssDNA required for *Pa*SSB binding is approximately 25 nt.

3.5 Two Different Complexes are Formed when *Pa*SSB Binds to dT60–80

To examine the minimum nucleotide length necessary for the binding of a second *Pa*SSB tetramer to ssDNA pre-bound to *Pa*SSB, we studied the binding of *Pa*SSB to longer dT homopolymers, from 60 to 80 nt (Fig. 5). Although dT60 is only 5 nt longer than dT55, it produced a very different pattern of *Pa*SSB–ssDNA complexes observed using EMSA. At lower protein concentrations (<100 nM), *Pa*SSB forms a single complex with dT60 (Fig. 5a), similar to that observed with dT55 (Fig. 4i); however, when the *Pa*SSB concentration is increased slightly, another slower-migrating complex appears. The appearance of the second complex results from the increasing *Pa*SSB concentration, which suggests that it may contain at least 2 *Pa*SSB tetramers per oligonucleotide. As the minimal size of the ssDNA binding site for *Pa*SSB is approximately 25 nt (see above), the presence of an extra 5 nt in dT60, as compared with dT55, provides enough interaction space for the binding of a second *Pa*SSB tetramer, which occupies around 30 nt ssDNA. In addition, the stoichiometry of the 2 *Pa*SSB molecules bound per ssDNA did not change when the length of the dT

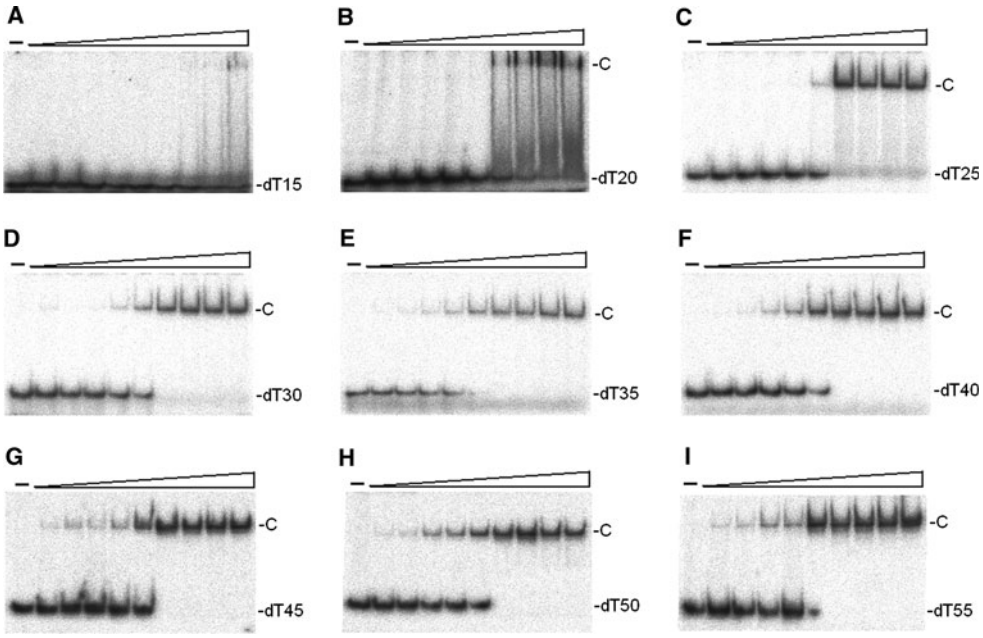

Fig. 4 Binding of *Pa*SSB to dT15–55. The reaction solutions contained 1.7 nM of (**a**) dT15, (**b**) dT20, (**c**) dT25, (**d**) dT30, (**e**) dT35, (**f**) dT40, (**g**) dT45, (**h**) dT50, or (**i**) dT55 and *Pa*SSB (0–5.0 μM)

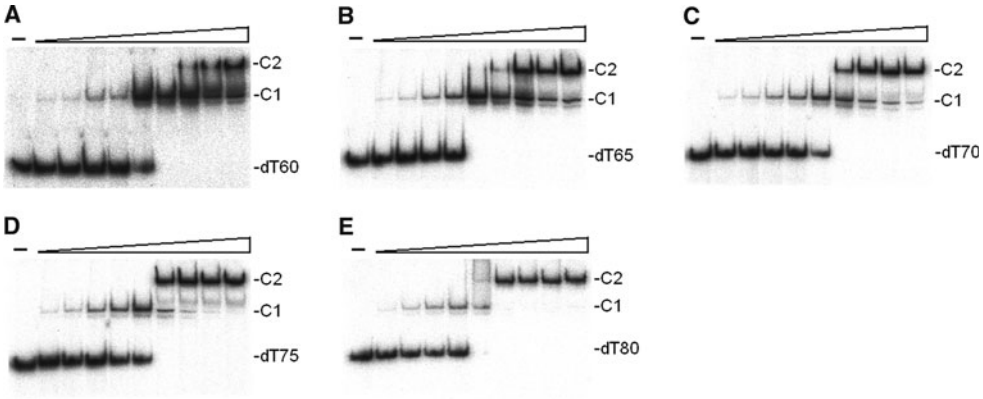

Fig. 5 Binding of *Pa*SSB to dT60–80. The reaction solutions contained 1.7 nM of (**a**) dT60, (**b**) dT65, (**c**) dT70, (**d**) dT75, or (**e**) dT80 and *Pa*SSB (0–5.0 μM)

homopolymers was further increased to 80 nt (Fig. 5e). These results suggest that the length of ssDNA required for efficient binding of *Pa*SSB is 29 ± 1 nt (Fig. 6).

3.6 The Binding Constants of the *Pa*SSB–ssDNA Complexes

The binding constants of the *Pa*SSB–ssDNA complexes (K_d values) are summarized in Table 1. The formation of *Pa*SSB–ssDNA complex 1 (C1) is nearly ssDNA-length independent, suggesting that the protein–DNA contact is similar for each C1 (Fig. 7). In contrast, the ability of a second *Pa*SSB tetramer (the K_{d2} value) to bind to ssDNA already bound by a *Pa*SSB tetramer was length dependent (Fig. 7). Indeed, increases in ssDNA length were associated with higher binding ability (lower K_{d2} value), indicating that the second *Pa*SSB tetramer prefers to bind to long ssDNA segments to which a *Pa*SSB tetramer is already bound.

4 Discussion

In this study, we describe the cloning, expression, purification, and characterization of SSB from *P. aeruginosa* PAO1, the most common opportunistic pathogen [43]. The sequence analysis (Fig. 1) indicates that the *Pa*SSB monomer possesses an OB-fold domain at its N-terminus and a flexible tail at its C-terminus, as in *Ec*SSB, although the glycine-rich hinge observed in *Ec*SSB is not evident. Analysis of *Pa*SSB by using gel filtration chromatography showed that the protein forms a tetramer in solution.

We showed that the binding of *Pa*SSB to dT50 results in tryptophan fluorescence quenching (Fig. 3). In the presence of 20 and 300 mM NaCl, the binding site sizes of *Pa*SSB was 24 ± 2 nt and 30 ± 2 nt per homotetramer, respectively; no distinct differences could be observed between low- and high-salt conditions. For *Hp*SSB, the stoichiometry was 25 ± 2 nt per homotetramer [2]. Two different

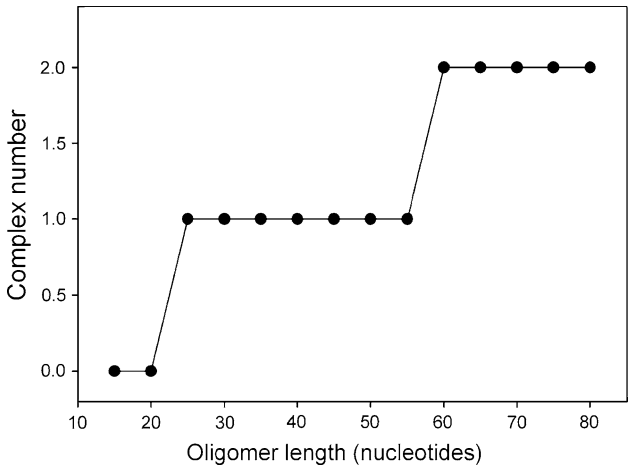

Fig. 6 Complex number of *Pa*SSB as a function of the length of the ssDNA determined using EMSA

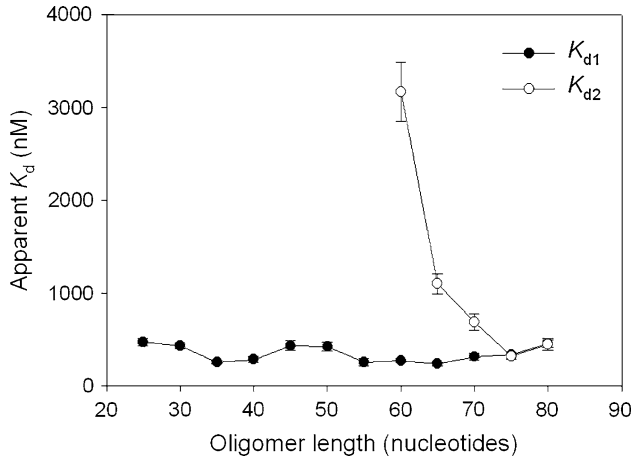

Fig. 7 Apparent K_d values of *Pa*SSB as a function of the length of the ssDNA. K_{d1}, K_d for the formation of the first complex (C1); K_{d2}, K_d for the formation of the second complex (C2)

Table 1 ssDNA-binding parameters of *Pa*SSB

	*Pa*SSB	
	K_{d1} (nM)	K_{d2} (nM)
dT25	470 ± 40	
dT30	427 ± 34	
dT35	255 ± 15	
dT40	281 ± 32	
dT45	432 ± 50	
dT50	419 ± 48	
dT55	254 ± 42	
dT60	267 ± 18	3,170 ± 320
dT65	236 ± 20	1,100 ± 108
dT70	312 ± 36	683 ± 90
dT75	333 ± 16	320 ± 38
dT80	453 ± 40	444 ± 66

Each K_d is calculated as the average of at least three measurements ± S.D

DNA-binding modes have been identified for *Ec*SSB [19]. Under high-salt conditions, 65 nt ssDNA binds per *Ec*SSB tetramer with almost 90% fluorescence quench; under low-salt conditions, 35 nt DNA produces a 53% fluorescence quench. Human replication protein A, a eukaryotic SSB, binds DNA noncooperatively and has a binding site of 20–30 nt per heterotrimer under most conditions [14, 16, 24, 41]. The constant binding stoichiometry of *Pa*SSB that was determined using fluorescence quench at high and low salt concentrations also has been reported in SSBs from the *Thermus/Deinococcus* group. Unlike *Ec*SSB [31], the C-terminal flexible region of *Deinococcus* SSB is clearly evident from its crystal structure, suggesting that this region of the *Deinococcus* SSB has lower dynamic. The OB-fold domain and the C-terminal tail of *Pa*SSB are similar to that of *Ec*SSB, with the exception of the flexible glycine-rich hinge in *Ec*SSB. Taken together, these data suggest that multiple binding modes $(SSB)_{35}$ and $(SSB)_{65}$ could not be identified with certainty in *Pa*SSB, possibly because of its low flexibility and/or lower number of glycine residues. However, this speculation needs to be confirmed by further biochemical experiments.

Many SSB proteins bind to ssDNA with some degree of positive cooperativity. Cooperativity can result from direct protein–protein interactions between the nearest neighbors, such as the LAST motif in the T4 gene-32 protein [1], and the arginine-mediated interaction motif in *Thermus* SSB [8, 38]. Cooperativity can also result from the protein-induced distortion of adjacent DNA as demonstrated by *Sulfolobus* SSB, PriB, and FOXK1a proteins [12, 15, 34]. The EMSA results indicate that *Pa*SSB binds to short ssDNAs (dT25–dT55) to form a complex in which a single tetramer is bound to the ssDNA (Fig. 4), and that 2 tetramers could bind to dT60–dT80 (Fig. 5). Thus, the apparent binding-site size of *Pa*SSB is 29 ± 1 nt (Fig. 6). For *Pa*SSB, binding appears to be noncooperative because, for several of the DNAs, essentially all of the DNA shifts into C1 before the appearance of the second complex (C2). In addition, the apparent K_d values are of the first and second complex also as expected for noncooperative binding (Table 1 and Fig. 7); for positively cooperative binding, K_{d2} should be less than K_{d1}. Increasing the length of C2 causes its K_d value to match that of C1, suggesting that the length dependence reflects the minimal amount of spacing that is optimal for steric considerations.

Acknowledgments We thank Ms. Hui-Chuan Hsieh for constructing the pET21b-*Pa*SSB. This research was supported a grant from the National Research Program for Genome Medicine (NSC 99-3112-B-040-001 to C.Y. Huang).

References

1. Casas-Finet JR, Fischer KR, Karpel RL (1992) Proc Natl Acad Sci USA 89:1050–1054
2. Chan KW, Lee YJ, Wang CH, Huang H, Sun YJ (2009) J Mol Biol 388:508–519
3. Chase JW, Williams KR (1986) Annu Rev Biochem 55:103–136
4. Curth U, Genschel J, Urbanke C, Greipel J (1996) Nucleic Acids Res 24:2706–2711
5. Curth U, Greipel J, Urbanke C, Maass G (1993) Biochemistry 32:2585–2591
6. Dabrowski S, Olszewski M, Piatek R, Brillowska-Dabrowska A, Konopa G, Kur J (2002) Microbiology 148:3307–3315
7. Fairall L, Buttinelli M, Panetta G (2000) In: Travers A, Buckle M (eds) DNA-protein interactions: a practical approach. Oxford University Press, New York, pp 65–74
8. Fedorov R, Witte G, Urbanke C, Manstein DJ, Curth U (2006) Nucleic Acids Res 34:6708–6717
9. Genschel J, Litz L, Thole H, Roemling U, Urbanke C (1996) Gene 182:137–143
10. Haseltine CA, Kowalczykowski SC (2002) Mol Microbiol 43:1505–1515
11. Huang CY, Chang YW, Chen WT (2008) Biochem Biophys Res Commun 375:220–224
12. Huang CY, Hsu CH, Sun YJ, Wu HN, Hsiao CD (2006) Nucleic Acids Res 34:3878–3886
13. Jedrzejczak R, Dauter M, Dauter Z, Olszewski M, Dlugolecka A, Kur J (2006) Acta Crystallogr D Biol Crystallogr 62:1407–1412
14. Kelly TJ, Simancek P, Brush GS (1998) Proc Natl Acad Sci USA 95:14634–14639
15. Kerr ID, Wadsworth RI, Cubeddu L, Blankenfeldt W, Naismith JH, White MF (2003) EMBO J 22:2561–2570
16. Kim C, Snyder RO, Wold MS (1992) Mol Cell Biol 12: 3050–3059
17. Larkin MA, Blackshields G, Brown NP, Chenna R, McGettigan PA, McWilliam H, Valentin F, Wallace IM, Wilm A, Lopez R, Thompson JD, Gibson TJ, Higgins DG (2007) Bioinformatics 23:2947–2948
18. Liu JH, Chang TW, Huang CY, Chen SU, Wu HN, Chang MC, Hsiao CD (2004) J Biol Chem 279:50465–50471
19. Lohman TM, Ferrari ME (1994) Annu Rev Biochem 63:527–570
20. Madden TL, Tatusov RL, Zhang J (1996) Methods Enzymol 266:131–141
21. Matos RG, Barbas A, Arraiano CM (2010) Protein J 29:394–397
22. Meyer RR, Laine PS (1990) Microbiol Rev 54:342–380
23. Murzin AG (1993) EMBO J 12:861–867
24. Oakley GG, Patrick SM (2010) Front Biosci 15:883–900
25. Olszewski M, Mickiewicz M, Kur J (2008) Arch Microbiol 190:79–87
26. Raghunathan S, Kozlov AG, Lohman TM, Waksman G (2000) Nat Struct Biol 7:648–652
27. Roy R, Kozlov AG, Lohman TM, Ha T (2007) J Mol Biol 369:1244–1257
28. Roy R, Kozlov AG, Lohman TM, Ha T (2009) Nature 461: 1092–1097
29. Saikrishnan K, Jeyakanthan J, Venkatesh J, Acharya N, Sekar K, Varshney U, Vijayan M (2003) J Mol Biol 331:385–393
30. Saikrishnan K, Manjunath GP, Singh P, Jeyakanthan J, Dauter Z, Sekar K, Muniyappa K, Vijayan M (2005) Acta Crystallogr D Biol Crystallogr 61:1140–1148
31. Savvides SN, Raghunathan S, Futterer K, Kozlov AG, Lohman TM, Waksman G (2004) Protein Sci 13:1942–1947
32. Schwarz G, Watanabe F (1983) J Mol Biol 163:467–484
33. Shereda RD, Kozlov AG, Lohman TM, Cox MM, Keck JL (2008) Crit Rev Biochem Mol Biol 43:289–318
34. Tsai KL, Huang CY, Chang CH, Sun YJ, Chuang WJ, Hsiao CD (2006) J Biol Chem 281:17400–17409
35. Wadsworth RI, White MF (2001) Nucleic Acids Res 29:914–920
36. Wang CC, Tsau HW, Chen WT, Huang CY (2010) Protein J 29:445–452
37. Winsor GL, Lo R, Sui SJ, Ung KS, Huang S, Cheng D, Ching WK, Hancock RE, Brinkman FS (2005) Nucleic Acids Res 33:D338–D343
38. Witte G, Fedorov R, Curth U (2008) Biophys J 94:2269–2279
39. Witte G, Urbanke C, Curth U (2003) Nucleic Acids Res 31: 4434–4440
40. Witte G, Urbanke C, Curth U (2005) Nucleic Acids Res 33: 1662–1670
41. Wold MS (1997) Annu Rev Biochem 66:61–92
42. Yang C, Curth U, Urbanke C, Kang C (1997) Nat Struct Biol 4:153–157
43. Zhao WH, Hu ZQ (2010) Crit Rev Microbiol 36:245–258

Protein J (2011) 30:102–108
DOI 10.1007/s10930-011-9309-1

Characterization of a Single-Stranded DNA Binding Protein from *Salmonella enterica* Serovar Typhimurium LT2

Yen-Hua Huang · Yen-Ling Lee · Cheng-Yang Huang

Published online: 26 January 2011
© Springer Science+Business Media, LLC 2011

Abstract Single-stranded DNA-binding protein (SSB) plays an important role in DNA metabolism, such as DNA replication, repair, and recombination, and is essential for cell survival. We characterized the single-stranded DNA (ssDNA)-binding properties of *Salmonella enterica* serovar Typhimurium LT2 SSB (*St*SSB) by using fluorescence quenching measurements and electrophoretic mobility shift analysis (EMSA). Analysis of purified *St*SSB by gel filtration chromatography showed a stable tetramer in solution. In fluorescence titrations, *St*SSB bound to 21–38 nucleotides (nt) per tetramer depending on the salt concentration. Using EMSA, we characterized the stoichiometry of *St*SSB complexed with a series of ssDNA homopolymers, and the size of the binding site was determined to be 22 ± 1 nt. Furthermore, EMSA results indicated that the dissociation constants of *St*SSB for the first tetramer were less than that for the second tetramer. On the basis of these biophysical analyses, the ssDNA binding-mode of *St*SSB is expected to be noncooperative.

Keywords SSB · DNA replication · EMSA · ssDNA binding mode

Y.-H. Huang · Y.-L. Lee · C.-Y. Huang (✉)
Department of Biomedical Sciences, Chung Shan Medical University, No.110, Sec.1, Chien-Kuo N. Rd., Taichung City, Taiwan
e-mail: cyhuang@csmu.edu.tw

C.-Y. Huang
Department of Medical Research, Chung Shan Medical University Hospital, No.110, Sec.1, Chien-Kuo N. Rd., Taichung City, Taiwan

Abbreviations

Ec	*Escherichia coli*
St	*Salmonella enterica* serovar Typhimurium LT2
Pa	*Pseudomonas aeruginosa* PAO1
Mt	*Mycobacterium tuberculosis*
Ms	*Mycobacterium smegmatis*
Hp	*Helicobacter pylori*
ssDNA	Single-stranded DNA
SSB	Single-stranded DNA-binding protein
SDS-PAGE	Sodium dodecyl sulphate–polyacrylamide gel electrophoresis
EDTA	Ethylenediamine tetraacetic acid
EMSA	Electrophoretic mobility shift analysis
nt	Nucleotides
K_d	The apparent dissociation constant

1 Introduction

Single-stranded DNA-binding protein (SSB) plays an important role in DNA replication, repair, and recombination [27, 29, 34]. During these reactions, SSB binds to and protects the susceptible single-stranded state of DNA (ssDNA) from nucleolytic digestion and prevents the secondary structure formation. Most bacterial SSBs are active as homotetramers where 4 oligonucleotide/oligosaccharide-binding folds (OB-folds) form a DNA-binding domain [1, 21, 26]. However, SSBs from the bacterial phylum *Deinococcus-Thermus* function as a homodimer in which each monomer contains 2 OB-folds linked by a conserved spacer sequence [5, 7, 39, 41]. SSB from *Sulfolobus solfataricus* is a monomer that includes 1 OB-fold and likely functions as a tetramer when in the presence of DNA [8, 13, 37].

Bacterial SSBs consist of two domains, an N-terminal ssDNA-binding/oligomerization domain and a flexible C-terminal protein–protein interaction domain [34]. The N-terminal domain is separated from the highly conserved and acidic tail of the last 10 C-terminal amino acids of SSB by a long either proline- [24] or glycine-rich hinge [16]. The C-terminal domain of SSB interacts with other auxiliary proteins that are essential for cell survival [3]. The binding of SSB to ssDNA makes the glycine-rich region more easily accessible to other proteins such as proteases and DNA polymerase III [3, 22, 40].

The most thoroughly studied SSB is that of *Escherichia coli* (*Ec*SSB), which binds cooperatively to ssDNA [16]. The estimated size of the binding sites of SSBs are dependent on the salt concentration in fluorescence titrations with poly(dT). *Ec*SSB mainly binds to 35- and 65-nucleotide (nt)-long ssDNA, using the $(SSB)_{35}$- and $(SSB)_{65}$-binding modes, respectively. In the $(SSB)_{35}$-binding mode, 2 subunits of the *Ec*SSB tetramer interact with ssDNA, whereas in the $(SSB)_{65}$-binding mode, all 4 subunits participate in ssDNA binding. These different binding modes of SSB may be required during different stages of DNA metabolism [28, 29].

In the present study, we examined the electrophoretic mobility shift patterns of *Salmonella enterica* serovar Typhimurium LT2 SSB (*St*SSB) bound to different length ssDNA. The expectation of EMSA is that, once the length of the nucleotides is sufficient for the binding of two or more SSB tetramers, the electrophoretic mobility of the higher SSB oligomeric tetramers will be lower than that of the smaller SSB oligomeric tetramers. Furthermore, we also studied the binding properties of *St*SSB between low- and high-salt conditions by using fluorescence quenching measurements. On the basis of these biophysical analyses, the ssDNA binding-mode of *St*SSB is discussed.

2 Materials and Methods

2.1 Materials

All restriction enzymes and DNA-modifying enzymes were purchased from New England Biolabs (Ipswich, MA, USA) unless explicitly stated otherwise. All chemicals were purchased from Sigma–Aldrich (St. Louis, MO, USA) unless explicitly stated otherwise. The *E. coli* strains TOP10F′ (Invitrogen, USA) and BL21(DE3)pLysS (Novagen, UK) were used for genetic construction and protein expression, respectively.

2.2 Cloning, Expression and Purification

The gene *STM4256* encoding the *St*SSB was PCR-amplified from *S. typhimurium* genomic DNA [19]. The forward (5′-CTGAACATATGGCCAGCAGAGGCGTAA-3′) and the reverse (5′-TGGAACTCGAGGAACGGAATGTCG TCG-3′) primers were designed to introduce unique NdeI and XhoI restriction sites (underlined) into *St*SSB, permitting the insertion of the amplified gene into the pET21b vector (Novagen Inc., Madison, WI, USA) for the protein expression in *E. coli*. *E. coli* cells were transformed with the expression vector and grown to OD_{600} of 0.9 at 37 °C in Luria–Bertani medium containing 250 μg/ml ampicillin [12, 38]. Overexpression of *St*SSB construct was induced with 1 mM isopropyl thiogalactoside (IPTG) for 3 h at 37 °C. The cells overexpressing the protein were chilled on ice, harvested by centrifugation, resuspended in Buffer A (20 mM Tris–HCl, 5 mM imidazole, 0.5 M NaCl; pH 7.9) and disrupted by sonication with ice cooling between pulses. The *St*SSB protein was then purified from the soluble supernatant by Ni^{2+}-affinity chromatography (HiTrap HP; GE Healthcare Bio-Sciences, Piscataway, NJ, USA). Protein purity remained greater than 95% as determined by Coomassie-stained SDS–PAGE.

2.3 Gel-Filtration Chromatography

Gel-filtration chromatography was carried out by the same protocol as previously described for DnaD using an AKTA-FPLC system [10]. Briefly, purified *St*SSB in buffer (0.1 M NaCl and 20 mM Tris–HCl at pH 8.0) was applied to a Superdex 200 HR 10/30 column (GE Healthcare Bio-Sciences, Piscataway, NJ, USA) equilibrated with the same buffer. The column was operated at a flow rate of 0.5 mL/min, and 0.5-mL fractions were collected. The proteins were detected by measuring absorbance at 280 nm. The column was calibrated with proteins of known molecular masses: γ-globulin (158 kDa), albumin (67 kDa), ovalbumin (43 kDa), chymotrypsinogen A (25 kDa), and ribonuclease A (13.7 kDa).

2.4 Fluorescence Measurement

Fluorescence titrations were carried out in a spectrofluorimeter (Hitachi F-2700; Hitachi High-Technologies, Tokyo, Japan) as described previously [2, 4, 12, 25]. The excitation and emission of tryptophan fluorescence were detected at 295 and 348 nm, respectively. The *St*SSB solution (0.1 μM; tetramer) in 2 mL Tris–HCl buffer (20 mM Tris–HCl, and pH 8.0) containing 20 mM or 300 mM NaCl was titrated with rising quantities of dT50 oligonucleotide. After the addition of the ssDNA, the complex solution was equilibrated for 300 s until no fluorescence change could be observed. The tryptophan fluorescence quenching is used to measure the diminution of fluorescence between the ssDNA-free and the

ssDNA-bound proteins. The ssDNA-binding site size (n) was analyzed by the ssDNA-binding curve using the model of Schwarz and Watanabe [33].

2.5 Gel Shifts

Various lengths of ssDNA oligonucleotides were custom synthesized by MdBio, Inc., Frederick, MD. Radiolabeling was carried out with [γ^{32}P]ATP (6,000 Ci/mmol; Perkin-Elmer Life Sciences) and T4 polynucleotide kinase (Promega, Madison, WI, USA). *St*SSB (0, 19, 37, 77, 155, 310, 630, 1,250, 2,500, and 5,000 nM) was incubated for 30 min at 25 °C with 1.7 nM DNA substrates (dT15–75) in a total volume of 10 µL in 20 mM Tris–HCl pH 8.0 and 100 mM NaCl. Aliquots (5 µL) were removed from each reaction solution and added to 2 µL of gel-loading solution (0.25% bromophenol blue and 40% sucrose). The resulting samples were resolved on a native 8% polyacrylamide gel at 4 °C in TBE buffer (89 mM Tris borate and 1 mM EDTA) for 1 h at 100 V and visualized by autoradiography. Complexed and free DNA bands were scanned and quantified. The binding dissociation constants for the *St*SSB-ssDNA complex 1 (K_{d1}) were estimated from the protein concentration that binds 50% of the input DNA [6, 9, 11, 12, 15, 18]; the binding dissociation constants for the *St*SSB-ssDNA complex 2 (K_{d2}) were estimated from the protein concentration that forms 50% of the complex 2; the binding dissociation constants for the *St*SSB-ssDNA complex 3 (K_{d3}) were estimated from the protein concentration that forms 50% of the complex 3. In this report, each K_d is calculated as the average of at least three measurements ±S.D.

3 Results

3.1 Sequence Analysis

The gene *STM4256*, encoding *S. typhimurium* SSB, was initially found using a database search through the National Center for Biotechnology Information (NCBI). Based on the known nucleotide sequence, the predicted *St*SSB monomer protein has a length of 176 amino acid residues and a molecular mass of 19 kDa. Analysis of the primary structure of *St*SSB by RPS-BLAST [17] revealed the presence of a putative OB-fold domain that is common in all known SSBs. Figure 1 shows an alignment of the amino acid sequences of *S. typhimurium*, *E. coli* [32], *Mycobacterium tuberculosis* [30], *Mycobacterium smegmatis* [31], *Helicobacter pylori* [1], and *Pseudomonas aeruginosa* PAO1 SSBs [12]. In the *Ec*SSB–ssDNA complex [26], 4 essential aromatic residues, Trp40, Trp54, Phe60, and Trp88, participate in ssDNA binding via stacking interactions. These residues are conserved in most SSB families as Phe/Tyr/Trp, and the corresponding residues in *St*SSB are Trp41, Trp55, Phe61, and Trp89. The C-terminal tail of SSBs containing several acidic residues, such as "DDDIPF" in *Ec*SSB, is also conserved in *St*SSB. In contrast to those motifs, 3 glycine residues in the glycine-rich hinge of *Ec*SSB (Gly125, Gly128, and Gly129) are not found in *St*SSB.

3.2 Oligomerization of *St*SSB in Solution

Analysis of purified protein by gel filtration chromatography revealed a single peak (Fig. 2). Assuming that *St*SSB has a shape and partial specific volume similar to the

```
StSSB   MASRGVNKVILVGNLGQDPEVRYMPSGGAVANLTLATSESWRDKQTGEMKE-QTEWHRVVMF  61
EcSSB   MASRGVNKVILVGNLGQDPEVRYMPNGGAVANITLATSESWRDKATGEMKE-QTEWHRVVLF  61
MtSSB   --MAGDTTITIVGNLTADPELRFTPSGAAVANFTVASTPRIYDRQTGEWKDGEALFLRCNIW  60
MsSSB   --MAGDTTITVVGNLTADPELRFTPSGAAVANFTVASTPRMFDRQSGEWKDGEALFLRCNIW  60
HpSSB   ----MFNKVIMVGRLTRNVELKYLPSGSAAATIGLATSRRFK-KQDGTLGE-EVCFIDARLF  56
PaSSB   -MARGVNKVILVGNVGGDPETRYMPNGNAVTNITLATSESWKDKQTGQQQE-RTEWHRVVFF  60

StSSB   GKLAEVAGEYLRKGSQVYIEGQLRTRKWTDQSGQERYTTEINVPQIGGVMQMLGGRQGGGAP 123
EcSSB   GKLAEVASEYLRKGSQVYIEGQLRTRKWTDQSGQDRYTTEV-VVNVGGTMQMLGGRQGGGAP 122
MtSSB   REAAENVAESLTRGARVIVSGRLKQRSFETREGEKRTVIEVEVDEIGPSLRYATAKVNKASR 122
MsSSB   REAAENVAESLTRGSRVIVTGRLKQRSFETREGEKRTVVEVEVDEIGPSLRYATAKVNKASR 122
HpSSB   GRTAEIANQYLSKGSSVLIEGRLTYESWMDQTGKKNSRHTITADSLQFMDKKSDNPQANAMQ 118
PaSSB   GRLAEIAGEYLRKGSQVYVEGSLRTRKWQGQDGQDRYTTEI-VVDINGNMQLLGGR-----P 119

StSSB   AG------GQQQGGWGQPQQPQQPQGGNQFSGGAQSRPQQSAP-APSNEPPMD-FDDDIPF  176
EcSSB   AGGNI-GGGQPQGGWGQPQQ---PQGGNQFSGGAQSRPQQSAPAAPSNEPPMD-FDDDIPF  178
MtSSB   SGG---FGSGSRPAPAQTS----------------SASGDDPWGSAPASGSFGGGDDEPPF  164
MsSSB   SGG---GGGGFGSGGGGSRQ----------------SEPKDDPWGSAPASGSFSGADDEPPF  165
HpSSB   DSIMHENSNNAYPANHNAPSQDPFNQAYAQNAYAKENLQAQPSKYQNSVPEINIDEEEIPF  179
PaSSB   SG------DDSQRAPREPMQ--RPQQAPQQ----QSRPAPQQQPAPQPAQDYDSFDDDIPF  165
```

Fig. 1 Multiple amino acid sequence alignment of SSB proteins. Sequence alignment of *St*SSB, with other SSB proteins from *E. coli* (*Ec*SSB), *Mycobacterium tuberculosis* (*Mt*SSB), *Mycobacterium smegmatis* (*Ms*SSB), *Helicobacter pylori* (*Hp*SSB), and *Pseudomonas aeruginosa* PAO1 (*Pa*SSB), was generated by CLUSTALW2 [14]. Amino acid residues displaying 100% identity are highlighted in *bold black*, and those displaying similarity are highlighted in *black*

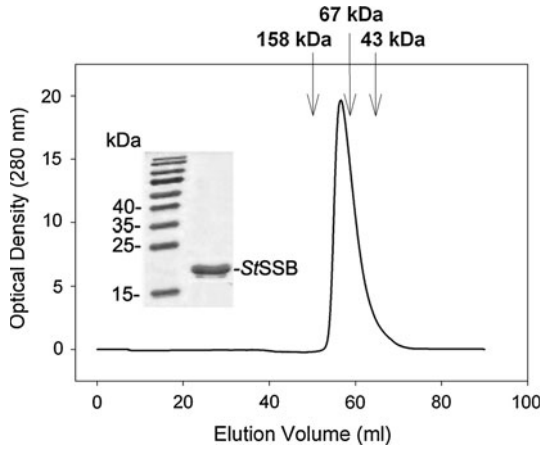

Fig. 2 Gel-filtration chromatographic analysis of *St*SSB. Purified *St*SSB protein in buffer (0.1 M NaCl and 20 mM Tris–HCl at pH 8.0) was applied to a Superdex 200 HR 10/30 column equilibrated with the same buffer. The proteins were detected by measuring absorbance at 280 nm. The column was calibrated with proteins of known molecular masses: γ-globulin (158 kDa), albumin (67 kDa), ovalbumin (43 kDa), chymotrypsinogen A (25 kDa), and ribonuclease A (13.7 kDa). The sizes of the molecular mass markers (in kDa) are indicated at the *top*. The corresponding peak shows the eluted *St*SSB. Coomassie Blue-stained SDS–PAGE (12%) of the purified *St*SSB and molecular mass standards are also shown. The sizes of the standard proteins, from the *top down*, are as follows: 170, 130, 100, 70, 55, 40, 35, 25, and 15 kDa. The purified *St*SSB migrated between the 25 and 15 kDa standards on the SDS–PAGE

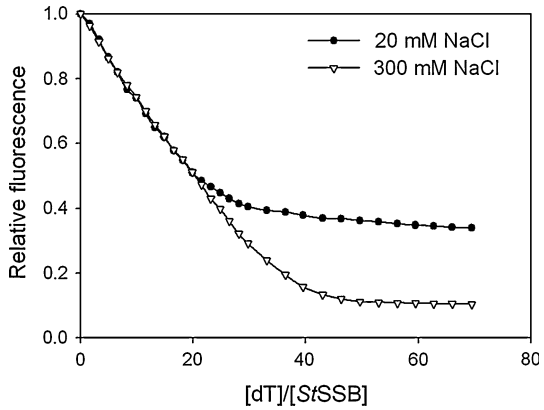

Fig. 3 Fluorescence titration of *St*SSB with ssDNA dT50. The excitation and emission of tryptophan fluorescence were detected at 295 and 348 nm, respectively. The *St*SSB solution (0.1 μM; tetramer) in 2 mL Tris–HCl buffer (20 mM Tris–HCl, and pH 8.0) containing 20 or 300 mM NaCl was titrated with rising quantities of dT50 oligonucleotide. After the addition of the ssDNA, the complex solution was equilibrated for 300 s until no fluorescence change could be observed. Tryptophan fluorescence quenching of *St*SSB in the presence of 20 mM (*filled circle*) or 300 mM NaCl (*open triangle*), is shown

standard proteins, the native molecular mass of *St*SSB was estimated to be ~80 kDa. The native molecular mass for *St*SSB is approximately 4.1 times the molecular mass of a *St*SSB monomer (19 kDa). Thus, we concluded that *St*SSB in solution is a stable tetramer, similar to *Ec*SSB.

3.3 DNA Binding Monitored by Quenching of Intrinsic Tryptophan Fluorescence

It is well established that the fluorescence quench and the estimated size of the binding sites of SSBs depend on the salt concentration of the SSB solution [16]. *St*SSB has 3 tryptophan residues (Trp41, Trp55, and Trp89) in the OB-fold domain, allowing an analysis of ssDNA binding by tryptophan fluorescence quenching (Fig. 3). The protein displayed strong intrinsic fluorescence with a peak wavelength of 348 nm when excited at 295 nm, consistent with tryptophan fluorescence (data not shown). As dT50 was titrated into the *St*SSB solution, the intrinsic fluorescence of the protein was progressively quenched. On addition of a saturating quantity of ssDNA in the presence of 20 and 300 mM NaCl, the intrinsic fluorescence at 348 nm was quenched by 66 and 90%, respectively. The estimated binding-site sizes of *St*SSB in 20 and 300 mM NaCl were about of 23 ± 2 nt and 36 ± 2 nt, respectively.

3.4 *St*SSB Binding to dT20–40 Forms a Single Complex

To investigate the length of nucleotides sufficient for the formation of the *St*SSB-ssDNA complex and the ssDNA-binding ability of *St*SSB, we studied the binding of *St*SSB to dT15 (Fig. 4a), dT20 (Fig. 4b), dT25 (Fig. 4c), dT30 (Fig. 4d), dT35 (Fig. 4e), and dT40 (Fig. 4f) with different protein concentrations using EMSA. As shown in Fig. 4a, a band shift was observed when *St*SSB was incubated with dT15. Because some significant smears were observed, it appears that *St*SSB interacts with dT15, but it could not form a very stable complex with dT15 during electrophoresis. It is considered that dT15 is too short to form a stable complex with *St*SSB. In contrast to dT15, longer dT homopolymers, dT20–40, bind to *St*SSB and form a single complex (Fig. 4b–f). Thus, the EMSA results suggest that the length of ssDNA required for *St*SSB binding ranges between 15 to 20 nt.

3.5 Two Different Complexes are Formed When *St*SSB Binds to dT45–60

To examine the minimal nucleotide length necessary for the binding of a second *St*SSB tetramer to ssDNA pre-bound to *St*SSB, we studied the binding of *St*SSB to longer dT homopolymers of 45–60 nt (Fig. 5). Although dT45 is only 5 nt longer than dT40, the pattern of the *St*SSB-ssDNA complexes observed using EMSA is very different. At lower protein concentrations, *St*SSB forms a single

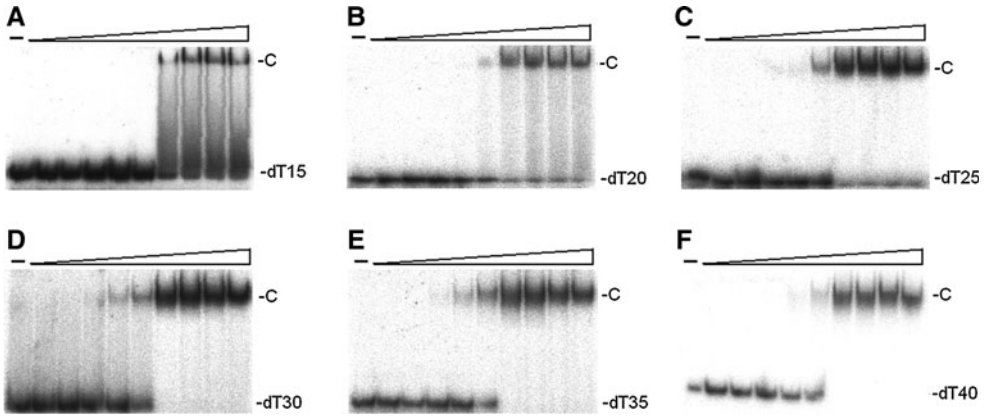

Fig. 4 Binding of *St*SSB to dT15–40. *St*SSB (0, 19, 37, 77, 155, 310, 630, 1,250, 2,500, and 5,000 nM) was incubated for 30 min at 25 °C with 1.7 nM of **a** dT15, **b** dT20, **c** dT25, **d** dT30, **e** dT35, or **f** dT40 in a total volume of 10 μL in 20 mM Tris–HCl pH 8.0 and 100 mM NaCl. Aliquots (5 μL) were removed from each reaction solution and added to 2 μL of gel-loading solution (0.25% bromophenol blue and 40% sucrose). The resulting samples were resolved on a native 8% polyacrylamide gel at 4 °C in TBE buffer (89 mM Tris borate and 1 mM EDTA) for 1 h at 100 V and visualized by autoradiography

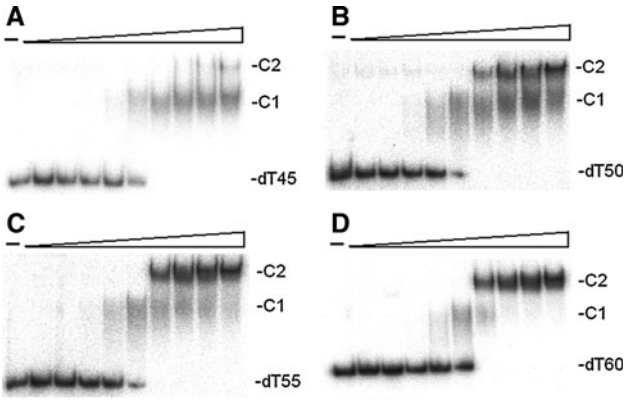

Fig. 5 Binding of *St*SSB to dT45–60. *St*SSB (0, 19, 37, 77, 155, 310, 630, 1,250, 2,500, and 5,000 nM) was incubated for 30 min at 25 °C with 1.7 nM of **a** dT45, **b** dT50, **c** dT55, or **d** dT60 in a total volume of 10 μL in 20 mM Tris–HCl pH 8.0 and 100 mM NaCl. Aliquots (5 μL) were removed from each reaction solution and added to 2 μL of gel-loading solution (0.25% bromophenol blue and 40% sucrose). The resulting samples were resolved on a native 8% polyacrylamide gel at 4 °C in TBE buffer (89 mM Tris borate and 1 mM EDTA) for 1 h at 100 V and visualized by autoradiography

complex with dT45 (Fig. 5a), similar to that observed with dT40 (Fig. 4f); however, when the *St*SSB concentration is increased, another slower-migrating complex appears. The appearance of the second complex results from the increasing *St*SSB concentration, which suggests that it may contain at least 2 *St*SSB tetramers per oligonucleotide. As the minimal length of ssDNA required for *St*SSB binding ranges between 15 to 20 nt (see above), the presence of an extra 5 nt in dT45, as compared with dT40, provides enough interaction space for the binding of a second *St*SSB tetramer, which occupies around 22 nt ssDNA. Furthermore, the stoichiometry of the 2 *St*SSB tetramers bound per ssDNA did not change when the length of the dT homopolymers was further increased to 60 nt (Fig. 5d).

3.6 *St*SSB Binding to dT65–75 Forms Three Distinct Complexes

To examine the minimal nucleotide length necessary for the binding of a third *St*SSB tetramer to ssDNA already bound by 2 *St*SSB tetramers, we studied the binding of *St*SSB to dT65–75 (Fig. 6). Although dT65 is only 5 nt longer than dT60, *St*SSB binding to dT65 forms 3 distinct complexes (Fig. 6a), unlike the binding of *St*SSB to dT60 which only forms 2 complexes (Fig. 5d). Taken together with these results from EMSA, the length of ssDNA required for efficient binding of *St*SSB is 22 ± 1 nt (Fig. 7).

3.7 The Binding Constants of the *St*SSB-ssDNA Complexes

The binding constants of the *St*SSB-ssDNA complexes (K_d values) are summarized in Table 1. The formation of the *St*SSB-ssDNA complex 1 (C1) is ssDNA-length independent (Fig. 7a), suggesting that the protein-DNA contact for each C1 is similar. In contrast, the ability of a second (the K_{d2} value) or a third (the K_{d3} value) *St*SSB tetramer to bind to ssDNA already bound by *St*SSB tetramer(s) was length-dependent (Fig. 7a). In fact, increases in ssDNA length were associated with higher binding ability (lower K_{d2} value), indicating that the second *St*SSB or the third *St*SSB prefers to bind to long ssDNA segments to which *St*SSB tetramer(s) is already bound.

4 Discussion

In this study, we described the cloning, expression, purification, and characterization of SSB from *Salmonella*

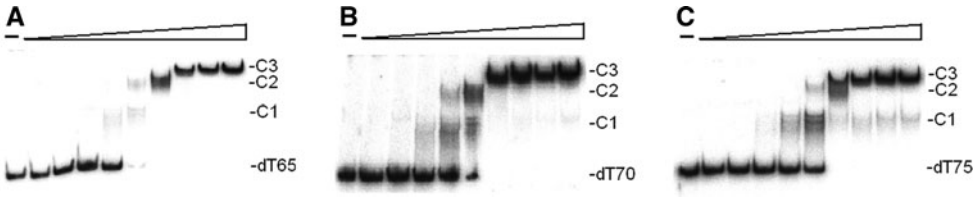

Fig. 6 Binding of *St*SSB to dT65–75. *St*SSB (0, 19, 37, 77, 155, 310, 630, 1,250, 2,500, and 5,000 nM) was incubated for 30 min at 25 °C with 1.7 nM of **a** dT65, **b** dT70, or **c** dT75 in a total volume of 10 µL in 20 mM Tris–HCl pH 8.0 and 100 mM NaCl. Aliquots (5 µL) were removed from each reaction solution and added to 2 µL of gel-loading solution (0.25% bromophenol blue and 40% sucrose). The resulting samples were resolved on a native 8% polyacrylamide gel at 4 °C in TBE buffer (89 mM Tris borate and 1 mM EDTA) for 1 h at 100 V and visualized by autoradiography

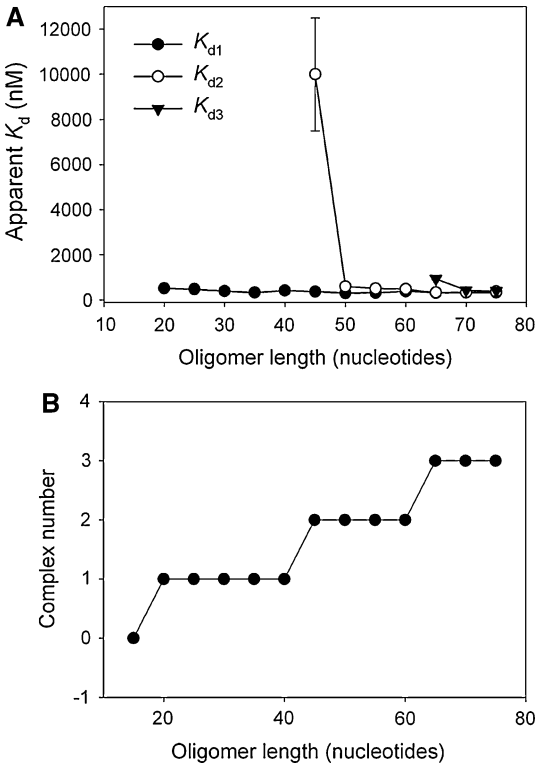

Fig. 7 **a** Apparent K_d values of *St*SSB as a function of the length of the ssDNA; K_{d1}, K_d for the formation of the first complex (C1); K_{d2}, K_d for the formation of the second complex (C2). K_{d3}, K_d for the formation of the third complex (C3). **b** Complex number of *St*SSB as a function of the length of the ssDNA determined using EMSA

Table 1 ssDNA-binding parameters of *St*SSB

	*St*SSB			
	K_{d1} (nM)	K_{d2} (nM)	K_{d3} (nM)	Complex number
dT15				0
dT20	520 ± 40			1
dT25	480 ± 30			1
dT30	400 ± 30			1
dT35	330 ± 30			1
dT40	420 ± 50			1
dT45	370 ± 50	10,000 ± 2,500		2
dT50	310 ± 40	600 ± 50		2
dT55	320 ± 40	510 ± 30		2
dT60	390 ± 50	490 ± 40		2
dT65	320 ± 70	330 ± 40	940 ± 60	3
dT70	330 ± 40	340 ± 30	430 ± 30	3
dT75	330 ± 30	390 ± 50	400 ± 30	3

Each K_d is calculated as the average of at least three measurements ±SD

enterica serovar Typhimurium LT2, which is the leading cause of human gastroenteritis and is used in generating a mouse model of human typhoid fever [19, 20, 35, 36]. Sequence analysis (Fig. 1) indicates that the *St*SSB monomer possesses an OB-fold domain at its N-terminus and a flexible tail at its C-terminus, as in *Ec*SSB. Analysis of *St*SSB by using gel filtration chromatography showed that the protein forms a tetramer in solution (Fig. 2).

We showed that the binding of *St*SSB to dT50 results in tryptophan fluorescence quenching (Fig. 3). In the presence of 20 and 300 mM NaCl, the binding site sizes of *St*SSB were 23 ± 2 nt and 36 ± 2 nt per tetramer, respectively; 2 distinct binding modes could be observed between low- and high-salt conditions, as observed in *Ec*SSB. In the case of *Ec*SSB, under high-salt conditions, a 65-nt ssDNA binds to each *Ec*SSB tetramer with almost 90% fluorescence quench; under low-salt conditions, a 35-nt ssDNA exhibits 53% fluorescence quench. In the case of *Hp*SSB, the stoichiometry was 25 ± 2 nt per homotetramer [1], but the salt effect on its ssDNA-binding mode(s) remains unclear. Human replication protein A, a eukaryotic SSB, binds to DNA noncooperatively and has a binding site of 20–30 nt per heterotrimer under most conditions [23, 42]. The constant binding mode (or "salt-independent" binding mode) of SSB determined using fluorescence quench at high- and low-salt concentrations has also been reported in SSBs from the *Thermus/Deinococcus* group [41], *Thermotoga maritima* [24], *Thermotoga neapolitana* [24], *Thermoanaerobacter tengcongensis* [25], and *Pseudomonas aeruginosa* PAO1 [12], possibly because of its low flexibility and/or low number of glycine residues [12, 24]. In fact, 8

glycine residues in the glycine-rich hinge that are found in *Ec*SSB are not found in *Pa*SSB (Fig. 1). The amino acid sequences of *St*SSB and *Ec*SSB share >80% identity, suggesting the presence of multiple binding modes, even though 3 glycine residues in the glycine-rich hinge of *Ec*SSB (Gly125, Gly128, and Gly129) are not found in *St*SSB. However, this speculation must be confirmed by further biochemical experiments.

Many SSBs bind to ssDNA with some degree of positive cooperativity. The EMSA approach used here allowed us to observe the formation of distinct complexes and to determine the ssDNA binding mode of *St*SSB. The EMSA results indicate that *St*SSB binds to short ssDNAs (dT20–40) to form a complex in which a single tetramer is bound to the ssDNA (Fig. 4), 2 tetramers are bound to dT45–60 (Fig. 5), and 3 tetramers are bound to dT65–75 (Fig. 6). Thus, the apparent binding-site size of *St*SSB is 22 ± 1 nt (Fig. 7). In the case of *St*SSB, binding appears to be noncooperative, for several DNAs, because essentially all the DNA shifts into the fist complex (C1) before the appearance of the second (C2) or third complex (C3). In addition, the apparent K_d values are of the first, second, and third complex, as expected for noncooperative binding (Table 1; Fig. 7); for positive cooperative binding, K_{d3} and/or K_{d2} should be less than K_{d1}. Increasing the length of C3 or C2 causes its K_d value to match that of C1 (Fig. 7a), suggesting that length dependence reflects the minimal amount of spacing that is optimal for steric considerations.

Acknowledgments We thank Ms. Hui-Chuan Hsieh for constructing the pET21b-*St*SSB. This research was supported a grant from the National Research Program for Genome Medicine (NSC 99-3112-B-040-001 to C.Y. Huang).

References

1. Chan KW, Lee YJ, Wang CH, Huang H, Sun YJ (2009) J Mol Biol 388:508–519
2. Chen CC, Huang CY (2011) Protein J. doi:10.1007/s10930-010-9302-0
3. Curth U, Genschel J, Urbanke C, Greipel J (1996) Nucleic Acids Res 24:2706–2711
4. Curth U, Greipel J, Urbanke C, Maass G (1993) Biochemistry 32:2585–2591
5. Dabrowski S, Olszewski M, Piatek R, Brillowska-Dabrowska A, Konopa G, Kur J (2002) Microbiology 148:3307–3315
6. Fairall L, Buttinelli M, Panetta G (2000) Bandshift, gel retardation or electrophoretic mobility shift assays. In: Travers A, Buckle M (eds) DNA-protein interactions: a practical approach. Oxford University Press, New York, pp 65–74
7. Fedorov R, Witte G, Urbanke C, Manstein DJ, Curth U (2006) Nucleic Acids Res 34:6708–6717
8. Haseltine CA, Kowalczykowski SC (2002) Mol Microbiol 43:1505–1515
9. Hsieh HC, Huang CY (2011) Biochem Biophys Res Commun 404:546–551
10. Huang CY, Chang YW, Chen WT (2008) Biochem Biophys Res Commun 375:220–224
11. Huang CY, Hsu CH, Sun YJ, Wu HN, Hsiao CD (2006) Nucleic Acids Res 34:3878–3886
12. Jan HC, Lee YL, Huang CY (2011) Protein J doi:10.1007/s10930-010-9297-6
13. Kerr ID, Wadsworth RI, Cubeddu L, Blankenfeldt W, Naismith JH, White MF (2003) EMBO J 22:2561–2570
14. Larkin MA, Blackshields G, Brown NP, Chenna R, McGettigan PA, McWilliam H, Valentin F, Wallace IM, Wilm A, Lopez R, Thompson JD, Gibson TJ, Higgins DG (2007) Bioinformatics 23:2947–2948
15. Liu JH, Chang TW, Huang CY, Chen SU, Wu HN, Chang MC, Hsiao CD (2004) J Biol Chem 279:50465–50471
16. Lohman TM, Ferrari ME (1994) Annu Rev Biochem 63:527–570
17. Madden TL, Tatusov RL, Zhang J (1996) Methods Enzymol 266:131–141
18. Matos RG, Barbas A, Arraiano CM (2010) Protein J 29:394–397
19. McClelland M, Sanderson KE, Spieth J, Clifton SW, Latreille P, Courtney L, Porwollik S, Ali J, Dante M, Du F, Hou S, Layman D, Leonard S, Nguyen C, Scott K, Holmes A, Grewal N, Mulvaney E, Ryan E, Sun H, Florea L, Miller W, Stoneking T, Nhan M, Waterston R, Wilson RK (2001) Nature 413:852–856
20. Meltzer E, Schwartz E (2010) Curr Opin Infect Dis 23:432–437
21. Murzin AG (1993) EMBO J 12:861–867
22. Naue N, Fedorov R, Pich A, Manstein DJ, Curth U (2010) Nucleic Acids Res. doi:10.1093/nar/gkq988
23. Oakley GG, Patrick SM (2010) Front Biosci 15:883–900
24. Olszewski M, Grot A, Wojciechowski M, Nowak M, Mickiewicz M, Kur J (2010) BMC Microbiol 10:260
25. Olszewski M, Mickiewicz M, Kur J (2008) Arch Microbiol 190:79–87
26. Raghunathan S, Kozlov AG, Lohman TM, Waksman G (2000) Nat Struct Biol 7:648–652
27. Reyes-Lamothe R, Sherratt DJ, Leake MC (2010) Science 328:498–501
28. Roy R, Kozlov AG, Lohman TM, Ha T (2007) J Mol Biol 369:1244–1257
29. Roy R, Kozlov AG, Lohman TM, Ha T (2009) Nature 461:1092–1097
30. Saikrishnan K, Jeyakanthan J, Venkatesh J, Acharya N, Sekar K, Varshney U, Vijayan M (2003) J Mol Biol 331:385–393
31. Saikrishnan K, Manjunath GP, Singh P, Jeyakanthan J, Dauter Z, Sekar K, Muniyappa K, Vijayan M (2005) Acta Crystallogr D Biol Crystallogr 61:1140–1148
32. Savvides SN, Raghunathan S, Futterer K, Kozlov AG, Lohman TM, Waksman G (2004) Protein Sci 13:1942–1947
33. Schwarz G, Watanabe F (1983) J Mol Biol 163:467–484
34. Shereda RD, Kozlov AG, Lohman TM, Cox MM, Keck JL (2008) Crit Rev Biochem Mol Biol 43:289–318
35. Tischler AD, McKinney JD (2010) Curr Opin Microbiol 13:93–99
36. Tsolis RM, Young GM, Solnick JV, Baumler AJ (2008) Nat Rev Microbiol 6:883–892
37. Wadsworth RI, White MF (2001) Nucleic Acids Res 29:914–920
38. Wang CC, Tsau HW, Chen WT, Huang CY (2010) Protein J 29:445–452
39. Witte G, Fedorov R, Curth U (2008) Biophys J 94:2269–2279
40. Witte G, Urbanke C, Curth U (2003) Nucleic Acids Res 31:4434–4440
41. Witte G, Urbanke C, Curth U (2005) Nucleic Acids Res 33:1662–1670
42. Wold MS (1997) Annu Rev Biochem 66:61–92

Protein J (2011) 30:59–65
DOI 10.1007/s10930-010-9302-0

Inhibition of *Klebsiella Pneumoniae* DnaB Helicase by the Flavonol Galangin

Cheng-Chieh Chen · Cheng-Yang Huang

Published online: 7 January 2011
© Springer Science+Business Media, LLC 2010

Abstract *Klebsiella pneumoniae* is a ubiquitous opportunistic pathogen that colonizes at the mucosal surfaces in humans and causes severe diseases. Many clinical strains of *K. pneumoniae* are highly resistant to antibiotics. Here, we used fluorescence quenching to show that the flavonols galangin, myricetin, quercetin, and kaempferol, bearing different numbers of hydroxyl substituent on the aromatic rings, may inhibit dNTP binding of the primary replicative DnaB helicase of *K. pneumoniae* (*Kp*DnaB), an essential component of the cellular replication machinery critical for bacterial survival. The binding affinity of *Kp*DnaB to dNTPs varies in the following order: dCTP ~ dGTP > dTTP > dATP. Addition of 10 μM galangin significantly decreased the binding ability of *Kp*DnaB to dATP, whereas the binding affinity of *Kp*DnaB to dGTP that was almost unaffected. Our analyses suggest that these flavonol compounds may be used in the development of new antibiotics that target *K. pneumoniae* and other bacteria.

Keywords Flavonol · Galangin · DnaB helicase · *Klebsiella pneumoniae*

Abbreviations

Kp	*Klebsiella pneumoniae*
K_d	The dissociation constant
dsDNA	Double-stranded DNA
ssDNA	Single-stranded DNA
Myr	Myricetin
Que	Quercetin
Kae	Kaempferol
Gal	Galangin

C.-C. Chen · C.-Y. Huang (✉)
Department of Biomedical Sciences, Chung Shan Medical University, No.110, Sec.1, Chien-Kuo N. Rd., Taichung, Taiwan
e-mail: cyhuang@csmu.edu.tw

C.-Y. Huang
Department of Medical Research, Chung Shan Medical University Hospital, No.110, Sec.1, Chien-Kuo N. Rd., Taichung, Taiwan

1 Introduction

DNA helicases are motor proteins essential for DNA replication, repair, and recombination [8, 15, 16, 18]. During DNA replication, the leading strand is directly synthesized by DNA polymerase. On the lagging strand, the primase interacts with the hexameric helicase to synthesize short RNA primers. These primers are used to generate the Okazaki fragments necessary for progression of the replication fork. The most widely studied replicative helicase is *Escherichia coli* DnaB helicase (*Ec*DnaB) [1, 21]. *Ec*DnaB is a multifunctional ATPase that catalyzes the unwinding of double-stranded DNA (dsDNA) into single-stranded DNA (ssDNA) intermediates at the replication fork to provide ssDNA templates for DNA polymerases [21]. Recently, we resolved the three-dimensional structures of the *Geobacillus kaustophilus* DnaB-family protein both in the apo state and complexed it with ssDNA and the non-hydrolysable NTP ATPγs, and showed that ATP hydrolysis may drive the movement of the helicase toward the 3′ end of the lagging strand [13].

Klebsiella pneumoniae (*Kp*) is a ubiquitous opportunistic pathogen that colonizes at the mucosal surfaces in humans and causes severe diseases such as septicemia, pneumonia, urinary tract infections, and soft tissue infections [17].

Despite advances in treatment and prevention, *K. pneumoniae* still poses a major threat to public health worldwide. Although *K. pneumoniae* strains are generally susceptible to some antibiotics, such as cephalosporins, many clinical strains of *K. pneumoniae* are highly resistant to antibiotics. Currently, few therapies are effective against these extended-spectrum β-lactamase (ESBL)-producing *K. pneumoniae* strains [7, 30]. Discovering virulence factors and identifying novel targets for drug development and new therapies against *K. pneumonia* are critical for public health [4, 27, 29]. Since DnaB is required for DNA replication, blocking the activity of DnaB would be detrimental to bacterial survival [22]. Because of the distinct differences between eukaryotic and prokaryotic DnaB-like helicases [21, 22], the *K. pneumoniae* DnaB helicase may be a promising target in developing antibiotics.

Flavonoids are the most common group of plant polyphenols, and are responsible for much of the flavor and color of fruits and vegetables [19]. To date, over 5,000 different flavonoids have been described; many of these compounds display structure-dependent biological and pharmacological activities [19, 23, 26]. The 6 major subclasses of flavonoids are: flavonols, flavones, flavanones, catechins (flavanols), anthocyanidins, and isoflavones [19]. Flavonols are polyphenol compounds with in vitro antioxidant and anti-radical activity [3, 26], as well as antibacterial activity [5]. A flavonol is composed of 2 aromatic rings linked by a heterocyclic pyran-4-one ring.

In this study, we have cloned, expressed, and purified *Kp*DnaB, and found that the 4 flavonols (Fig. 1) myricetin (Myr), quercetin (Que), kaempferol (Kae), and galangin (Gal) can interact with *Kp*DnaB and prevent dNTP binding. These flavonols may be potential leads in anti-*Kp* drug development.

2 Materials and Methods

2.1 Materials

All restriction enzymes and DNA-modifying enzymes were purchased from New England Biolabs (Ipswich, MA, USA) unless explicitly stated otherwise. All custom oligonucleotide primers were obtained from Invitrogen Corporation (Carlsbad, CA, USA). All chemicals were purchased from Sigma–Aldrich (St. Louis, MO, USA) unless explicitly stated otherwise.

2.2 Construction of the *Kp*DnaB Expression Plasmid

KPN04439, the gene encoding the putative *Kp*DnaB, was amplified by PCR using genomic DNA of *K. pneumoniae* subsp. *pneumoniae* MGH 78578 as the template. The forward (5′-GGGGAATTCACAGCACAATCCCAGGTATTGAAA-3′) and the reverse (5′-GGGAAGCTTCTCATCATCATACTGAGGACCGGC-3′) primers were designed to introduce unique *Eco*RI and *Hind*III restriction sites (underlined) into *Kp*DnaB, permitting the insertion of the amplified gene into the pET21e vector. The pET21e vector was engineered from the pET21b vector (Novagen Inc., Madison, WI, USA), to avoid having the *N*-terminal T7 tag fused with the gene product [24]. Briefly, the region containing the *Nhe*I site of the pET21b vector (CATATGGCTAGC) was mutated to introduce a new *Eco*RI site (CATATGGAATTC) by using the primers E1 (5′-AAGGAGATATACATATGGAATTCATGACTGGTGGACAG-3′) and E1′ (5′-TGCTGTCCACCAGTCATGAATTCCATATGTATATCTCCT-3′). The resultant plasmid was digested with *Eco*RI to remove the DNA fragment spanning from the original *Nhe*I site to the *Eco*RI site, and then religated onto itself at the *Eco*RI site to generate the expression vector pET21e. The *Kp*DnaB DNA fragment was then inserted into pET21e to produce the plasmid pET21e-*Kp*DnaB for *Kp*DnaB expression. Therefore, the expected gene product expressed by pET21e-*Kp*DnaB will have 2 additional artificial residues, EF, introduced by the *Eco*RI site located at the *N*-terminus, and a *C*-terminal His tag (KLAAALEHHHHHH), useful for purifying the recombinant protein.

2.3 Protein Expression and Purification

Recombinant *Kp*DnaB protein was expressed and purified using the same protocol as described previously for the protein PriB [10], with a minor modification. Briefly, *E. coli* BL21(DE3) cells were transformed with the wild-type pET21e-*Kp*DnaB plasmid and grown to 0.9 OD_{600} at 37 °C in Luria–Bertani medium containing 250 μg/mL

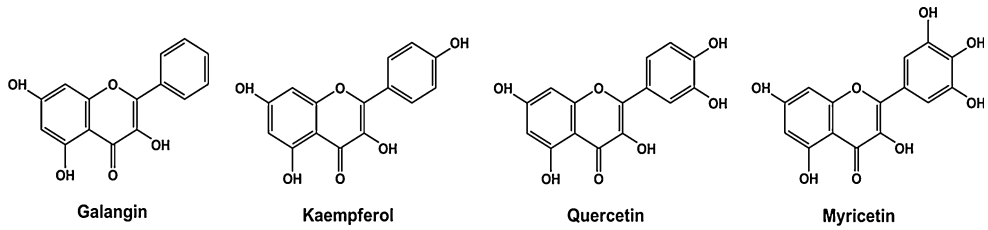

Fig. 1 Molecular structure of Gal, Kae, Que and Myr

ampicillin with rapid shaking. Overexpression of the *Kp*DnaB construct was induced by incubating with 1 mM isopropyl thiogalactoside (IPTG) for 3 h at 37 °C. The cells overexpressing the protein were chilled on ice, harvested by centrifugation, resuspended in Buffer A (20 mM Tris–HCl, 5 mM imidazole, 0.5 M NaCl; pH 7.9) and disrupted by sonication with ice cooling between pulses. The *Kp*DnaB was purified from the soluble supernatant by Ni^{2+}-affinity chromatography (HiTrap HP; GE Healthcare Bio-Sciences, Piscataway, NJ, USA). Protein purity remained greater than 95% as determined by Coomassie-stained SDS–PAGE.

2.4 Dissociation Constant of dNTPS and *Kp*DnaB Determined by Fluorescence Spectrophotometer

An aliquot amount of nucleotides was added into the solution containing *Kp*DnaB (1 μM), 50 mM HEPES at pH 7.0 with a final volume of 2 mL in a quartz cuvettes of 1 cm square cross-section. The decrease in intrinsic fluorescence of protein was measured at 330 nm upon excitation at 280 nm and 25 °C with a spectrofluorimeter (Hitachi F-2700; Hitachi High-Technologies, Tokyo, Japan). Each data point was duplicated, and the difference was within 10%. An aliquot amount of nucleotides was added with or without 10 μM flavonol to a predetermined concentration of *Kp*DnaB to obtain at least 7 data points for each dissociation constant (K_d). The K_d was obtained by the equation: $\Delta F = \Delta F_{max} - K_d(\Delta F/[\text{nucleotide}])$ (Enzyme Kinetics module of SigmaPlot; Systat Software, Chicago, IL, USA).

3 Results

The purpose of this study was to identify some naturally occurring compounds that can inhibit the activity of bacterial replicative helicase(s). The results presented here show that 4 flavonol compounds may be useful in developing anti-*K. pneumoniae* antibiotics.

3.1 Fluorescence Quenching of *Kp*DnaB by dATP, dTTP, dCTP, or dGTP

The fluorescence emission spectra of *Kp*DnaB quenched with dATP, dTTP, dCTP, and dGTP are shown in Fig. 2a–d. Fluorescence intensity of *Kp*DnaB decreased remarkably with increasing concentrations of dNTP (0–10^{-3} M). At 10^{-3} M, dCTP (Fig. 2c) and dGTP (Fig. 2d) quenched

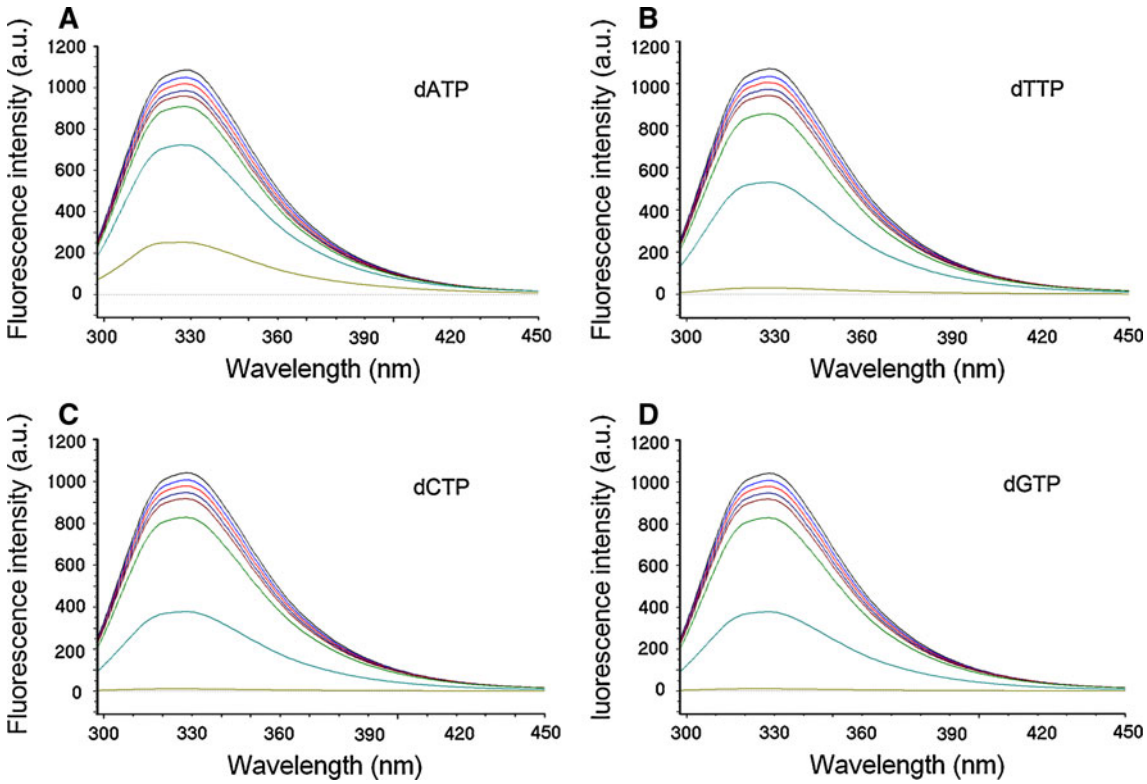

Fig. 2 The fluorescence quenching of *Kp*DnaB by **a** dATP, **b** dTTP, **c** dCTP or **d** dGTP. dNTP, from the *top down*, are as follows: 0, 10^{-9}, 10^{-8}, 10^{-7}, 10^{-6}, 10^{-5}, 10^{-4}, and 10^{-3} M. An aliquot amount of the nucleotide was added into the solution containing *Kp*DnaB (1 μM), 50 mM HEPES at pH 7.0 and 25 °C. After the addition of the nucleotide, the reaction solution was equilibrated for 10 min until no fluorescence change could be observed

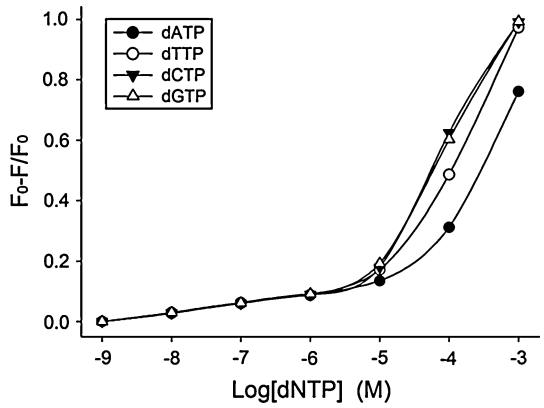

Fig. 3 The fluorescence quenching of *Kp*DnaB plotted as relative fraction of $(F_0-F)/F_0$ against the concentrations of the dNTP

the fluorescence intensity of *Kp*DnaB almost completely, whereas dATP (Fig. 2a) only quenches approximately 80% of the *Kp*DnaB fluorescence intensity. Adding dNTPs resulted in a significant blue shift (~10 nm) of the emission wavelength (λ_{em}) of *Kp*DnaB, indicating an interaction between dNTP and *Kp*DnaB and suggesting formation of a dNTP-*Kp*DnaB complex. The dissociation constant (K_d) values of *Kp*DnaB bound to dATP, dTTP, dCTP, and dGTP determined from the titration curves (Fig. 3) were 159.8 ± 60, 106.0 ± 30, 60.3 ± 13, and 63.2 ± 16 μM, respectively, meaning that *Kp*DnaB exhibited the strongest binding activity towards dCTP.

3.2 Fluorescence Quenching of *Kp*DnaB by Flavonols

The fluorescence emission spectra of *Kp*DnaB quenched by Gal, Kae, Que, and Myr are shown in Fig. 4a–d. Due to the compounds' solubility, 10 μM of each flavonol was used. *Kp*DnaB fluorescence intensity decreased significantly with increasing concentrations of flavonols (0–10 μM). The maximum λ_{em} of these flavonols alone in response to excitation at 280 nm was approximately 520 nm (data not shown). In addition, these 4 flavonols resulted in a slight blue shift (~1 nm) of the maximum λ_{em} of *Kp*DnaB. Thus, the quenching of *Kp*DnaB fluorescence mainly depended on the formation of a complex between the flavonol and *Kp*DnaB (Fig. 4). The titration curves shown in Fig. 5 suggest that *Kp*DnaB binds most strongly to Myr, and, in the order of decreasing affinity, to the other flavonols as follows: Myr > Kae > Gal > Que.

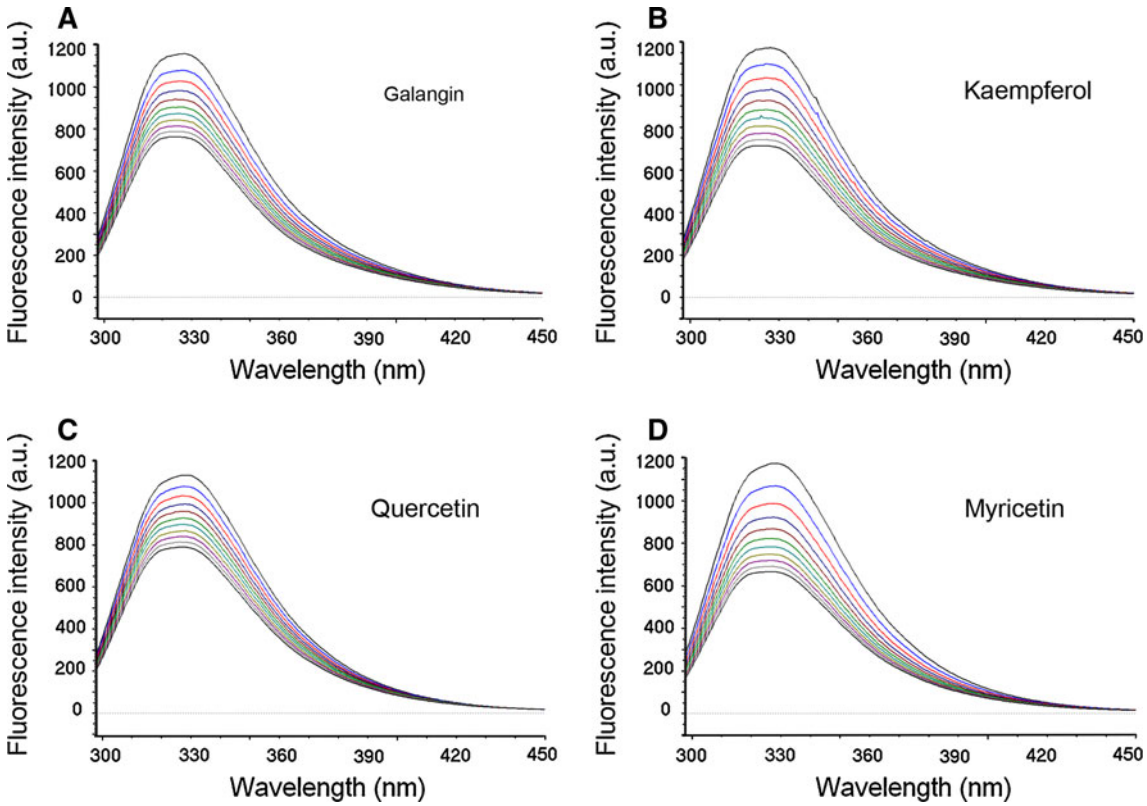

Fig. 4 The fluorescence quenching of *Kp*DnaB by **a** Gal, **b** Kae, **c** Que or **d** Myr. Flavonol, from the *top down*, are as follows: 0, 1, 2, 3, 4, 5, 6, 7, 8, 9, and 10 μM. An aliquot amount of the flavonol was added into the solution containing *Kp*DnaB (1 μM), 50 mM HEPES at pH 7.0 and 25 °C. After the addition of the flavonol, the reaction solution was equilibrated for 10 min until no fluorescence change could be observed

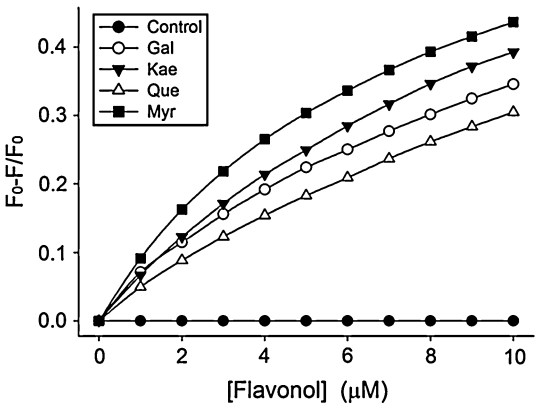

Fig. 5 The fluorescence quenching of *Kp*DnaB plotted as relative fraction of $(F_0-F)/F_0$ against the concentrations of the flavonol

3.3 Fluorescence Quenching of *Kp*DnaB by dATP, dTTP, dCTP and dGTP in the Presence of Myr, Kae, Gal, or Que

To investigate whether the flavonols can inhibit the binding of *Kp*DnaB to dNTP, we analyzed *Kp*DnaB fluorescence quenching by dATP in the presence of Myr, Kae, Gal, or Que (Fig. 6a). The interaction of *Kp*DnaB with dATP was much more sensitive to Gal than to Que. Fluorescence quenching of *Kp*DnaB was not obvious until the concentration of dATP increased to 10^{-4} M, indicating that the binding affinity between *Kp*DnaB and dATP was decreased by the presence of Gal, Kae, Que, or Myr in the reaction solution.

To test whether the flavonols inhibit the binding of *Kp*DnaB to other dNTPs, we also analyzed *Kp*DnaB fluorescence quenching by dTTP (Fig. 6b), dCTP (Fig. 6c), and dGTP (Fig. 6d) in the presence of Myr, Kae, Gal, or Que. However, the results of these experiments were quite different from those of the experiment with dATP. dTTP, dCTP, and dGTP quenched *Kp*DnaB fluorescence by almost 50% even at 10^{-4} M of the flavonols, suggesting that Myr, Kae, Gal, and Que specifically disrupt the *Kp*DnaB-dATP interaction (Fig. 6).

3.4 Inhibition of *Kp*DnaB-dNTP Interaction by Gal was the Strongest

Figure 7 shows the effects of flavonol on the interaction between *Kp*DnaB and dATP, dTTP, dCTP, or dGTP. *Kp*DnaB-dATP binding was inhibited by flavonoids as follows, in the order of decreasing efficiency: Gal > Myr > Kae > Que (Fig. 7a). None of the 4 flavonols disrupted dGTP binding to *Kp*DnaB (Fig. 7d). Among the flavonols, Gal inhibited *Kp*DnaB-dNTP interaction most strongly, although Myr showed the strongest binding to *Kp*DnaB (Fig. 5). Thus, the ability of flavonols to inhibit *Kp*DnaB action in general may be dNTP-dependent.

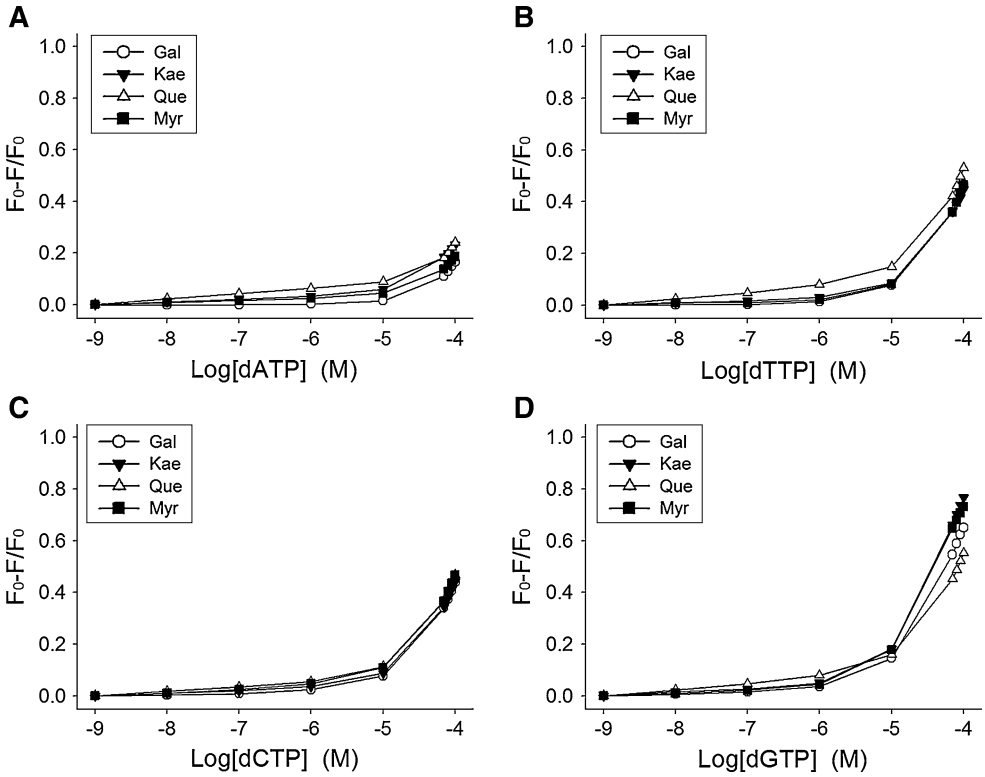

Fig. 6 The fluorescence quenching of *Kp*DnaB in the presence of 10 μM flavonol plotted as relative fraction of $(F_0-F)/F_0$ against the concentrations of **a** dATP, **b** dTTP, **c** dCTP or **d** dGTP. The reaction solution (1 μM *Kp*DnaB, 50 mM HEPES at pH 7.0) was pre-incubated with 10 μM flavonol for 10 min, and then an aliquot amount of the nucleotide was added to the *Kp*DnaB solution. After the addition of the nucleotide, the reaction solution was equilibrated for further 10 min until no fluorescence change could be observed

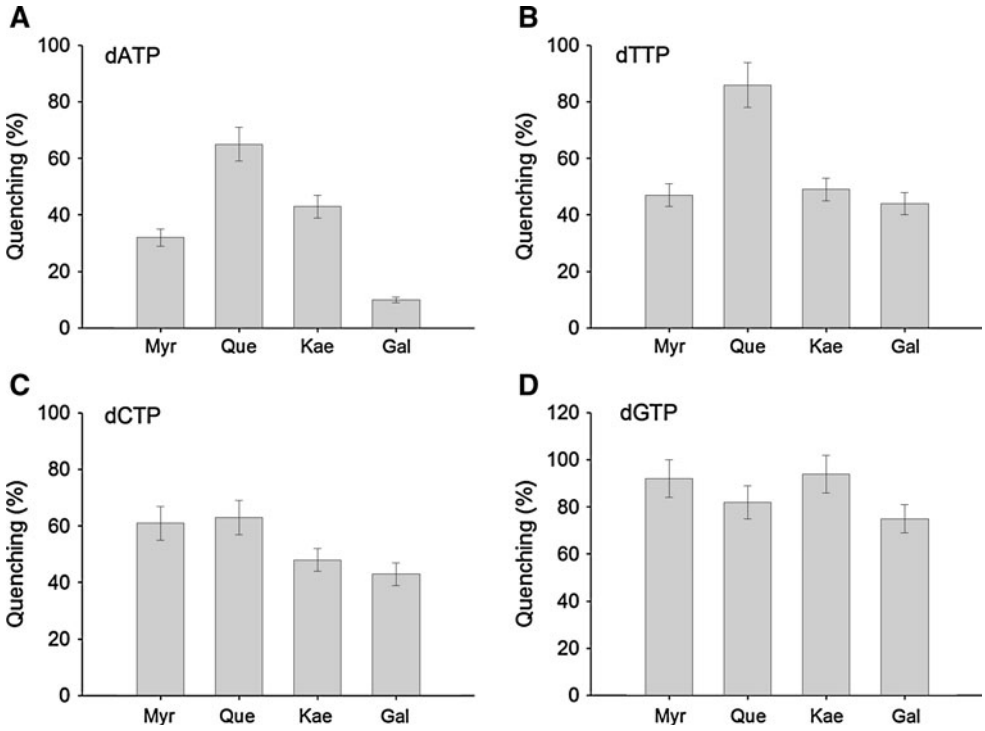

Fig. 7 The quantitative analysis of fluorescence quenching of *Kp*DnaB plotted as relative fraction of $(F_0-F)/F_0$ in the presence of 10 μM flavonol and 10 μM of **a** dATP, **b** dTTP, **c** dCTP or **d** dGTP

3.5 The Flavonoids Inhibited Growth of *K. Pneumoniae*

To test whether these flavonoids can inhibit growth of *K. pneumoniae*, *K. pneumoniae* cells were grown to 0.5 OD_{600} at 37 °C, and then added 10 μM of Gal, Kae, Que, or Myr into the medium. Figure 8 shows that these 4 flavonoids inhibited growth of *K. pneumoniae*; Gal had a greater inhibitory effect than the others.

4 Discussion

DNA replication is one of the most basic biological functions and should be a prime target in antibiotic development. In fact, it is the target of the bactericidal fluoroquinolone class of antibiotics that interferes with DNA gyrase [9] and topoisomerase [2]. Since DNA helicases are important components of the cellular replication machinery in all organisms, inhibition of helicase activity would be detrimental to bacterial survival as well [1, 6, 20, 21, 28]. In this study, we used fluorescence quenching to analyze the interaction of *Kp*DnaB with 4 flavonols, Gal, Kae, Que, and Myr (Fig. 1), which contain different numbers of hydroxyl substituent on the aromatic rings. Our results demonstrated that these flavonols were capable of inhibiting the interaction of *Kp*DnaB with dNTPs. The extent of *Kp*DnaB fluorescence quenching induced by dATP in the presence of a flavonol was much smaller than that of dATP alone, indicating inhibition of *Kp*DnaB-dATP binding by the flavonol (Figs. 3, 6). In addition, the inhibition depended not only on the flavonol (with Gal displaying the strongest inhibition), but also on the dNTP used (the inhibition was most specific to dATP binding).

Binding and hydrolysis of NTP cofactors by the DnaB helicase before association with ssDNA are essential processes that induce and modulate a high affinity conformation of the enzyme that can bind to ssDNA [14, 21, 25]. Although the primary replicative helicase can hydrolyze all NTPs [20], our studies indicate that *Kp*DnaB has a preference for dCTP over other nucleotides (Fig. 3). Thus, other compounds similar to dCTP may be useful in inhibiting *Kp*DnaB.

Other studies have shown that Myr non-competitively inhibits *E. coli* DnaB helicase [6] and RSF1010 RepA helicase [28], with IC_{50} of approximately 10 and 50 μM, respectively. In this study, we found that 10 μM of Gal, Kae, Que, or Myr can inhibit dNTP binding to *Kp*DnaB. Although it is well established that flavonoids have several hydroxyl groups and thus have marked potentials to bind (any) proteins, the strength of the inhibition in dNTP binding of *Kp*DnaB was not correlated with the number of hydroxyl substituent on the aromatic rings of the flavonols (Fig. 7).

Although Myr binds to *Kp*DnaB with the highest affinity among the flavonols (Fig. 5), it did not display the highest inhibition of dNTP-*Kp*DnaB binding (Fig. 7). Based on these results, we propose that these flavonols may inhibit

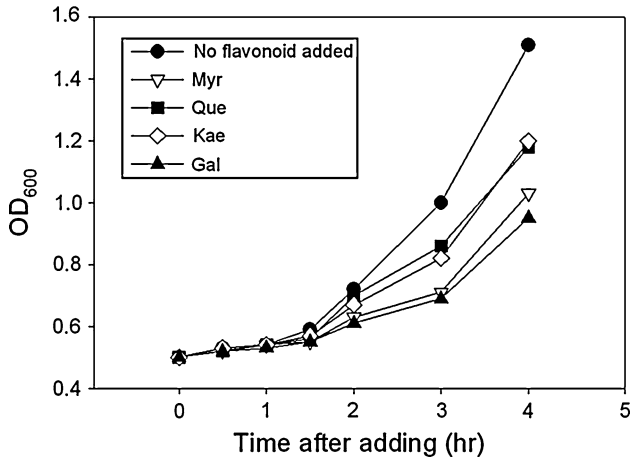

Fig. 8 Growth of *K. pneumoniae* cells in Luria–Bertani medium supplemented with 10 μM of the flavonoids (Myr, Que, Kae, or Gal)

dNTP binding to *Kp*DnaB in 2 possible ways. First, these 4 flavonols may not bind to the active site of *Kp*DnaB, or only partially occupy the active site. Second, since DnaB helicase binding to dNTP causes a large conformational change [11, 12, 20], these flavonols may inhibit the conformational change itself, thereby causing varying degree of inhibition. The inhibition of *Kp*DnaB by these flavonols appeared to be dNTP-dependent, and, thus, neither of these possibilities can be dismissed.

Our crystal structure of *Geobacillus kaustophilus* helicase in complex with ssDNA and the non-hydrolysable NTP analogue ATPγs [13] revealed that ATP hydrolysis may drive the movement of the helicase toward the 3′ end of the lagging strand. In addition, the dNTP-binding site of the helicase at loop I, part of the Walker B motif, is adjacent to the DNA interaction site. From these results, we speculate here that 1 flavonol molecule is enough to bind to the empty active sites of 6 *Kp*DnaB subunits to shut down and lock the enzyme in the dNTP-unbound state. We have prepared a crystal of *Kp*DnaB in complex with Gal to further investigate this hypothesis, and the resulting information may be useful in designing compounds that fit more precisely into helicase active sites.

Acknowledgments We thank Mr. Shun-Chuan Yang for constructing the pET21e-*Kp*DnaB plasmid. This research was supported a grant from the National Research Program for Genome Medicine (NSC 99-3112-B-040-001 to C.Y. Huang).

References

1. Baker TA, Bell SP (1998) Cell 92:295–305
2. Black MT, Coleman K (2009) Curr Opin Investig Drugs 10:804–810
3. Burda S, Oleszek W (2001) J Agric Food Chem 49:2774–2779
4. Chen L, Yang J, Yu J, Yao Z, Sun L, Shen Y, Jin Q (2005) Nucleic Acids Res 33:D325–D328
5. Cushnie TP, Lamb AJ (2005) Int J Antimicrob Agents 26: 343–356
6. Griep MA, Blood S, Larson MA, Koepsell SA, Hinrichs SH (2007) Bioorg Med Chem 15:7203–7208
7. Gupta A, Ampofo K, Rubenstein D, Saiman L (2003) J Perinatol 23:439–443
8. Heller RC, Marians KJ (2006) Nat Rev Mol Cell Biol 7:932–943
9. Hopkins KL, Davies RH, Threlfall EJ (2005) Int J Antimicrob Agents 25:358–373
10. Huang CY, Hsu CH, Sun YJ, Wu HN, Hsiao CD (2006) Nucleic Acids Res 34:3878–3886
11. Jezewska MJ, Bujalowski W (1996) J Biol Chem 271:4261–4265
12. Jezewska MJ, Kim US, Bujalowski W (1996) Biophys J 71:2075–2086
13. Lo YH, Tsai KL, Sun YJ, Chen WT, Huang CY, Hsiao CD (2009) Nucleic Acids Res 37:804–814
14. Lohman TM, Bjornson KP (1996) Annu Rev Biochem 65: 169–214
15. McGlynn P, Lloyd RG (2002) Nat Rev Mol Cell Biol 3:859–870
16. Mott ML, Berger JM (2007) Nat Rev Microbiol 5:343–354
17. Podschun R, Ullmann U (1998) Clin Microbiol Rev 11:589–603
18. Reyes-Lamothe R, Sherratt DJ, Leake MC (2010) Science 328:498–501
19. Ross JA, Kasum CM (2002) Annu Rev Nutr 22:19–34
20. Roychowdhury A, Szymanski MR, Jezewska MJ, Bujalowski W (2009) Biochemistry 48:6730–6746
21. Singleton MR, Dillingham MS, Wigley DB (2007) Annu Rev Biochem 76:23–50
22. Soultanas P (2005) Structure 13:839–844
23. Teillet F, Boumendjel A, Boutonnat J, Ronot X (2008) Med Res Rev 28:715–745
24. Wang CC, Tsau HW, Chen WT, Huang CY (2010) Protein J 29:445–452
25. West SC (1996) Cell 86:177–180
26. Wolfe KL, Liu RH (2008) J Agric Food Chem 56:8404–8411
27. Wu HJ, Wang AH, Jennings MP (2008) Curr Opin Chem Biol 12:93–101
28. Xu H, Ziegelin G, Schroder W, Frank J, Ayora S, Alonso JC, Lanka E, Saenger W (2001) Nucleic Acids Res 29:5058–5066
29. Yang J, Chen L, Sun L, Yu J, Jin Q (2008) Nucleic Acids Res 36:D539–D542
30. Yu WL, Chuang YC, Walther-Rasmussen J (2006) J Microbiol Immunol Infect 39:264–277

國科會國外研討會心得報告

計畫名稱 ： 阻斷克雷伯氏菌複製叉重啟之研究 2/2

(NSC 99-3112-B-040-001)

主持人 ： 黃晟洋

撰寫人 ： 陳政傑

服務單位名稱 ： 中山醫學大學生物醫學科學研究所

出國地點 ： 菲律賓 (Philippines)

出國日期 ： 2011/2/24~2011/3/1

一、會議簡介

本次會議是在菲律賓首都馬尼拉(Manila)舉辦的6th APOCB Congress (The Asian-Pacific Organization for Cell Biology)國際研討會。本次會議的時間為2011年2月25日至2月28日。內容包含十六個主題如下：

1. Protein Quality Control and Cellular Homeostasis
2. Nucleus and Gene Expression
3. Cancer signaling and Metastasis
4. Cell differentiation
5. Bioclips
6. Protistology
7. Developmental Biology
8. Organelles
9. Viral-Cell interactions
10. Biosafety
11. Cytoskeleton and Cell Motility
12. Biobanking
13. Young Investigators Forum
14. Infectious Diseases
15. Drug Discovery and Emerging Technologies
16. Free Papers

與會人員來自世界各地十六個國家，以亞洲地區的菲律賓、台灣、日本、中國、韓國居多。此次會議包含生物醫學各個領域不同的研究方向，如發育生物學、蛋白質體學、神經生物學、病毒學、癌症與訊號路徑、重大疾病研究、藥物研發等，是一個很好的知識交流平台，對於未來生醫方面的發展有很大的助益。

此行讓我收益良多，不論是對於傳統發育模式的顛覆及突破，以及神經傳導方面蛋白訊息的研究，或是心血管疾病利用幹細胞組織來治療的方法，都是相當新穎且走在生醫領域最尖端潮流的知識系統。相信在不久以後，這些知識將會引領人類進入更高水準的醫療時代。

二、會議心得內容

此次會議由於探討主題甚多，所以分成三個演講廳同時進行，對於想多方面了解各國在不同領域研究現況的我，是一項有利的安排。雖然可惜有些主題因為時間重疊無法參與，但幸好主辦單位有把各個論文題目內容做整理，故也可以對於沒有聽到的主題進行了解。以下就對於一些精彩的演講做心得摘要：

Generation of Neural Primordia in Vertebrate Embryos by Mechanism that Challenge the Classical Models *Professor Hisato Kondoh , Japan*

這個演講主題是在挑戰傳統發育生物學的模式，一開始教授在台上就把教科書的發育路徑畫了一個大叉，這個動作令我印象深刻，並引起大家熱烈的掌聲。內容主要是在探討傳統模式中，脊椎動物胚胎發育時期的三個胚層會去決定細胞分化的命運，但教授的研究成果推翻了這個論點，以paraxial mesoderm和neural plate去證明了細胞的命運是從似幹細胞的前驅細胞所分化而來，而這個機制需要Tbx6去抑制Sox2訊號的產生。這項結果除了是發育生物學的突破，也為幹細胞方面的研究開啟一個新的觀點。

Intracellular Transport and Kinesin Superfamily Moleculor Motors (KIFs) : Key Regulators for Neuronal Function, Development and Tumorigenesis
Professor Nobutaka Hirokawa , Japan

這個演講主題以kinesin superfamily proteins (KIFs)為主軸，展開了對於細胞的形態發育、功能性和生存能力的探討。KIF對於神經細胞的發育有很大的影響，如軸突的生成、神經訊號的傳遞、NMDA型與AMPA型受器的作用等。首先教授用影片的方式，展現神經細胞實際生成的狀況以及訊號傳遞的情形，接下來以水迷宮實驗證明了KIF17會影響老鼠的學習能力以及記憶能力，再來用圖片方式拍下老鼠的器官發育狀況，證明了KIF3會影響器官發育的左右對稱性，最後以數據方式去計算，證明了KIF4與神經細胞的存活率有關。教授的研究跨足了神經生物學以及發育生物學領域，並且實驗結果明確的表達出KIF蛋白對於生物整體影響的重要性，這是現今醫學發展以及疾病研究的一項重大突破。

三、海報張貼過程與心得

此次所投稿的論文是以海報形式呈現研究成果，海報尺寸原本是100cmX120cm，但在會議前兩天寫信告知變更規格為75cmX100cm，因時間倉促來不及修改尺寸，幸好海報板夠大，當天早上7:30在工作人員熱情的幫忙下，順利貼上海報。

海報展示時間為2/26日下午5:15~6:00以及2/28日早上11:00~12:00，不過因為放置海報的房間在會議進行中一直都是開放的，所以實際展示時間還要更長。

展示的海報共有70篇，內容跟會議探討的主題一樣廣泛，而令我印象深刻的是有篇植物根部細胞分裂的研究，因為是在這整個會議中，極少數幾個跟植物相關的題目，其他還有像是綠螢光蛋白(GFP)的改良、肌肉萎縮症(MD)的訊號傳導路徑等研究，都讓我很感興趣，並且在與人問答應對之間也加強了我對實驗研究的邏輯思考，以及英文表達能力，對我而言是個很寶貴的學習機會。

在此要感謝旁邊的商品銷售工作人員，很熱情地幫我拍了一張照片。

四、結論

首先要感謝老師肯給我這個機會，讓我能夠到國外增廣見聞，以及國科會提供在參與國際會議經費上的補助。能夠接觸到這些國際知名的學術演講者，對我有極大幫助，也了解現今世界生醫領域的潮流方向為何，同時可以增加台灣在國際間的能見度與地位，也算是盡了個人的一份心力。

整體來講，這次能夠出國參與國際會議，對我來說是個一生難得的重要經驗，不管在英文表達方面，或是研究方向思考，都讓我學到了很多，對於實驗與研究工作也有更深的體會。要想有一天在這國際舞台上獲得掌聲，只有不斷地努力，精益求精，秉持著自我要求的信念，終有一天，才能夠有更加璀璨的研究成果，為人類醫學方面做出些微貢獻。希望下次還能有這樣的機會，出國學習成長，並為台灣的外交盡一己綿薄之力。

五、附上幾張會議照片以及一份會議流程表和參加證明

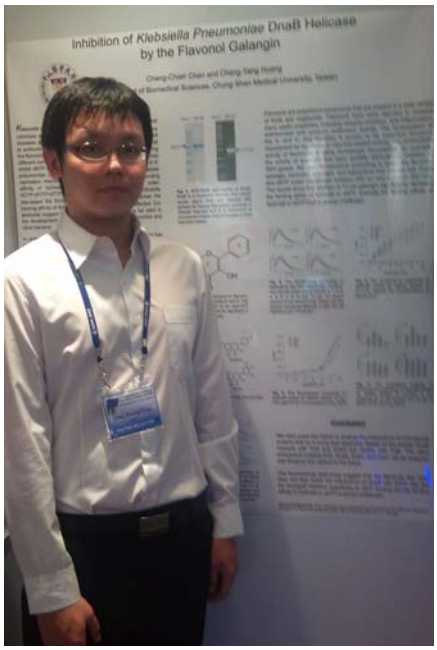

THE CONGRESS AT A GLANCE

	Friday, 25 February 2011	Saturday, 26 February 2011	Sunday, 27 February 2011	Monday, 28 February 2011
	9:00-5:00 **REGISTRATION** *Secretariat Room, SULU*	8:00-5:00 **REGISTRATION** Registration Booth at Foyer	8:00-11:00 **REGISTRATION** Registration Booth at Foyer	9:00-12:00 **REGISTRATION** Registration Booth at Foyer
MORNING SESSION	8:30-12:00 **PRE-CONGRESS WORKSHOP** *BORACAY* **"Teaching Cell Biology with Limited Resources"**	8:30-9:30 **OPENING CEREMONY** *ISLA 2* 9:30-9:50 **PHOTO OPPORTUNITY** *ISLA 2* 9:50-10:10 **RIBBON CUTTING AND POSTER VIEWING** *ISLA 3* 10:10-10:30 **COFFEE BREAK** *Foyer* 10:30-11:00 **PLENARY LECTURE 1** *ISLA 2* 11:00-11:30 **PLENARY LECTURE 2** *ISLA 2* 11:30-12:00 **PLENARY LECTURE 3** *ISLA 2*	7:50-8:20 **PLENARY LECTURE 4** *ISLA 2* 8:20-8:50 **PLENARY LECTURE 5** *ISLA 2* 8:50-9:20 **PLENARY LECTURE 6** *ISLA 2* 9:20-9:50 **PLENARY LECTURE 7** *ISLA 2* *(Coffee will be served)* 9:50-11:15 **EDUCATION SESSION** *ISLA 2* **CONFERENCE TOUR** 11:30 **ASSEMBLY** at staircase near ISLA1 11:40 **DEPARTURE**	9:00-9:30 **PLENARY LECTURE 8** *ISLA 2* 9:30-10:00 **PLENARY LECTURE 9** *ISLA 2* 10:00-10:30 **PRODUCT PRESENTATION** *(Coffee will be served)* *ISLA 2* 10:30 – 11:00 **PLENARY LECTURE 10** *ISLA 2* 11:00-12:00 **POSTER SESSION** *ISLA 3*
AFTERNOON SESSION	12:00-1:00 **LUNCH BREAK** *ISLA 1*	12:00-1:00 **LUNCH BREAK** *ISLA 1*	*(Packed lunch will be provided to all participants)*	12:00-1:00 **LUNCH BREAK** *ISLA 1*
	1:30-5:00 **PRE-CONGRESS WORKSHOP** *BORACAY* **"Scientific Writing and Publishing for Non-native Speakers of English"**	1:00-3:15 **SIMULTANEOUS SESSIONS** *(BATANES 1 & 2)* *SS1: PROTEIN QUALITY CONTROL & CELLULAR HOMEOSTASIS* *SS2: NUCLEUS & GENE EXPRESSION* *(ISLA 2)* *SS3: CANCER SIGNALING & METASTASIS* *SS4: CELL DIFFERENTIATION* *(E's BAR)* *SS5: BIOCLIPS* *SS6: PROTISTOLOGY* 3:15-3:45 **PRODUCT PRESENTATION** *(Coffee will be served)* *ISLA 2* 3:45-5:15 **SIMULTANEOUS SESSIONS** *(BATANES 1 & 2)* *SS7: DEVELOPMENTAL BIOLOGY* *SS8: ORGANELLES* *(ISLA 2)* *SS9: VIRAL-CELL INTERACTIONS* *SS10: BIOSAFETY* *(E's BAR)* *SS11: CYTOSKELETON & CELL MOTILITY* *SS12: BIOBANKING* 5:15-6:00 **POSTER SESSION** *ISLA 3*	**CONFERENCE TOUR to "VILLA ESCUDERO" Tiaong, Quezon** 2:00 **ARRIVAL** at Villa Escudero (Cultural Show, Museum Visit, Carabao Ride, etc.) 6:00 **DINNER** at Villa Escudero 8:00 **RETURN TO MANILA**	1:00-3:15 **SIMULTANEOUS SESSIONS** *(MACTAN 1 & 2)* *SS13: YOUNG INVESTIGATORS* *(ISLA 2)* *SS14: INFECTIOUS DISEASES* *SS15: DRUG DISCOVERY & EMERGING TECHNOLOGIES* *(BORACAY)* *SS16: FREE PAPERS* 3:15-3:30 **COFFEE BREAK** *Foyer* 3:30-4:00 **APOCB PLENARY LECTURE** *ISLA 2* 4:00 **CLOSING CEREMONY** *ISLA 2* 5:15 **ASSEMBLY** Staircase near ISLA1 5:30 **DEPARTURE** for St. Luke's Medical Center-Global City 6:00-10:00 **FAREWELL BANQUET AND CULTURAL NIGHT** *(including presentation by country)*
	6:00 **WELCOME RECEPTION** *e's Bar* *2nd Floor, EDSA Shangri-La*	6:00 **FREE TIME** APOCB Executive Committee Meeting *Summer Palace* *2nd Floor, EDSA Shangri-La*		

6th Asian-Pacific Organization for Cell Biology International Congress (6APOCB)

25~28 February 2011, Manila, Philippines

Theme: "Challenges in Cell Biology: Health, Agriculture, Industry and Education"

presents this

Certificate of Attendance

to

Cheng-Chieh Chen

Given this 28th of February 2011, at EDSA Shangri-La Manila

Nobutaka Hirokawa, MD, PhD
President of APOCB

Filipinas F. Natividad, PhD
Secretary-General of 6APOCB

國科會補助計畫衍生研發成果推廣資料表

日期:2011/07/04

國科會補助計畫	計畫名稱: 阻斷克雷伯氏菌複製叉重啟之研究(2/2)
	計畫主持人: 黃晟洋
	計畫編號: 99-3112-B-040-001- 學門領域: 基因體醫學國家型研究計畫

無研發成果推廣資料

99 年度專題研究計畫研究成果彙整表

計畫主持人：黃晟洋	計畫編號：99-3112-B-040-001-
計畫名稱：阻斷克雷伯氏菌複製叉重啟之研究(2/2)	

成果項目			量化			單位	備註（質化說明：如數個計畫共同成果、成果列為該期刊之封面故事...等）
			實際已達成數（被接受或已發表）	預期總達成數(含實際已達成數)	本計畫實際貢獻百分比		
國內	論文著作	期刊論文	0	0	100%	篇	
		研究報告/技術報告	0	0	100%		
		研討會論文	2	2	100%		
		專書	0	0	100%		
	專利	申請中件數	0	0	100%	件	
		已獲得件數	0	0	100%		
	技術移轉	件數	0	0	100%	件	
		權利金	0	0	100%	千元	
	參與計畫人力（本國籍）	碩士生	2	0	100%	人次	
		博士生	0	0	100%		
		博士後研究員	0	0	100%		
		專任助理	1	0	100%		
國外	論文著作	期刊論文	4	8	100%	篇	
		研究報告/技術報告	0	0	100%		
		研討會論文	1	1	100%		
		專書	0	0	100%	章/本	
	專利	申請中件數	0	0	100%	件	
		已獲得件數	0	0	100%		
	技術移轉	件數	0	0	100%	件	
		權利金	0	0	100%	千元	
	參與計畫人力（外國籍）	碩士生	3	3	100%	人次	
		博士生	0	0	100%		
		博士後研究員	0	0	100%		
		專任助理	2	2	100%		

其他成果 (無法以量化表達之成果如辦理學術活動、獲得獎項、重要國際合作、研究成果國際影響力及其他協助產業技術發展之具體效益事項等，請以文字敘述填列。)	無

	成果項目	量化	名稱或內容性質簡述
科教處計畫加填項目	測驗工具(含質性與量性)	0	
	課程/模組	0	
	電腦及網路系統或工具	0	
	教材	0	
	舉辦之活動/競賽	0	
	研討會/工作坊	0	
	電子報、網站	0	
	計畫成果推廣之參與（閱聽）人數	0	

國科會補助專題研究計畫成果報告自評表

請就研究內容與原計畫相符程度、達成預期目標情況、研究成果之學術或應用價值（簡要敘述成果所代表之意義、價值、影響或進一步發展之可能性）、是否適合在學術期刊發表或申請專利、主要發現或其他有關價值等，作一綜合評估。

1. 請就研究內容與原計畫相符程度、達成預期目標情況作一綜合評估

□達成目標

■未達成目標（請說明，以 100 字為限）

□實驗失敗

□因故實驗中斷

■其他原因

說明：

抑制劑的有效強度不夠

2. 研究成果在學術期刊發表或申請專利等情形：

論文：■已發表 □未發表之文稿 □撰寫中 □無

專利：□已獲得 □申請中 ■無

技轉：□已技轉 □洽談中 ■無

其他：（以 100 字為限）

3. 請依學術成就、技術創新、社會影響等方面，評估研究成果之學術或應用價值（簡要敘述成果所代表之意義、價值、影響或進一步發展之可能性）（以 500 字為限）

These results may provide deeper knowledge of the KP replication restart primosome, whereby to advance our understanding as to how DNA replication restart of KP can be blocked. These finding may be also used for drug developments for bacterial infection disease.